Petrology of very high temperature crustal xenoliths in the Puente Negro intrusion: a sapphire-spinel-bearing Oligocene andesite, Mixteco terrane, southern Mexico

Fernando Ortega-Gutiérrez*, Barbara M. Martiny, Dante J. Morán-Zenteno, A. Margarita Reyes-Salas, and Jesús Solé-Viñas

Instituto de Geología, Universidad Nacional Autónoma de México
Ciudad Universitaria, C.P. 04510, Mexico City, Mexico.
** fortega@servidor.unam.mx*

ABSTRACT

This study presents petrologic, chemical, geochronological and isotopic data, as well as petrogenetic interpretations about a unique subvolcanic locality in southern Mexico that contains deep-seated xenoliths and xenocrysts (igneous and metamorphic), albeit affected by extreme pyrometamorphism during rapid ascent in a composite andesitic dike. The intrusion has a K-Ar age of 29.2 ± 0.3 Ma on volcanic matrix and 30.5 ± 0.6 Ma on hornblende xenocrysts,and it is part of an arc-related regional magmatic event in southern Mexico. This magma at Puente Negro intruded quartzo-feldspathic gneisses and micaceous schists of the Paleozoic Acatlán Complex. Xenoliths consist of high-grade garnet-bearing gneisses, aluminous metapelites, impure quartzites, and abundant hornblende-rich gabbroic rocks. Garnet, corundum (including purple-blue sapphire), spinel, and aluminous orthopyroxene constitute the main types of deep-seated xenocrysts derived from disaggregation of metamorphic rocks in the andesite. Low pressure assemblages with tridymite, spinel, Al-silicates (mullite and sillimanite), two pyroxenes, Fe-Ti oxides, and high-silica anatectic glasses indicate peak temperatures of pyrometamorphism above 1100 ºC. Decompression coronas of spinel-plagioclase-orthopyroxene ± corundum ± glass about polyphase garnet porphyroblasts in plagioclase-orthopyroxene-spinel restitic gneisses, Al-rich orthopyroxene coring Al-poor orthopyroxene xenocrysts, spinel-plagioclase-corundum xenocrystic pseudomorphs probably after garnet, and local preservation of orthopyroxene-sillimanite and garnet-hypersthene-spinel-quartz assemblages strongly support interaction of original basaltic magmas with the lower crust. Aluminum in orthopyroxene (up to 11.6 Al_2O_3 wt. %) coexisting with spinel, ilmenite-magnetite pairs, and Fe/Mg partitioning between orthopyroxene and spinel in garnet coronas yield decompression metamorphic temperatures around 990 ºC, whereas coexisting hornblende-plagioclase and two pyroxenes in gabbroic xenoliths yield magmatic temperatures of 800 to 950 ºC. The first basaltic hydrous magma represented by the gabbroic xenoliths differentiated in a magmatic chamber in the middle crust at 4–6 kbar based on Al-in-hornblende barometry. The subsequent injection of this partially to totally crystallized magma chamber by a new basaltic batch apparently caused disaggregation of the hornblende-rich rocks and transported the xenolith-xenocryst load to the surface. Based on major and trace elements and Sr, Pb, and Nd isotope data, we conclude that the Puente Negro "andesite" was the end product of a mantle-derived, relatively long-lived plumbing system of original basaltic composition that in the early Oligocene (29–30

Ortega-Gutiérrez, F., Martiny, B.M., Morán-Zenteno, D.J., Reyes-Salas, A.M., Solé-Viñas, J., 2011, Petrology of very high temperature crustal xenoliths in the Puente Negro intrusion: a sapphire-spinel-bearing Oligocene andesite, Mixteco terrane, southern Mexico: Revista Mexicana de Ciencias Geológicas, v. 28, núm. 3, p. 593-629.

Ma) interacted with the continental crust at lower, middle and shallow levels, which are represented, respectively, by xenoliths of granulite facies quartzites and metapelites, mafic and ultramafic gabbroic rocks, and sanidinite facies quartzo-feldspathic buchites.

Key words: crustal xenoliths, pyrometamorphism, sapphire xenocrysts, arc basalt, Mixteco terrane, southern Mexico.

RESUMEN

Este estudio presenta datos petrológicos, químicos, geocronológicos e isotópicos, así como interpretaciones petrogenéticas sobre una localidad volcánica única en el sur de México que contiene xenolitos y xenocristales ígneos y metamórficos de origen profundo, afectados por pirometamorfismo extremo durante su ascenso rápido en un dique andesítico compuesto. La intrusión tiene una edad de de 29.2± 0.3 Ma (matriz volcánica) y de 30.5±0.6 Ma (xenocristales de hornblenda), y es parte de un evento magmático regional en el sur de México que, localmente en Puente Negro, intrusionó gneisses cuarzo-feldespáticos y esquistos micáceos del Complejo Acatlán paleozoico. Los xenolitos consisten en gneisses granatíferos, metapelitas aluminosas, cuarcitas impuras y abundantes rocas gabroicas ricas en hornblenda. Granate, corindón (incluyendo safiro azul-púrpura), espinela y ortopiroxena aluminosa constituyen los tipos principales de xenocristales profundos procedentes de rocas metamórficas disgregadas en la andesita. Asociaciones de presión baja con tridimita, espinela, mullita, silimanita, clinopiroxena y ortopiroxena, óxidos de Fe y Ti y vidrios anatexíticos altos en sílice indican temperaturas pico en el campo del pirometamorfismo superiores a 1100 ºC. Las coronas de descompresión alrededor de granates polimetamórficos formadas por espinela-plagioclasa-ortopiroxena ± corindón ± vidrio en gneisses restíticos de plagioclasa-ortopiroxena-espinela, ortopiroxena aluminosa en los centros de xenocristales de ortopiroxena pobre en aluminio, pseudomorfos de espinela-plagioclasa-corindón probablemente reemplazando granate, y la preservación local de asociaciones de ortopiroxena-silimanita y granate-hiperstena-espinela-cuarzo, claramente apoyan la interacción de un magma basáltico original con la corteza inferior. El contenido de aluminio en ortopiroxena (hasta 11.6 % Al_2O_3), que coexiste con espinela, pares de ilmenita-magnetita y la distribución Fe/Mg entre ortopiroxena y espinela en las coronas alrededor de granate, indican temperaturas metamórficas durante la descompresión cercanas a los 990 ºC, mientras que pares coexistentes de hornblenda-plagioclasa o de dos piroxenas en los xenolitos gabroicos, proporcionan temperaturas de cristalización de 800 a 950 ºC. Este primer magma basáltico hidratado, representado por los xenolitos gabroicos, se diferenció en la corteza media a presiones de 4–6 kbar, calculadas por barometría del contenido de aluminio en las anfíbolas. La inyección subsecuente a través de esta cámara magmática parcial o totalmente cristalizada de nuevos magmas basálticos, aparentemente causó la desintegración de sus rocas ricas en hornblenda, emplazándose muy cerca de la superficie con su carga de xenolitos y fundiendo parcialmente los gneisses encajonantes. Con estas bases y datos isotópicos (Sr, Pb y Nd) y geoquímicos adicionales, concluimos que la "andesita" Puente Negro fue el producto final de un sistema magmático de larga duración relativa y composición basáltica derivado del manto, el cual, durante el Oligoceno temprano (30–29 Ma), interactuó con niveles inferiores, intermedios y someros de la corteza continental representados respectivamente por xenolitos de metapelitas y cuarcitas en facies de granulita, rocas gabróicas máficas y ultramáficas y buchitas cuarzofeldespáticas en facies de sanidinita.

Palabras clave: xenolitos corticales, pirometamorfismo, xenocristales de safiro, basalto de arco, terreno Mixteco, sur de México.

INTRODUCTION

The study of deep-seated xenoliths in volcanic rocks provides direct information about the nature and processes at depth that remain otherwise difficult or impossible to sample and understand (Rudnick and Fountain, 1995). In particular, xenoliths constitute samples from the buried crust and upper mantle, which in many important ways constrain the tectonic history and crustal genesis at a given area (Halliday *et al.*, 1993; Lee, *et al.*, 2001; Ghent *et al*., 2008; Ray *et al*., 2008), and also illuminate fundamental aspects of magmatic processes such as ascent rates and thermal interactions of the magma with the traversed crust (*e.g.*, Beard *et al*., 2005). Moreover, whilst deep-seated xenoliths in intraplate-type volcanics of central and northern Mexico have been used successfully to trace the nature of the local lower crust and upper mantle (Ruiz *et al.*, 1988; Hayob *et al.*, 1989; Luhr *et al.*, 1989; Rudnick and Cameron, 1991; Cameron *et al.*, 1992; Schaaf *et al.*, 1994; Luhr and Aranda-Gómez, 1997), with few exceptions (*e.g.*, Blatter and Carmichael, 1998;

Aguirre-Diaz *et al*., 2002) this has not been possible in southern and central Mexico essentially because of the lack of volcanic rocks bearing deep crustal xenoliths. Thus, the rather unique nature of the Puente Negro shallow intrusion and its xenoliths located in southern Mexico constitutes an invaluable opportunity for assessing the lithotectonic structure of the crust underlying the polyphase metamorphic Acatlán Complex in the forearc region of the Trans-Mexican Volcanic Belt, and also provides extraordinary information about the thermal and petrologic evolution of basaltic-andesitic orogenic magmas as they traverse the entire crust. Thus, the main goals of this work are a) to present the first detailed petrographic, mineralogical, and petrogenetic study of both the andesitic host rock and its diverse load of xenoliths and xenocrysts, and b) to discuss important physical aspects of the magma-xenolith system evolution. In particular, the presence of corundum/sapphire, green spinel, and aluminous orthopyroxene xenocrysts in the andesitic rock, together with the polyphase, very high temperatures documented in the metamorphic xenoliths, provide intriguing insights into the P-T history of Puente Negro magmas.

TECTONOSTRATIGRAPHIC SETTING

Puente Negro is a subvolcanic intrusion emplaced in rocks of the Paleozoic Acatlán Complex, basement of the Mixteco terrane, state of Puebla in southern Mexico (Figure 1a), which is one of the most extensive pre-Mesozoic metamorphic complexes exposed in the forearc region of the Trans-Mexican Volcanic Belt (Campa and Coney 1983; Sedlock *et al*., 1993). The oldest basement of southern Mexico includes the Grenvillian Oaxacan Complex (Zapoteco terrane) juxtaposed against the Acatlán Complex along the Caltepec Permian fault exposed 75 km to the east of Puente Negro (Elías-Herrera and Ortega-Gutiérrez, 2002). The western limit of the Acatlán Complex is marked by the Laramidic Papalutla thrust against the Morelos Cretaceous carbonate platform (Guerrero terrane), the basement of which is not exposed. The host rocks of the Puente Negro intrusion (Figure 1b, 2a) consist of retrograde quartzo-feldspathic gneisses (Esperanza Granitoids) with polyphase metamorphic fabrics of Paleozoic age composed of white mica, chlorite, quartz, and epidote, with amphibole, epidote, garnet, and albite as common porphyroclasts. The

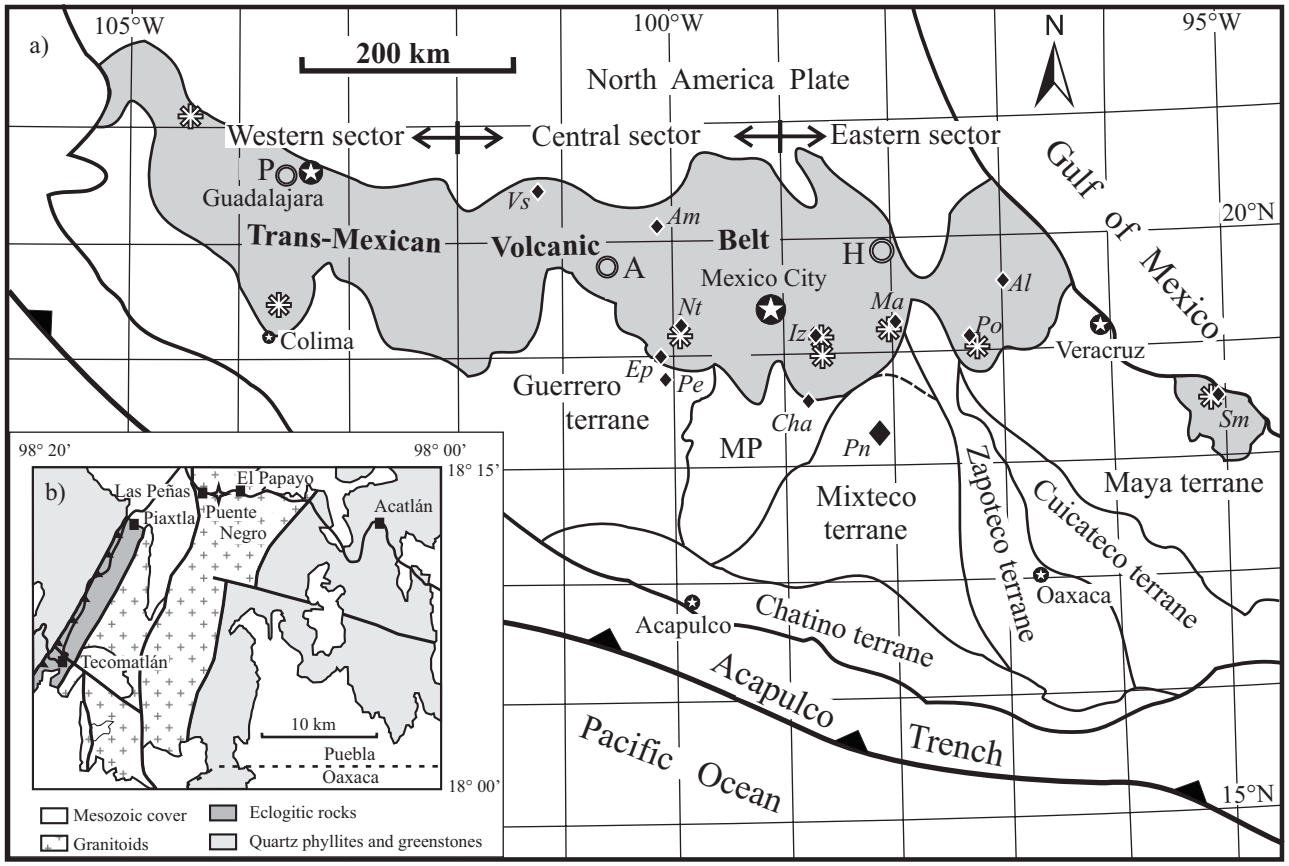

Figure 1. (a) Tectonostratigraphic location. Location of the Puente Negro (*Pn*) xenolith locality (large filled rhomb) in relation to the Transmexican Volcanic Belt, and localities where granulite or mantle xenoliths (small filled rhombs) have been reported in the volcanic arc (see Ortega-Gutierrez *et al*., 2008). Valle de Santiago (*Vs*), Amealco (*Am*), El Peñon (*Ep*), Pepechuca (*Pe*), Nevado de Toluca (*Nt*), Chalcatzingo (*Cha*), Iztaccihuatl (*Iz*), Malinche (*Ma*), Pico de Orizaba (*Po*), Alto Lucero (*Al*), San Martin Tuxtla (*Sm*), Los Humeros caldera (H), Los Azufres caldera (A), La Primavera caldera (P). Major stratovolcanoes are shown by white asterisks, and largest calderas by double circles. (b) General geologic setting of the Puente Negro intrusion area.

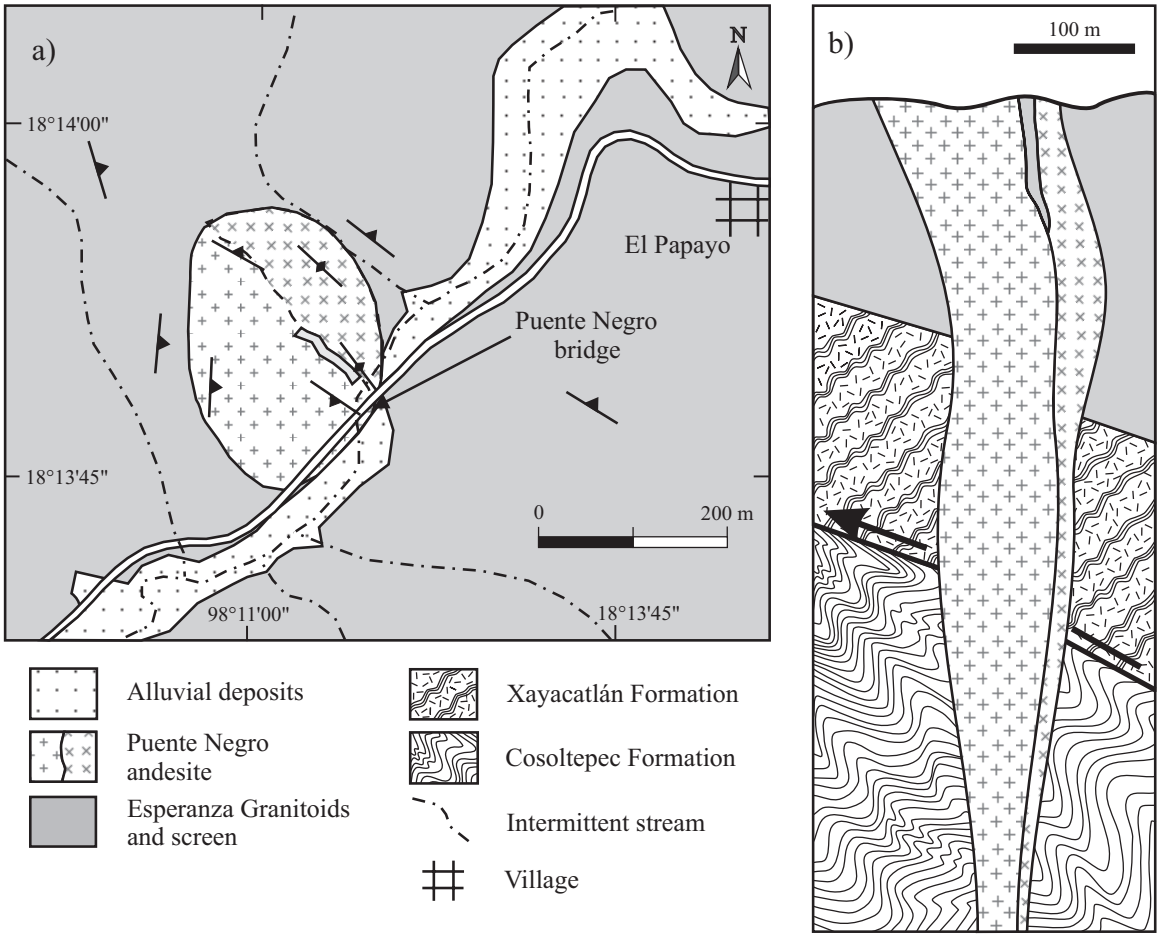

Figure 2. a) Local geology, and b) schematic cross section of the Puente Negro dike complex intruded into the Acatlán Complex

unexposed rocks intruded by the andesitic dike (Figure 2b) probably consist of retrograde eclogitic mafic and ultramafic rocks of the Xayacatlán Formation, and low-grade quartzose phyllites of the Cosoltepec Formation, which form elsewhere the main part of the exposed Acatlán Complex (Ortega-Gutiérrez, 1978).

Puente Negro intrusion

The igneous body is exposed at 18˚13.74' north latitude, and 98˚ 10.98' west longitude, between the towns of El Papayo and Las Peñas (Figures 1b and 2a). The intrusion (Figures 2b and 3a) apparently represents a splayed and tapered shallow dike complex termination with an oval outcrop expression, and a maximum apparent total width of about 160 meters. It is composed of at least three separate bodies (Figure 2b), two of which contain abundant xenoliths and xenocrysts showing throughout a steep igneous foliation trending NW to WNW. A discontinuous screen about 3 m wide of glassy rocks interpreted as partially melted country gneiss (buchite) is located between the two main dikes.

Although high-grade metamorphic xenoliths (Figure 3b to 3f) and quartz, garnet, and amphibole xenocrysts are common, igneous gabbroic and quartzitic gneisses predominate in the xenolith population. The gabbros are highly porphyritic, rich in amphibole, and attain a maximum size of about 10 cm, whereas the largest quartzose xenolith found is a rounded block 40 × 30 cm across. Many of the quartzose xenoliths show mantles or narrow veins of glass and rare ultramafic xenoliths (hornblende orthopyroxenites) attain sizes up to a few centimeters. Amphibole megacrysts in the gabbroic xenoliths may be several centimeters long, whereas the largest garnet xenocryst found was about one centimeter in diameter.

The maximum depth for the intrusive body is estimated to be a few hundred meters (a few tens of bars), as deduced from the aphanitic texture of the igneous matrix and perfect preservation of glass in both andesite and xenoliths. Similar dikes, sills and plugs with xenoliths and garnet xenocrysts intruding the Acatlán Complex are common elsewhere (*e.g.*, Las Minas plug located about 40 km NNW of Puente Negro, and Reyes Metzontla, 65 km to the east of Puente Negro), but none is as diverse or with xenoliths as large as those at Puente Negro.

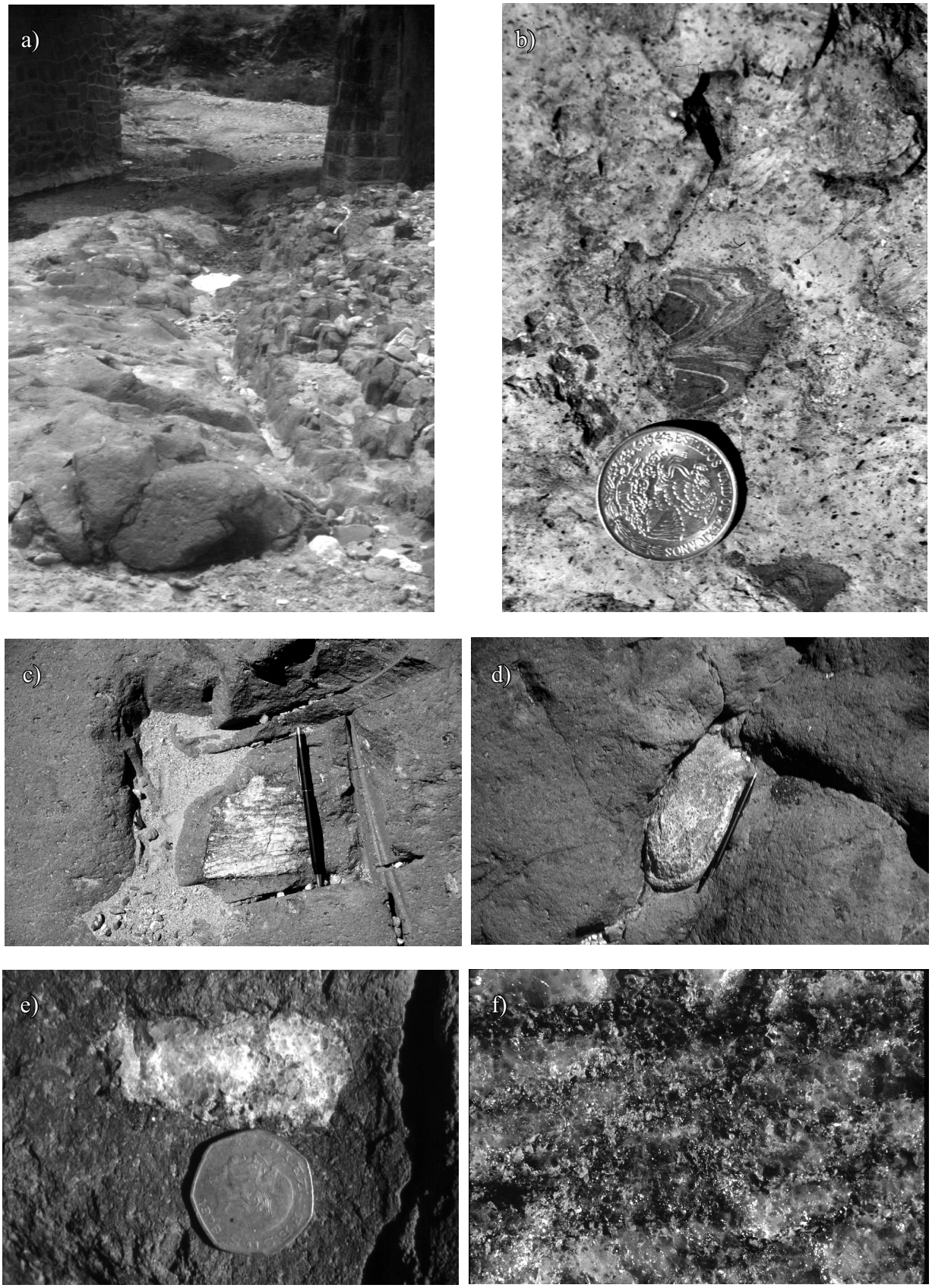

Figure 3. Field aspects of Puente Negro intrusion and its xenoliths. a) Puente Negro main outcrop. b) Rheomorphic xenolith entrained in the andesitic magma; coins in b) and e) are 3 cm across. c) Quartzo-feldspathic banded gneiss; pen in c) and d) is 13 cm long. d) Calcsilicate xenolith. e) Quartzite xenolith. f) Close up of the equigranular (granulitic) texture of a metapelitic xenolith; the image is about 2 cm across.

PETROGRAPHY OF INTRUSION AND XENOLITHS

Because the Puente Negro xenolith locality is described for the first time and both, host andesite and its xenoliths show a very complex mineralogy and unusual textural features, the following detailed petrographic descriptions and petrologic discussion of the rocks and minerals are considered essential to this and future petrogenetic studies of the locality. A petrographic summary based on the study of over 70 thin sections of the Puente Negro andesite and xenoliths is shown in Table 1. Six domains were distinguished in the andesite: aphanitic volcanic matrix, phenocrysts, "glomerocrysts", xenoliths (gabbroic and metamorphic), xenocrysts, and xenocrystic polycrystalline pseudomorphs, all of which provide important petrogenetic information on the conditions that controlled the evolution of the magma-xenolith system *en route* to the surface.

The dikes in outcrop show porphyritic and aphanitic textures, but in thin section the dominant microtexture is defined by pilotaxitic plagioclase (2–200 μm) set in a fine-grained matrix rich in Fe-Ti oxides (1–20 μm), orthopyroxene, and minor clinopyroxene; often, abundant brown glass is also present (Figure 4a). The matrix of a representative glass-rich sample (PN21) is formed by Pl (63%), glass (20%), Opx (15%), TiMag (titanomagnetite) (2%), and Cpx (<1%).

Abbreviations for minerals in this work are after Whitney and Evans (2010), except when indicated. Note that modal percentages were visually estimated. Microphenocrysts (250–400 μm) and phenocrysts (>400 μm) are plagioclase, orthopyroxene, and some clinopyroxene. Amphibole is the main mafic phase in the andesite (Figure 4b), but occurs in large to small crystals that at first sight may be considered phenocrysts and therefore cogenetic with the andesite. However, the intense alteration to anhydrous gabbroic assemblages (often 100 %), and strong resemblance to amphiboles in the gabbroic xenoliths suggest a xenocrystic origin; it is characterized by simple twinning, magmatic embayment, and multiple oscillatory zoning marked by alternating bands of brown to colorless or greenish brown colors. Orthopyroxene occurs in the aphanitic matrix with opaque oxides, plagioclase microlites and glass, and as faintly pleochroic (pale yellow to colorless phenocrysts up to 2.2 mm long); a few crystals contain abundant inclusions of hercynite. Plagioclase "phenocrysts" (probably xenocrysts) are up to 1.3 mm, sharply zoned, and commonly show sieve texture, as well as inclusions of orthopyroxene, opaque phases, green spinel (Figure 4c), and corundum. Primary clinopyroxene present

Table 1. Petrographic summary of the Puente Negro andesite-xenolith system.

Sample	Qz	Trd	Sa	Pl	Glass	Spl	Sil	Mul	Crn	Opx	Cpx	Grt	Hbl	Bt	Cal	Rt	Fe/Ti oxide	Ap	Zrn	Crd	Rock type
PN21*				X	X					X							X				Andesite
PN0	X	X	X	X	X							X					X		X		Quartzite
PN1	X	X	X	X	X	X	?	?	X	X	X	X				X	X		X	?	Quartzite
PN3				X	X						X		X				X				Hbl gabbro
PN4				X	X	X				X	X		X					X			Websterite
PN6				X	X					X		X	X			X	X				Grt gneiss
PN9	X	X		X	X	X			?	X		X		X		X	X		X		Grt gneiss
PN10				X	X								X	X					X		Hbl gabbro
PN12				X	X						X		X				X				Hbl gabbro
PN14	X	X		X	X	X				X		X				X	X		X		Quartzite
PN17				X		X			X	X		X					X				Grt gneiss
PN18				X	X	X				X	X	X	X	X							Grt gneiss
PN19	X	X	X	X													X				Quartzite
PN23	X	X		X	X	X			X	X	X	X					X				Quartzite
PN24	X	X	X	X						X						X	X		X	?	Buchite
PN27	X	X		X	X					X	X						X				Quartzite
PN29				X	X	X			X	X		X					X	X	X	?	Grt gneiss
PN41				X						X	X		X								Hbl gabbro
PN42	X	X	?	X	X						X				X		X	X	X		Calcsilicate
FO29698	X	X	X	X	X	X		X		X						X	X	X	X	?	Quartzite
FO29998				X	X			X		X	X		X	X		X	X				Hbl gabbro
FO6605	X	X	X	X	X					X	X						X	X	X		Buchite
FO7505	X	X		X	X		X			X											Qz gneiss
FO11679	X			X	X					X	X						X		X		Buchite
FO21098	X	X		X	X	X				X							X				Qz gneiss

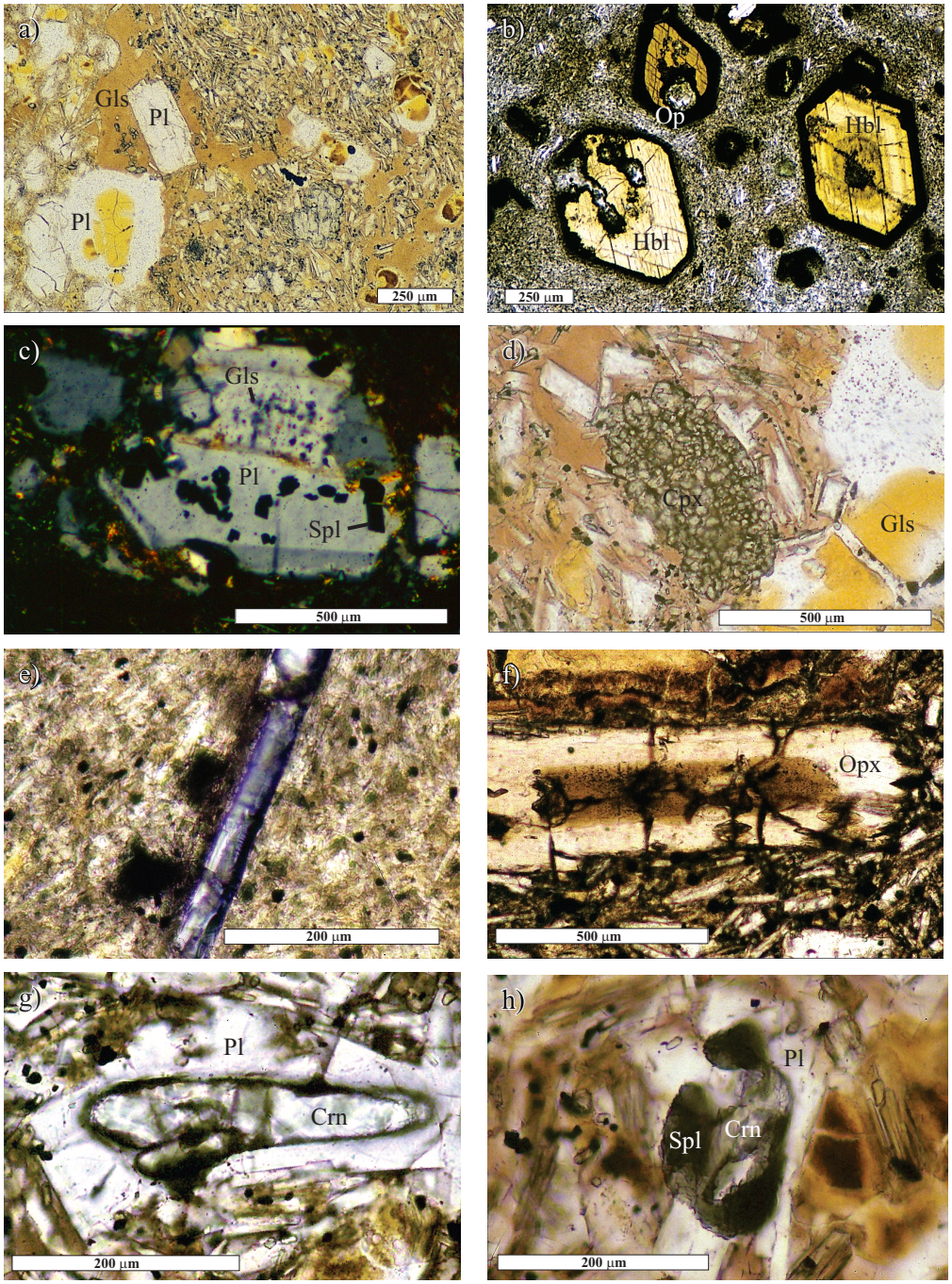

Figure 4. Photomicrographs of: a) abundant glass (Gls) in the andesite matrix, probably derived from melting of the adjacent gneiss xenolith (plane polarized light, PN23a). b) A group of amphibole crystals (Hbl) with sharp opacite (Op) rims set in aphanitic volcanic groundmass (plane polarized light, FO375). c) Sharply zoned plagioclase xenocryst with abundant glass and spinel (Spl) inclusions (crossed nicols, FO375). d) Total replacement of quartz xenocrysts by clinopyroxene (plane polarized light, PN23a). e) Purplish-blue sapphire xenocryst or phenocryst (?) inside the matrix of the andesite (plane polarized light, PN32). f) Sharply zoned orthopyroxene xenocryst displaying intense pleochroism (Al-rich) in the core (green along Z and brown along X), and colorless in the outer rims (Al-poor) (plane polarized light, PN6). g) Colorless corundum enclosed by calcic plagioclase inside the andesitic matrix of PN21 (plane polarized light). h) Corundum rimmed by spinel in the andesitic matrix of PN24 (plane polarized light).

in "glomerocrysts" may show ilmenite inclusions cored by rutile (PN 22), whereas secondary clinopyroxene rimming or completely replacing quartz xenocrysts forms clusters up to 1.2 cm in size (Figure 4d). Clinopyroxene also is found in the gabbroic coronas of amphibole, and as polycrystalline euhedral grains rimming glass patches. Xenocrysts of orthopyroxene may show opacitic reaction rims and ductile deformation revealed by wavy extinction and mechanical twinning. "Glomerocrysts" are common in most thin sections studied; they consist of all possible combinations

of plagioclase, pyroxene, hornblende, and rare biotite, thus ranging in petrographic composition from gabbroic, anorthositic and pyroxenitic to hornblenditic; the textural arrangement and euhedral aspect of the composing minerals indicate a cumulitic origin. Decompression affected these inclusions because most show reaction coronas against the volcanic matrix. Rare clusters of plagioclase-apatite, apatite-Fe/Ti oxide-zircon, and plagioclase-spinel were also observed. When present, glass is abundant (up to 60% of the thin section), brown in color, and usually associated with quartzose xenoliths indicating local anatectic derivation.

Wall-rock Paleozoic gneiss

The Paleozoic gneiss next to the intrusion remained essentially unaffected, suggesting quick cooling of the intrusion, although meter-sized mylonitic rafts of the gneiss inside the intrusion (FO11679, PN 9, FO6605) were substantially melted (≥ 30%) and pervasively reconstituted to the assemblage glass-Qz-Trd-Opx-Pl-TiMag-Hem-Rt-Zrn. In these rocks, which are interpreted as buchites according to the definition of Grapes (2006, p. 2): "…glassy, pyrometamorphic rock with partial to total melting", feldspar acquired a mottled appearance and it is composed of symplectitic intergrowths of altered brown glass and ternary feldspar. These pseudomorphs and isolated plagioclase grains are always separated from the quartz/tridymite groundmass by a wide rim of colorless glass, indicating dry melting of feldspar in the presence of quartz or tridymite. Amphibole was pseudomorphosed by composite aggregates of orthopyroxene, clinopyroxene, Fe/Ti oxides, and possibly calcic plagioclase (sausuritized); epidote appears replaced by fine aggregates of plagioclase-titanomagnetite, whereas most quartz and rarely tridymite in contact with glass were mantled by prismatic to acicular crystals (10–20 μm) of orthopyroxene or clinopyroxene. Other pseudomorphs formed during contact metamorphism in the gneiss consist of tiny titanomagnetite grains associated with broad zones of glass and acicular clinopyroxene. These xenolithic rafts occasionally preserved unaltered vestiges of the original gneiss minerals such as chlorite, epidote, zircon, titanite, and garnet.

Gabbroic (PN2, PN3, PN20, PN26, PN41) and ultramafic xenoliths (PN4, PN5)

Most xenoliths in the Puento Negro intrusion are of gabbroic composition. Texturally and mineralogically, they may be classified as plutonic and hypabyssal rocks, with the latter forming fine to coarse-grained amphibole-plagioclase ± clinopyroxene ± glass porphyries and a marked idiomorphic texture consisting of amphibole crystals up to several centimeters long set in a feldspathic, fine-grained hypocrystalline groundmass. In thin section, amphibole shows exsolution of ilmenite in bands and irregular zones; it defines short prismatic to quenched skeletal or arborescent shapes dispersed in a matrix of smaller grains composed of three types of plagioclase: (a) sieve-textured, (b) hollow, and (c) microlitic, all inside large patches of altered glass, chalcedony and calcite. Isolated prisms of clinopyroxene, rare orthopyroxene, dark red rutile, and needles of apatite probably were derived from the total dehydration of amphibole, which more commonly remained mantled by Cpx-Pl-Fe/Ti oxides, except when isolated inside plagioclase. The anhydrous assemblage Opx + Kfs + Fe/Ti oxides replaced biotite developed from the breakdown of amphibole. In extreme cases (*e.g.*, FO7405) the originally hydrated, hornblende-rich xenoliths were almost completely dehydrated to the pseudomorphic assemblage Pl-Cpx-Opx-TiMag ± Bt ± glass, and in one case to a fine aggregate very rich in spinel, but retaining in some cases (hypabyssal samples) the intersertal, formerly hornblende-rich matrix texture of the original rock. Deuteric CO_2 and H_2O-rich fluids often caused a strong alteration of the quenched matrix to carbonates and clays.

Although rare, small ultramafic xenoliths are present in the Puente Negro intrusion. Two samples examined in thin section have the primary modal assemblage Opx (60-80%)-Cpx (7%)-Hbl (10-30%)-glass (<5%)-Pl (<5%)-Hc (<1%), in which most amphibole was partly dehydrated to Pl-glass, or recrystallized to Cpx-Pl-Bt-opaque aggregates. Orthopyroxene shows ragged grain boundaries and commonly is weakly altered to chlorite; it shows faint pleochroism in contrast to the strongly pleochroic orthopyroxene associated with glass in metamorphic xenoliths and xenocrysts within the andesite. Some grains contain inclusions of clinopyroxene and rounded prisms or blebs of Fe-Ti oxides. Amphibole is strongly pleochroic with brown, yellow and reddish shades. It may show inclusions of ilmenite/rutile, clinopyroxene, and orthopyroxene. Clinopyroxene occurs in minor quantities as small, subhedral to anhedral inclusions in orthopyroxene, and as twinned crystals in the ultramafic assemblage. Clinopyroxene crystallized first because it is found as inclusions within orthopyroxene and amphibole. Rare crystals of olive green spinel occur in contact with clinopyroxene and may be an early magmatic phase. Most glassy matrix was devitrified to spherulitic smectite, enclosing acicular plagioclase. A cumulate origin for these xenoliths is inferred from the euhedral arrangement of mafic phases touching each other in a quenched plagioclase-glass (altered) minor groundmass, which demonstrates very rapid cooling after entrainment because some of the glass remained fresh inside sieve plagioclase.

Quartzose gneiss and quartzite xenoliths

Xenoliths of this type (*e.g.*, PN0, PN1, PN9, PN14, PN19, PN27, FO29698, FO8305, PN605) are dominated by quartz and tridymite (often epitaxially inverted to quartz

paramorphs), accompanied by variable amounts of garnet, plagioclase, orthopyroxene, clinopyroxene, green spinel, Al-silicate$_{ss}$ (aluminum silicates solid solutions, *cf.* Cameron, 1977), corundum, zircon, rutile, hematite, opaque phases, rarely cristobalite, and glass. Quartz, usually mantled by tridymite (Figure 5a), occurs in fine to coarse-grained (0.1–7.5 mm) granoblastic mosaics with abundant curved fractures, commonly enclosing pockets of brown glass with numerous crystals of clinopyroxene or plagioclase. Rare, globular inclusions in quartz formed by Al-orthopyroxene, green spinel and needles of rutile immersed in glass may represent former inclusions of incongruently melted biotite. Other symplectitic pseudomorphs in these xenoliths consisting of Ilm-Rt-Spl ± Zrn, Rt-Ilm, Opx-Spl-glass, Pl-Opx-TiMag-Crn-glass, and Opx-Spl-Pl, may represent, respectively, pseudomorphs after armalcolite, ferropseudobrookite, biotite, amphibole, and garnet, but no vestiges of these phases, with the exception of garnet, were preserved. Zircon probably was exsolved from high temperature rutile because it is very often a companion phase of rutile-ilmenite aggregates in the quartzose matrix.

Almost pure quartzite xenoliths display a granoblastic texture with quartz grains defined by curved broad contacts occupied by colorless glass, plagioclase, clinopyroxene and tridymite, which commonly merge into tridymitite or pockets of quenched magma (brown glass + plagioclase laths). In addition to quartz and tridymite, quartzites include small amounts of strongly pleochroic orthopyroxene (brown to pale orange with occasional inclusions of green spinel and corundum) coexisting with plagioclase, Al-silicate$_{ss}$, titanomagnetite, rutile, and brown glass. This orthopyroxene sometimes reacted with intergranular anatectic melts (glass) acquiring narrow mantles of clinopyroxene. Elsewhere, orthopyroxene defines slender to stubby pleochroic euhedral crystals up to 250 μm long that are embedded in glass (Figure 5b), and it is also present as polycrystalline pseudomorphs and coronas replacing garnet. It has a marked pleochroism in shades of green, yellow-brown and brown, and is commonly accompanied by rounded grains or rhombs of green spinel. Multiple microlites of plagioclase and tridymite (quartz paramorphs) nucleated at right angle to most quartz grain margins or in quenched pockets, although plagioclase also occurs in symplectitic aggregates with spinel, Al-silicate$_{ss}$, and orthopyroxene. Microprobe analyses (see below) and optical properties of plagioclase indicate a bytownite composition. Glass, occasionally associated with clinopyroxene, forms an intergranular matrix enclosing most quartz grains. Garnet is found as fractured, colorless porphyroblasts up to 8 mm across mantled by polycrystalline coronas with abundant symplectites of spinel and plagioclase in a matrix of orthopyroxene, plagioclase and glass. Absence of cordierite in these coronas indicates an original calcium-rich garnet source. Some of the largest garnet crystals were rotated in the foliated matrix of the original metamorphic rock, whereas small crystals are completely altered to a spinel, orthopyroxene, plagioclase and glass aggregate. Zircon occurs inside glass as rounded to subhedral stubby grains up to 170 μm, commonly with euhedral overgrowths and granular aggregates possibly related to thermal recrystallization and neocrystallization.

Other types of quartzose xenoliths (PN9) show lens-shaped foliated domains of Qz/Trd-Zrn-Rt-opaque-glass alternating with the assemblages Opx-glass, Pl-glass, and Opx-Pl-glass that probably represent incongruently melted biotite or garnet. Thus, many of the "quartzite" xenoliths may be restites after strong melting of original quartz-biotite-plagioclase-garnet gneisses. Other zones in the quartzites show the assemblage Pl-Spl-Al silicate$_{ss}$-Opx-Trd/Qz-glass-opaque. Tridymite, mostly inverted to quartz, forms thin rinds about all original quartz grains, whereas dark green, dark brownish green, or opaque spinel occurs in squared and rhombic shapes always associated with orthopyroxene, glass and Al-silicate$_{ss}$. Orthopyroxene also occurs as stubby, distinctly pleochroic prismatic crystals within patches of dark brown glass containing a few long needles of Al-silicate$_{ss}$.

Metapelitic gneiss xenoliths

The extremely aluminous assemblages Pl-Sil-Spl-Crn-St, and Spl-Crn-Mul/Sil (Al-silicate$_{ss}$) were noticed in only one xenolith (FO8305), with staurolite and sillimanite partly replaced by spinel or corundum. Commonly, corundum and sillimanite are mantled by green spinel, suggesting the high-temperature reducing reactions Mag + 3Crn = 3Hc + ½O_2, and Mag + 3Sil = 3Hc + 3Trd + ½O_2, whereas coronas of Spl-Qz-Opx around relict garnets and fine aggregates of Al-silicate$_{ss}$, Opx, Qz, and Spl indicate decompression of the xenoliths at ultrahigh temperature by the reactions Grt = 2Opx + Spl + Qz, and Spl + 2Qz = Al-silicate$_{ss}$ + Opx.

Some of these xenoliths are garnet-rich and show granoblastic textures typical of granulites (Figure 3f) with finely banded structure. Their high-temperature assemblages include Opx-Al-silicate$_{ss}$-Pl-Spl-Rt-Zrn-Fe/Ti oxides (FO29678), and Grt-Pl-Spl-Qz-Opx-Zrn-glass (PN5, PN17), where relict garnets form porphyroblasts up to 7 mm in size. Garnet displays clean, unfractured cores surrounded by a thick fractured zone that in turn is mantled by coronas of Opx-Spl-Pl, or Pl-Crn-Mag (see Figures 5c-5d). The close spatial association of spinel, glass, and orthopyroxene in both matrix and coronas around garnet may be ascribed to garnet breakdown during xenolith ascent in the magma by the reaction 4Grt + Qz + ½O_2 = 5Opx + 4An + Mag, implying in this case an increase in the activity of oxygen. Calcium-rich plagioclase enclosing euhedral orthopyroxene and spinel forms discontinuous anorthositic bands; orthopyroxene is strongly pleochroic in shades of green, yellow or brown. Most of these xenoliths also show coronas of Al-Opx about spinel in contact with plagioclase probably originated by the reaction Spl + Pl = Opx + melt

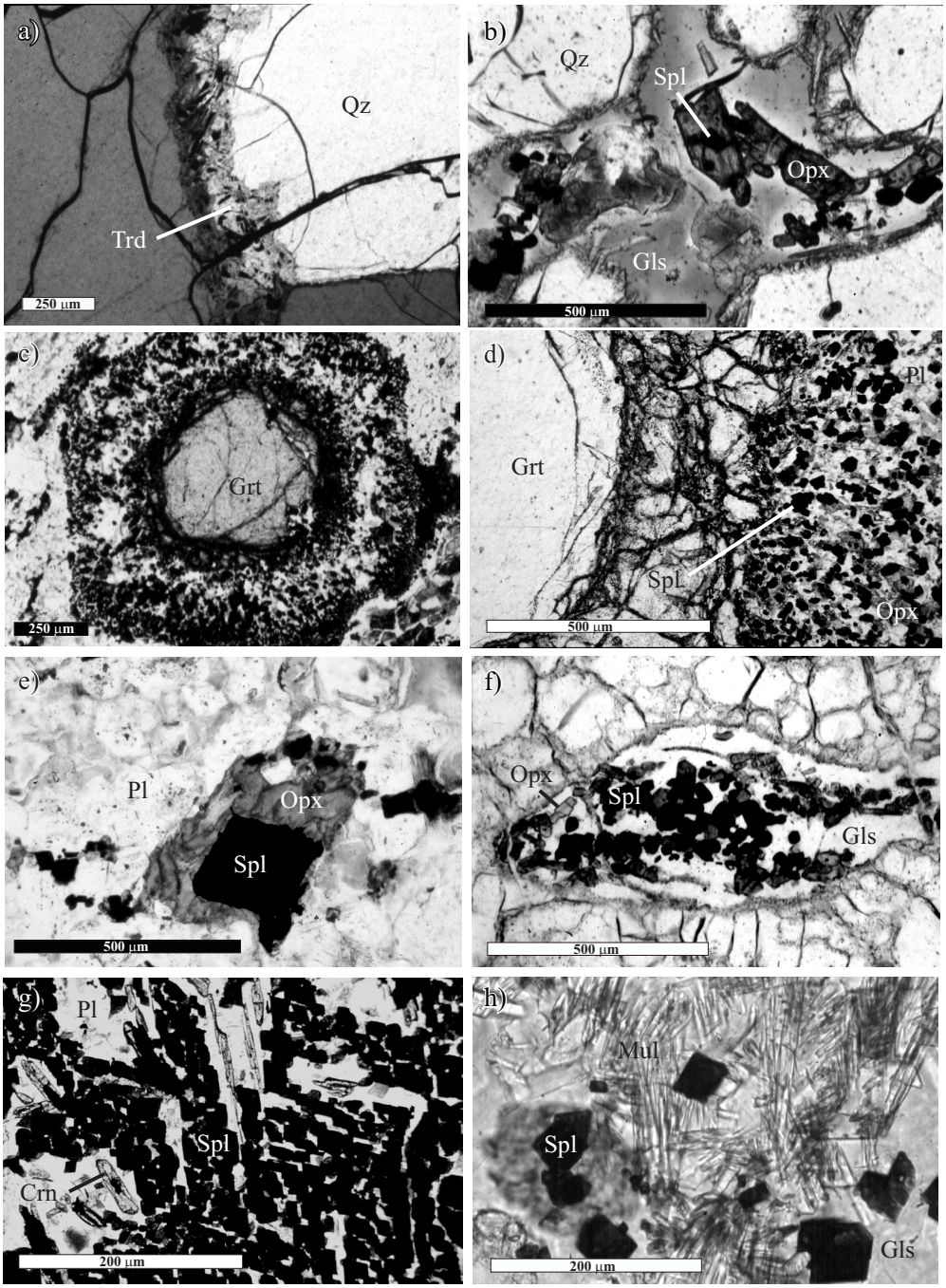

Figure 5. Photomicrographs of: a) Fractured quartz rimmed by former high tridymite (Trd) laths (crossed nicols, FO7405). b) High-Al orthopyroxene (Opx) (dark gray, plane polarized light) with inclusions of spinel (black) in a matrix of glass (gray, Gls) and quartz (white) (PN1). c) Multiple decompression coronas of Spl-Pl-Opx-Crn-glass around a garnet porphyroblast set in a plagioclase-rich foliated matrix (plane polarized light, PN29). d) Detail of the decompressional corona shown in c) (plane polarized light). e) Al-Opx rims around spinel in contact with plagioclase in garnetiferous gneiss xenolith (plane polarized light, PN29a). f) Pseudomorph after biotite (?) melted incongruently to the assemblage Opx-Spl-glass (plane polarized light). g) Pseudomorph of spinel (black), plagioclase (white) and corundum (gray) probably after sapphirine or staurolite (crossed nicols, PN32). h) Spinel-mullite-glass assemblage probably formed by the incongruent melting of an aluminous silicate (plane polarized light, FO29988).

(Figure 5e). The reaction MgTs Opx (tschermackitic Opx) = Spl + Trd was also texturally observed (PN23b), indicating decompression and very high temperatures. Additional pseudomorphic aggregates include symplectites of titanomagnetite and glass (PN17) probably after biotite, and of Al-silicate$_{ss}$-Crd?-Spl, interpreted as former sapphirine. Euhedral, primary anhydrite crystals and strontian barite were also found together with zircon, whereas opaque minerals include titanomagnetite and ilmenite, which were used for geothermometry (see below). Other poorly

defined bands composed of garnet-plagioclase-orthopyroxene, plagioclase-hercynite-biotite-corundum (mantled by hercynite), and orthopyroxene-plagioclase-glass zones are present in some of these xenoliths (PN18a). A small xenolith immersed in the andesite (PN23) shows all the stages of garnet breakdown to the ultimate pseudomorphic assemblages Spl-Pl, Spl-Pl-Crn, and Spl-Pl-Opx that preserved the former external shape of garnet porphyroblasts and remnants of the original mineral. The differences in mineralogy may be ascribed to differential reaction of garnets with the metamorphic matrix enclosing the garnet consisting of Pl-Spl-Opx-Crn-TiMag-Cpx-glass. Orthopyroxene and corundum, although not in direct contact, coexist within a distance of tens of microns, and are probably related to the decompression reaction Spl + Qz_{melt} = Opx + Crn.

Quartzo-feldspathic gneiss xenoliths

Granitic gneiss xenoliths up to 10 cm across are coarse-grained and have a well developed banded structure with alternating mafic and felsic domains and abundant glass (Figure 3c). One of these gneisses examined in thin section (PN24) showed a foliated texture of intermediate grain size formed by the assemblage Trd/Qz-Opx-Pl-glass-opaque-Zrn. Quartz, with occasional inclusions of rutile and zircon, forms polycrystalline ribbons typical of quartzo-feldspathic granulitic gneisses. All crystals of quartz in contact with glass show a reaction corona formed by tiny laths of plagioclase and tridymite. Occasionally, orthopyroxene rimmed by tridymite occurs as inclusions inside quartz. Several pseudomorphic aggregates composed of Opx-Spl-glass, Pl-glass, or Opx-Crd?-Spl-opaque suggest the total breakdown or partial melting of phases such as biotite, amphibole, plagioclase, and probably garnet in the original gneiss. Complex dendritic, micrographic and symplectitic intergrowths of sanidine and quartz/tridymite were observed, indicating partial melting with rapid crystallization. Most importantly, sample FO7505 contains possible relicts of the ultrahigh-temperature, deep-seated association Opx-Sil, albeit these phases were not observed in direct contact.

Glass of these xenoliths occurs in a matrix traversed by acicular plagioclase and rare orthopyroxene, and as distinct patches with large, euhedral prisms of orthopyroxene forming an intersertal texture within the glass. The first type of glass is dark brown, whereas the second type is of a lighter color. A considerable proportion of both glasses was altered to radial clay aggregates.

Calcsilicate xenoliths

Xenolith PN42 **(**Figure 3d) shows in thin section a roughly banded structure with the composite high-T assemblage Cpx-Pl-Trd/Qz-Mw(?)-Ttn-Ilm-Zrn-Ap-glass. Almost pure quartzite bands are in contact with the andesitic magma, followed inside the xenolith by another band of Cpx-glass, and its core is composed of calcic plagioclase and clinopyroxene accompanied by a phase optically resembling merwinite. Most quartz is rimmed by tridymite, and ilmenite by titanite, which may also form symplectitic aggregates with clinopyroxene cores. Primary carbonate is coarse-grained and has straight contacts against plagioclase, glass and clinopyroxene, but it may be secondary, because it is also present as patches in the andesite hosting the xenolith. Clinopyroxene is commonly color-zoned, with brown cores and green rims; it displays a poikiloblastic texture enclosing numerous grains of plagioclase and glass, suggesting the breakdown of hornblende in the presence of quartz and calcite. Titanite forms mantles around ilmenite, whereas "merwinite" is abundant in patches as polycrystalline, rounded to euhedral grains in textural equilibrium with tridymite, bytownite, and glass. Some feldspar (plagioclase or sanidine) shows complex micrographic intergrowths with glass. Pyrrhotite is quite abundant, indicating reducing conditions during high temperature crystallization. This xenolith is considered positive evidence for a non-local source of many of the Puente Negro xenoliths because calcsilicate-quartzite banded rocks are not present in the underlying or exposed Acatlán Complex.

Xenocrysts and xenolithic polycrystalline pseudomorphs

In outcrop, the main xenocrysts found in the Puente Negro dike are amphibole, quartz, and red garnet. In thin section, additional small xenocrysts of colorless and purplish-blue corundum (sapphire) (Figure 4e), green spinel, rutile, zoned Al-orthopyroxene (Figure 4f), ilmenite, and zircon, as well as polycrystalline pseudomorphs probably after biotite (Figure 5f), and highly aluminous aggregates of spinel, corundum and $Al\text{-}silicate_{ss}$ were discovered. Quartz commonly forms oval xenocrysts with complete or incomplete coronas of clinopyroxene, although many crystals and quartzite fragments did not react with the andesitic matrix, while others were completely replaced by clinopyroxene. Orthopyroxene xenocrysts are distinguished by their intense pleochroism (Z = brown, X = green) in grains up to 250 μm mantled by colorless hypersthene overgrowths. All garnets show kelyphitic rims 50 to 500 μm wide consisting of spinel, plagioclase, orthopyroxene, and minor corundum or glass. Garnets yield low Mg and high Mn contents, with a calcium-rich fractured zone mantling Ca-poor, unfractured cores. Most importantly, andesite samples PN43, PN32, PN24, and PN16 contain oval pseudomorphic xenocrysts up to 1 cm in size consisting of Spl-Pl-Crn ± Opx ± Rt ± Bt (Figure 5g) with modal abundances of spinel (20–70%), plagioclase (20–65%) and corundum (10–30%). These minerals and their relative proportions are remarkably similar to metasomatized orthogneissic

and paragneissic xenoliths in the Voisey's Bay troctolitic intrusion of Labrador, Canada (Mariga *et al*., 2006a) and in principle could have a comparable origin at depth before entrainment in the andesite, as discussed later. Euhedral calcic labradorite (An_{65}) mantles the pseudomorphs in contact with the enclosing volcanic matrix. Abundance of spinel and corundum suggests that some pseudomorphs probably formed after calcium-rich garnet; other aluminous phases such as sapphirine, staurolite, pargasite, or metasomatized anorthite are considered less likely precursor minerals. Additional highly aluminous pseudomorphs found (FO29698) show symplectites of Al-silicate$_{ss}$-Crd?-Spl, and Al-silicate$_{ss}$-Spl-Crn-Pl. Staurolite was found coring one of the corundum-bearing pseudomorphs (FO7505) formed by about 50–65% spinel, 20–40% plagioclase, 0–10% corundum, and 5–10% staurolite. Indeed, probably the most important petrogenetic features found in the Puente Negro andesite are the common presence of subhedral crystals of corundum mantled by plagioclase (Figure 4g) or spinel (Figure 4h), and a xenocryst of purplish-blue sapphire about 300 μm long isolated in the volcanic groundmass of sample PN32 (see Figure 4e); this type of sapphire in volcanic rocks may be unique because of its very small size and association with calc-alkaline magmatism, as opposed to the megacrystic, gem-quality sapphires described from several alkali (extensional) basaltic or syenitic fields of the world (Guo *et al.*, 1996; Sutherland *et al.*, 1998; Garnier *et al.*, 2005). The sapphire xenocryst was identified by its specific optical properties (uniaxial negative, negative elongation, straight extinction, extreme relief, and characteristic pleochroism (pale green along ε and deep purplish-blue along ω), and also confirmed by microprobe analysis (see below).

AGE OF PUENTE NEGRO INTRUSION

The isolated character of the Puente Negro dike, intruded only into Paleozoic metamorphic rocks lacking a younger cover, prompted the need to better constrain its age by isotopic methods. Because the intrusion and its igneous xenoliths are rich in fresh hornblende, this mineral, together with the volcanic matrix were the materials chosen to date the magmatic event.

Analytical methods and results

Samples PN10, PN22 and PN44 were crushed with a steel jaw and sieved at 180–250 μm. After cleaning in ultrasonic bath, both amphibole and matrix were separated using a Frantz magnetic separator. The concentrates were cleaned, dried and split in two parts, one for K determination and the other for Ar measurement. K for the matrix sample was obtained following the method of Solé and Enrique (2001). Briefly, 100 mg of sample were fused with 50% lithium metaborate + 50% lithium tetraborate. The fused pearl was measured with a Siemens 3000 XRF spectrometer calibrated against several international standards prepared in the same way. Results were accurate to 1% (1σ) or better. Potassium from amphiboles has been measured by ID-TIMS, because measurements by XRF were not reproducible. Results from ID-TIMS are accurate to 1% (1σ) or better.

Argon was measured by isotope dilution (^{38}Ar tracer) with a MM1200B noble gas mass spectrometer operated in static mode. Between 8 and 22 mg of sample were fused with a 50 W infrared CO_2 laser in a UHV chamber. After fusion, evolving gases were purified with a cold finger and two SAES getters, one operated at 400ºC and the other at room temperature. Eight series of measurements of each mass were made sequentially and extrapolated to gas inlet time. The signal was acquired with a secondary electron multiplier. Variation coefficients for ^{40}Ar and ^{38}Ar are generally below 0.1% and below 0.5% for ^{36}Ar. All analyses were made at the Instituto de Geología, UNAM. The constants recommended by Steiger and Jäger (1977) were used throughout. The obtained ages are shown in Table 2. The weighted mean age of amphibole is 30.5 ± 0.6 Ma, which is about 1 Ma older than the age of volcanic matrix, dated at 29.2 ± 0.3 Ma. Thus, it is possible to assume that the amphibole and hence the gabbroic source may be somewhat older than the andesite. In conclusion, we assign an age of 29.2 ± 0.3 Ma (Oligocene, Rupelian) to the Puente Negro intrusive event, which is part of the extensive magmatism that formed the Sierra Madre del Sur volcanic province in the Mixteca region of southern Mexico (Morán-Zenteno *et al.*, 2000), but is older than the earliest magmatism associated with the Trans-Mexican Volcanic Belt considered to be at around 19 Ma (Gómez-Tuena *et al.*, 2005). The common presence of andesitic dikes throughout the Mixteco terrane where the Paleogene volcanic rocks have been eroded suggests that these dikes are feeders of the Oligocene volcanic province.

Table 2. Analytical data for K-Ar measurements. Mean data for amphiboles and matrix have been calculated using a weighted mean and a weighted standard deviation. A minimum of 1% uncertainty has been applied to the standard deviation.

Analysis number	Sample	K %	^{40}Ar* moles/g	^{40}Ar* %	Age Ma (± 1σ)
Amphiboles					
712	PN-10	0.480	$2.540 \cdot 10^{-11}$	70.5	30.3 ± 0.8
889	PN-22	0.507	$2.778 \cdot 10^{-11}$	58.8	31.3 ± 1.8
892	”	”	$2.716 \cdot 10^{-11}$	64.2	30.6 ± 1.5
1380	PN-44	0.465	$2.486 \cdot 10^{-11}$	40.5	30.6 ± 1.8
				Mean	**30.5 ± 0.6**
Matrix					
1321	PN-44	1.32	$6.732 \cdot 10^{-11}$	78.4	29.2 ± 0.8
1375	”	”	$6.753 \cdot 10^{-11}$	76.8	29.3 ± 0.9
				Mean	**29.2 ± 0.3**

CHEMISTRY AND PETROLOGY OF THE PUENTE NEGRO INTRUSION AND ITS METAMORPHIC AND IGNEOUS XENOLITHS

Whole rock chemistry

Major whole rock element chemical analyses of eight representative samples performed on the andesitic intrusion (three analyses), four xenoliths and the intruded gneiss (PN39W) are shown in Table 3. Although the silica content and bulk composition of the dikes are typical of andesite (Gill, 1981; Le Bas *et al.*, 1986), the average normative labradorite (An_{52}), and relatively high TiO_2 content correspond more with an original basaltic composition considering that small but common quartz xenocrysts (estimated at *ca*. 2% modal for <500 μm grains), only evident in thin section, could not be all eliminated from the analyzed rocks, thus rising their bulk silica. Metamorphic xenoliths studied are mainly quartzose gneisses (*e.g.*, PN1, PN19), a high-Al metapelite (PN17), and a buchite (FO6605). Note the close chemical correspondence between the buchite and the country gneiss (PN39W), indicating a local source for this xenolith. The quartzitic xenolith (PN1) yields 83.91 wt. % normative quartz and 1 wt. % corundum. The excess alumina is probably fixed in modal Al-orthopyroxene and spinel, whereas sodium and calcium are fixed in plagioclase ($Ab_{67}An_{33}$). PN17 is a fine-grained garnetiferous gneiss with 4 wt. % normative corundum, very low quartz (1 wt. %), very high feldspar (70 wt. %), and high zirconium (356 ppm), possibly reflecting a sedimentary, somewhat desilicated protolith. PN4, the only ultramafic xenolith analyzed, shows (CIPW norm) 55 wt. % of hypersthene, 17 wt. % quartz, and about 24 wt. % plagioclase ($Ab_{32}An_{68}$). It apparently represents cumulate assemblages in a magma chamber differentiated at high water pressure. The high silica content of the ultramafic xenolith may be due to late-stage hydrothermal silicification (chalcedony). Major elements of three xenoliths were analyzed by ICP-OES and trace elements by ICP-MS in the laboratories at the Centre de Recherches Pétrographiques et Géochimiques of the Centre National de la Recherche Scientifique in Nancy, France. Major and trace elements of one xenolith (FO6605) were carried out by X-ray fluorescence at the Instituto de Geología, UNAM , using procedures described in Lozano and Bernal (2005). Major and trace elements of the intrusive rocks and intruded gneiss were carried out using different methods at the Instituto de Geología, UNAM (see Table 3). Isotope determinations were measured by thermal ionization mass spectrometry at LUGIS (Laboratorio Universitario de Geoquìmica Isotópica) at the National University of Mexico using a Finnigan MAT 262 system, following the procedures outlined in Schaaf *et al.* (2005).

Mineral chemistry

Chemical microanalyses of major elements in igneous and metamorphic minerals and glasses were made by WDS and complementary EDS electron probe at the petrologic laboratories of the Instituto de Geología and Instituto de Geofísica, both at the National University of Mexico, using a Jeol JXA 8900R superprobe, and a Jeol C35 SEM, respectively. For WDS, a beam current of 10–20 nA and accelerating voltage of 15–20 kV were used, with counting times of 20 to 40 seconds and a focused beam (1 μm), except for the glasses, in which case the counting time was lowered to 10 seconds and the beam defocused to 5 μm. Natural minerals (albite, diopside, kaersutite, jadeite, sanidine, obsidian, apatite, quartz, pyrope, almandine, plagioclase, and Cr-diopside), as well as synthetic products (rutile, chromium oxide, and ilmenite) were used as standards. Corrections were made using the ZAF software provided by Jeol.

Puente Negro intrusion and related gabbroic and ultramafic xenoliths

Microprobe chemical analyses of selected phases composing the Puente Negro andesite and an ultramafic igneous xenolith are shown in Tables 4 and 5, respectively.

Pyroxenes. Various kinds and compositions of igneous orthopyroxene are present in the Puente Negro andesite but were not systematically analyzed: (a) Colorless to distinctly pleochroic phenocrysts up to 1.4 mm, (b) colorless microphenocrysts and microlites in the andesitic groundmass, and (c) in "glomerocrysts". Orthopyroxene forms the main phase in the hornblende pyroxenite xenolith. All orthopyroxenes fall near the enstatite-ferrosilite base of the pyroxene quadrilateral, with Mg# numbers [100*Mg/(Mg+Fe)] up to 77 in the ultramafic xenolith and 78 in the matrix, but note that the Al_2O_3 content of the orthopyroxene in the andesite matrix (3.89 wt. %) is higher than that of the ultramafic xenolith (average of 2.22 wt. %), but both contain much less alumina than those in the metamorphic xenoliths. Zoning towards a more ferrosilitic margin is shown by the core-to-rim traverse across the ultramafic orthopyroxene (see Table 5). Clinopyroxene of the ultramafic xenolith falls in the ferroaugite field (av. $En_{42.7}Wo_{42.7}Fs_{10.4}$), but is rare in the andesite groundmass and absent as phenocrysts; it is common in "glomerocrysts" together with abundant amphibole, plagioclase, and orthopyroxene and also as partial to complete replacement of quartz xenocrysts. Note also that clinopyroxene in the ultramafic xenolith shows a relatively high content of alumina and chromium and the same tendency as orthopyroxene to slight iron enrichment from core to rim.

Amphibole. Amphibole xenocrysts are abundant in the andesite (2–20% of thin section area) and it is a characteristic phase in gabbroic and ultramafic (pyroxenites) igneous xenoliths, but it is completely absent in the metamorphic xenoliths. Table 4 shows selected amphibole analyses from the andesite, and Table 5 from the ultramafic xenolith. All amphiboles, gabbroic and xenocrystic, are pargasites with Mg# varying from 59 to 77 and moderate

contents of TiO_2 that are slightly higher in the xenocrysts (up to 2.39 wt. %). Aluminum is quite variable in the xenocrysts (10.49–14.33 Al_2O_3 wt. %), probably reflecting the polybaric differentiation and contamination of the andesite, and is quite uniform (11.56–12.47 Al_2O_3 wt. %) in the ultramafic xenolith (PN4). Sodium is moderate in the gabbroic amphiboles (av. 2.21 wt. %), but much higher in xenocrysts of the andesite (av. 4.23 wt. %). The MgO/FeO ratio is about the same in xenocrysts and ultramafic xenoliths. Amphibole in the latter bears inclusions of titanomagnetite with TiO_2 up to 9.4 wt. %.

Plagioclase. Plagioclase associated with gabbroic xenoliths (Table 5) is calcic to intermediate bytownite (An_{81}–An_{74}), whereas microlitic plagioclase in the andesite (Table 4) yields an average calcic andesine (An_{45}) with minor amounts of iron. Measured plagioclase in the dehydration rims of amphibole xenocrysts of the ultramafic xenolith is close to pure anorthite (An_{97}). EDS analyses performed on plagioclase in the quenched matrix of the ultramafic xenolith show a calcic bytownite composition, but potassium, when analyzed, was always very low.

Glass. Magmatic residual glasses from several andesitic dike samples and glass from a partially melted gabbroic xenolith were analyzed by electron microprobe, with results shown in Table 4 for the andesitic glasses and in Table 5 for the gabbroic xenoliths. Glasses in the andesite yield a rhyolitic composition, with silica contents from 75.5 to 77.6 SiO_2 wt. % and normative corundum up to 5.78 wt. %. Glasses in the coarse gabbroic xenoliths are strongly altered to a clay phase and were not analyzed, but those in the fine-grained quenched types (PN20) show a similar composition to andesite glasses (Table 5) except for their more hydrated state.

High-Al xenocrysts and xenolithic pseudomorphs

Xenocrysts and xenolithic pseudomorphs with high contents of aluminum are characteristic of the Puente Negro andesite inclusions. Spinel and corundum may be found

Table 3. Major and trace element compositions of the intrusive body, xenoliths and local country rocks at Puente Negro.

Sample Rock type	119-79* Andesite	PN15b§ Dacite	PN44§ Andesite	Av. And Andesite	PN1b ◊ Xenolith	PN17 ◊ Xenolith	PN4 ◊ Xenolith	FO6605 ‡ Xenolith	PN39W ‡ Gneiss
Major elements (wt. %)									
SiO_2	56.19	63.00	56.03	57.60	90.43	53.65	58.87	64.48	59.85
TiO_2	1.11	1.00	1.03	0.77	0.13	1.17	0.57	0.53	0.64
Al_2O_3	15.50	15.51	17.26	17.30	3.70	21.39	7.16	15.53	15.44
FeO	4.50			3.10					
Fe_2O_3	3.46	5.13	7.43	4.30	1.22	7.75	8.89	5.26	6.78
MnO	0.11	0.10	0.13	0.15	<d.l.	0.36	0.10	0.13	0.13
MgO	5.61	3.03	4.82	3.60	0.56	3.34	15.14	2.61	4.42
CaO	6.93	6.66	7.47	7.20	0.72	4.78	3.64	3.90	5.02
Na_2O	3.05	2.66	3.08	3.20	0.78	4.79	0.87	3.07	2.46
K_2O	1.50	1.27	1.46	1.50	0.18	1.05	0.13	2.11	0.91
P_2O_5	0.22	0.24	0.25	0.21	0.05	0.11	0.13	0.11	0.13
H_2O+	1.02	1.90	0.96	1.00	2.02	1.52	4.40	2.30	3.52
H_2O-	0.57	n.d.	n.d.	n.d.	n.d.	n.d.	n.d.	n.d.	n.d.
Total	99.77	100.50	99.92	99.93	99.79	99.91	99.90	100.03	99.30
Trace elements (ppm)									
Sc		23.5	26.5						
V		205	229		17	135	212	143	121
Cr		127	111		16	107	442	102	76
Co		24	47		1	14	54	20	24
Ni		74	21		<d.l..	20	64	28	29
Cu		34	29		8	24	68	11	23
Zn		128	242		14	158	171	81	104
Ga					3	23	11		
Be		2.3	2.2		<d.l.	3.2	<d.l.		
Rb		24	40		25	19	6	109	66
Sr		700	784		143	424	422	529	242
Y		21.2	27.3		10.0	46.4	11.2	32	28
Zr		147	165		277	356	65	244	173
Nb		7.2	8.6		2.5	19.2	3.0	14	14
Sn		1.7	1.8		<d.l.	0.53	0.60		

continues

isolated as xenocrysts and within plagioclase, whereas peculiar pseudomorphs (Table 6) probably after garnet or other original phases of unknown nature (sapphirine?) are composed of symplectitic aggregates of spinel, plagioclase, corundum, with some orthopyroxene, Fe/Ti oxides, and minor zircon, biotite, and rare ternary feldspar grains ($Ab_{64.8}Or_{26.8}An_{8.6}$).

Three forms of xenocrystic corundum are found in the Puente Negro andesite: (a) Purplish-blue sapphire xenocrysts, (b) pale-blue to colorless corundum in aluminous pseudomorphs, and (c) colorless corundum inclusions in calcic plagioclase. Table 6 shows analyses of the first two types. Note that sapphire shows a higher iron content than colorless corundum in the pseudomorphs, consistent with its possibly igneous and deeper crystallization (*e.g.*, Garnier *et al.*, 2005). Colorless corundum (not analyzed) in Ca-rich plagioclase, on the other hand, may be the product of magmatic precipitation at high pressure, or of the incongruent melting of plagioclase during magmatic recharge through the reaction NaCa-rich Pl = Crn + CaNa-rich Pl + Na-Si-rich melt (*e.g.*, Mariga *et al.*, 2006b). Spinel in the pseudomorphs (Table 6) is hercynite with an average Mg# of 27, and the associated symplectitic plagioclase is bytownite ($An_{69}Ab_{28}Or_3$). Spinel also exists in other forms (not analyzed) within the andesite as: (a) somewhat corroded euhedral green crystals, (b) dark green subhedral xenocrysts isolated in the volcanic matrix,

Table 3 (continued). Major and trace element compositions of the intrusive body, xenoliths and local country rocks at Puente Negro.

Sample **Rock type**	**119-79*** **Andesite**	**PN15b§** **Dacite**	**PN44§** **Andesite**	**Av. And** **Andesite**	**PN1b ◊** **Xenolith**	**PN17 ◊** **Xenolith**	**PN4 ◊** **Xenolith**	**FO6605 ‡** **Xenolith**	**PN39W ‡** **Gneiss**
Trace elements (ppm)									
Sb		0.25	0.52		<d.l.	0.46	0.76		
Cs		2.06	0.74		7.61	1.57	3.62		
Ba		393	384		68	423	132	630	654
La		19.89	20.22		8.82	65.10	6.80		
Ce		46.01	44.00		17.75	131.52	15.59		
Pr		5.55	5.80		2.21	15.65	2.27		
Nd		23.89	25.73		7.77	59.38	9.84		
Sm		5.22	5.72		1.49	10.53	2.25		
Eu		1.38	1.60		0.43	2.46	0.56		
Gd		4.80	5.33		1.36	8.51	2.17		
Tb		0.75	0.85		0.24	1.28	0.33		
Dy		3.86	4.60		1.50	8.30	2.11		
Ho		0.76	0.94		0.33	1.72	0.38		
Er		2.14	2.62		1.03	5.01	1.12		
Tm		0.276	0.378		0.15	0.81	0.16		
Yb		2.00	2.57		0.98	5.87	1.15		
Lu		0.30	0.40		0.15	0.92	0.17		
Hf		3.91	4.17		6.54	9.28	1.82		
Ta		0.21	0.49		0.22	1.34	0.24		
W					0.303	2.032	0.772		
Pb		11.1	21.9		6.7	30.5	21.6	16	27
Th		5.21	4.68		2.18	17.50	1.91	8	12
U		1.371	0.950		0.660	3.983	0.569		
CIPW Norm									
Q	10.46	22.28	5.94	12.48	83.91	0.94	17.43	23.03	20.66
Or	9.04	7.62	8.75	8.98	1.06	6.32	0.83	12.76	5.61
Ab	26.32	22.85	26.32	27.33	6.77	41.21	7.70	26.57	21.75
An	24.61	26.99	29.26	28.73	3.35	23.39	15.97	19.08	25.08
C	-	-	-	-	1.04	4.00	0.00	1.40	1.67
Di	7.17	4.08	5.44	4.86	-	-	1.63	-	-
Hy	14.65	13.69	21.75	11.11	3.50	21.64	55.00	15.88	23.64
Mag	5.10	-	-	4.54	-	n.d.	-	-	-
Il	2.15	1.92	1.98	1.48	0.25	2.26	1.14	1.03	1.27
Ap	0.51	0.56	0.58	0.49	0.12	0.26	0.32	0.26	0.32

Major elements are in wt. % and trace elements in ppm. PN1b: quartzitic gneiss; PN17: garnetiferous gneiss; PN4: amphibole orthopyroxenite; FO6605: buchitic xenolith; PN39W: adjacent country rock. * Wet chemical analysis; § major elements, Cr, Co, Ni by XRF, and remaining trace elements by ICP-MS; ◊ major elements and Sc by ICP emission, trace elements by ICP-MS; ‡ XRF. d.l.: detection limit; n.d.: not determined. Average andesite after Gill (1981).

Table 4. Electron microprobe chemical analyses of major phases composing the Puente Negro andesite.

	Plagioclase microlites				Opx	Amphibole xenocrysts									Dehydrated rims on amphibole xenocrysts				Glasses				
															Cpx	Opx	Pl	Ilm					
Oxide wt. %																							Average
SiO_2	56.54	56.33	64.63	64.84	52.80	43.42	43.40	41.10	40.54	41.99	41.02	40.3	41.20	40.8	42.88	51.60	40.89	0.00		75.50	77.10	77.60	76.72
TiO_2	0.02	0.04	0.05	0.05	1.40	2.24	2.01	2.17	2.26	2.14	2.16	2.32	2.23	2.39	1.50	0.60	0.99	48.3		0.30	0.28	0.48	0.35
Al_2O_3	26.00	25.91	22.36	22.33	3.89	10.49	10.68	11.91	11.71	10.91	11.34	13.4	14.33	13.5	1.56	2.92	28.04	0.07		11.6	12.0	11.1	11.58
FeOTotal	0.37	0.43	0.33	0.35	13.36	12.51	8.85	13.55	13.5	9.89	14.06	12.1	12.2	12.8	8.03	19.37	0.26	49.3		1.54	1.59	1.50	1.54
MnO	n.d.	n.d.	n.d.	n.d.	0.54	0.12	0.10	0.09	0.13	0.08	0.03	0.45	0.00	0.54	n.d.	n.d.	n.d.	n.d.		0.00	0.01	0.02	0.01
MgO	0.01	0.03	0.04	0.02	24.84	12.83	14.92	11.93	12.1	14.20	11.50	13.5	13.7	13.9	14.12	22.89	0.00	1.63		0.16	0.18	0.13	0.16
CaO	8.93	9.96	8.69	8.64	1.13	11.31	11.83	11.57	11.6	11.95	11.19	10.9	11.3	11.7	27.50	1.38	27.10	0.00		0.55	0.55	0.62	0.57
Na_2O	6.95	6.67	5.35	5.10	n.d.	3.60	4.21	5.92	6.00	5.97	5.74	2.14	2.22	2.25	0.00	0.00	0.41	0.00		1.75	1.80	1.64	1.73
K_2O	n.d.	n.d.	n.d.	n.d.	n.d.	0.73	0.68	0.66	0.68	0.69	0.73	0.86	0.88	0.74	0.00	n.d.	0.14	0.17		2.59	2.34	2.44	2.46
Total	98.82	99.37	101.45	101.33	97.98	97.25	96.68	98.90	98.45	97.82	97.77	95.96	98.14	98.69	95.59	98.76	97.83	99.41		94.03	95.84	95.50	95.12
Cations	8 Oxygens					23 Oxygens													*CIPW norm*				
Si	2.574	2.56	2.815	2.823	1.93	6.46	6.41	6.13	6.09	6.23	6.20	6.08	6.05	6.01	1.66	1.92	2.01	0.00	Qz	56.3	57.4	59.0	57.57
Ti	0.001	0.001	0.002	0.002	0.04	0.25	0.22	0.24	0.26	0.24	0.25	0.26	0.25	0.26	0.04	0.02	0.04	1.87	C	5.29	5.78	4.81	5.29
Al	1.395	1.387	1.148	1.146	0.17	1.84	1.86	2.09	2.07	1.91	2.02	2.37	2.48	2.35	0.07	0.13	1.63	0.00	Ab	15.7	15.9	14.6	15.40
Fe^{2+}	0.014	0.016	0.012	0.013	0.41	1.56	1.09	1.69	1.69	1.23	1.78	1.53	1.50	1.57	0.26	0.60	0.01	2.13	An	2.88	2.83	3.22	2.98
Mn	n.d.	n.d.	n.d.	n.d.	0.02	0.02	0.01	0.01	0.02	0.01	0.00	0.06	0.00	0.07	0.00	0.00	0.00	0.00	Or	16.3	14.4	15.1	15.25
Mg	0.001	0.002	0.003	0.001	1.35	2.85	3.29	2.65	2.70	3.14	2.59	3.03	3.00	3.06	0.82	1.27	0.00	0.13	Hy	2.91	3.06	2.44	2.80
Ca	0.436	0.485	0.405	0.403	0.04	1.8	1.87	1.85	1.86	1.90	1.81	1.76	1.78	1.85	1.14	0.06	1.43	n.d.	Ilm	0.61	0.55	0.95	0.70
Na	0.613	0.588	0.452	0.43	n.d.	1.04	1.21	1.71	1.75	1.72	1.68	0.63	0.63	0.64	0.00	n.d.	0.04	n.d.					
K	0.000	n.d.	n.d.	n.d.	n.d.	0.14	0.13	0.13	0.13	0.13	0.14	0.17	0.16	0.14	0.00	n.d.	0.01	n.d.					
Total	5.034	5.039	4.836	4.818	3.95	15.96	16.10	16.50	16.56	16.51	16.47	15.87	15.86	15.95	4.00	4.00	5.16	4.13					
An	41.5	49.2	47.3	42.3													97.0						
Mg#					78	64	75	63	61	72	59	66	67	66	76	68		6					

Table 5. Electron microprobe chemical analyses of main phases in the ultramafic xenolith PN4.

	Plagioclase				**Amphibole**								**Clinopyroxene**						**Orthopyroxene**					**Glass**
Oxide wt. %													Core					Rim	Core				Rim	
SiO_2	49.92	49.00	50.61	48.97	42.96	42.09	43.81	43.21	43.03	41.44	41.22	41.28	52.03	51.41	52.95	52.12	52.20	51.98	54.07	54.00	53.91	54.75	52.75	73.00
TiO_2	0.01	0.02	0.01	0.02	1.98	2.07	1.91	2.25	1.95	2.07	2.03	1.98	0.53	0.54	0.30	0.55	0.45	0.49	0.18	0.14	0.15	0.11	0.28	0.27
Al_2O_3	30.65	31.30	30.20	31.29	12.43	12.27	11.63	12.30	11.56	12.46	12.47	12.46	3.25	3.45	2.22	3.24	3.28	3.00	2.61	2.30	2.27	2.06	1.84	10.32
Cr_2O_3	0.00	0.00	0.00	0.00	0.00	0.00	0.04	0.00	0.00	0.00	0.00	0.00	0.96	0.97	0.60	0.82	0.70	0.87	0.08	0.01	0.00	0.02	0.04	n.d.
FeO_{Tot}	0.36	0.12	0.35	0.12	12.99	13.53	9.96	8.06	10.10	13.66	12.91	13.11	5.75	5.99	6.07	6.66	6.39	6.83	14.81	14.80	14.42	14.17	22.01	1.91
MnO	n.d.	n.d.	0.00	0.03	0.14	0.13	0.12	0.09	0.14	0.25	0.16	0.27	0.08	0.14	0.14	0.12	0.11	0.16	0.26	0.20	0.90	0.22	0.37	0.02
MgO	0.03	0.02	0.03	0.02	13.17	12.42	15.33	14.45	14.53	12.09	12.57	12.84	14.64	14.53	14.96	14.51	14.57	14.83	25.55	27.14	26.96	27.16	22.43	0.16
CaO	14.27	15.32	14.34	15.78	11.23	11.21	11.41	11.34	11.47	11.15	11.12	11.22	20.87	20.57	20.95	20.27	19.74	20.05	1.08	0.91	0.93	0.90	1.09	0.83
Na_2O	2.73	1.93	2.73	1.99	2.22	2.13	2.20	2.50	2.19	2.14	2.10	2.18	1.07	0.78	1.11	0.99	1.38	1.29	0.39	0.12	0.19	0.08	0.03	0.27
K_2O	0.21	0.16	0.21	0.16	0.60	0.67	0.61	1.07	0.60	0.67	0.67	0.60	n.d.	n.d.	n.d.	n.d.	n.d.	n.d.	n.d.	n.d.	n.d.	n.d.	n.d.	2.28
Total	98.18	97.87	98.48	98.38	97.72	96.52	97.02	95.27	95.57	95.93	95.25	95.94	99.18	99.38	99.30	99.28	98.82	99.50	99.03	99.62	99.73	99.47	100.84	89.06
Cations	16 Oxygens				23 Oxygens								6 Oxygens						6 Oxygens					*CIPW norm*
Si	2.316	2.281	2.340	2.273	6.332	6.310	6.413	6.405	6.410	6.270	6.260	6.230	1.92	1.92	1.96	1.93	1.94	1.93	1.97	1.95	1.95	1.97	1.95	Qtz 66.59
Ti	0.000	0.001	0.000	0.001	0.219	0.233	0.210	0.251	0.220	0.240	0.230	0.230	0.01	0.02	0.01	0.02	0.01	0.01	0.01	0.00	0.00	0.00	0.01	Or 15.13
Al	1.676	1.717	1.645	1.711	2.159	2.168	2.006	2.149	2.030	2.220	2.230	2.220	0.14	0.15	0.10	0.15	0.14	0.13	0.11	0.10	0.10	0.09	0.08	Ab 2.54
Cr	0.000	0.000	0.000	0.000	0.000	0.000	0.005	0.000	n.d.	n.d.	n.d.	n.d.	0.03	0.03	0.02	0.02	0.02	0.03	0.00	0.00	0.00	0.00	0.00	An 4.61
Fe^{2+}	0.014	0.005	0.014	0.005	1.601	1.696	1.219	0.999	1.260	1.730	1.640	1.650	0.18	0.19	0.19	0.21	0.20	0.21	0.45	0.45	0.44	0.43	0.68	Hy 3.92
Mn	0.000	0.000	0.000	0.001	0.017	0.017	0.015	0.011	0.020	0.030	0.020	0.040	0.03	0.00	0.00	0.00	0.00	0.01	0.01	0.01	0.03	0.01	0.01	C 6.64
Mg	0.002	0.001	0.002	0.001	2.894	2.776	3.345	3.193	3.230	2.730	2.840	2.890	0.81	0.81	0.83	0.80	0.80	0.82	1.39	1.46	1.45	1.46	1.23	Ilm 0.57
Ca	0.709	0.764	0.710	0.785	1.773	1.800	1.789	1.801	1.830	1.810	1.810	1.810	0.83	0.82	0.83	0.81	0.79	0.80	0.04	0.04	0.04	0.04	0.04	
Na	0.246	0.174	0.245	0.179	0.634	0.619	0.624	0.718	0.630	0.630	0.620	0.640	0.08	0.06	0.08	0.07	0.10	0.09	0.03	0.01	0.01	0.01	0.00	
K	0.012	0.009	0.012	0.009	0.113	0.128	0.114	0.202	0.110	0.130	0.130	0.120	n.d.	n.d.	n.d.	n.d.	n.d.	n.d.	n.d.	n.d.	n.d.	n.d	n.d.	
Total	4.975	4.952	4.967	4.965	15.743	15.747	15.741	15.729	15.740	15.790	15.780	15.830	4.03	4.00	4.02	4.01	4.00	4.03	4.00	4.01	4.02	3.99	4.00	
An	75	81	74	81									72	71	71	68	70	68	75	77	77	77	65	
Mg#					64	62	73	77	72	61	64	64												
En													42.69	43.03	42.83	42.47	42.62	42.60	72.36	74.65	73.95	75.70	62.67	
Fs													9.34	10.18	9.94	11.12	10.63	11.19	24.00	23.12	23.54	22.50	35.03	
Wo													43.73	43.78	43.10	42.64	41.5	41.39	2.20	1.80	1.83	1.80	2.19	
Ac													4.06	3.00	4.13	3.77	5.25	4.82	1.44	0.43	0.68	n.d.	0.11	

Table 6. Electron microprobe chemical analyses of main phases composing the "sapphirine" pseudomorph and a sapphire xenocryst in PN32. Coexisting TiMag and Ilm were used for geothermometry of the pseudomorph formation.

Oxide wt%	Spl			TiMag		Ilm			Opx		Pl	Crn	Sapphire	Bt
SiO_2	0.31	0.48	0.07	0.02	0.05	0.04	0.21	0.00	48.80	49.64	55.34	0.03	0.01	38.93
TiO_2	0.44	0.59	0.77	10.29	9.76	46.28	43.09	48.53	0.24	0.33	0.00	0.34	0.33	4.74
Al_2O_3	58.82	58.82	50.36	4.74	3.88	0.09	0.25	0.08	5.06	5.91	27.47	100.6	97.92	12.62
Cr_2O_3	0.00	0.00	0.09	0.04	0.07	0.03	0.07	0.06	0.04	0.00	0.00	0.06	0.06	0.00
FeO_{Total}	28.53	28.17	37.43	78.79	80.46	51.39	52.06	50.12	20.98	20.58	0.07	0.36	1.38	11.17
MnO	0.13	0.14	0.98	0.42	0.40	0.32	0.57	0.38	3.40	1.84	0.00	0.00	0.01	0.05
MgO	11.72	12.17	10.28	4.89	4.64	2.20	3.18	1.36	20.85	21.77	0.01	0.04	0.03	16.41
CaO	0.08	0.10	0.03	0.15	0.08	0.01	0.11	0.02	0.22	0.13	11.24	0.01	0.02	0.05
Na_2O	n.d.	n.d.	n.d.	n.d.	n.d.	n.d.	n.d.	n.d.	n.d.	n.d.	2.55	n.d.	n.d.	0.27
K_2O	n.d.	n.d.	n.d.	n.d.	n.d.	n.d.	n.d.	n.d.	n.d.	n.d.	0.38	n.d.	n.d.	11.06
Total	100.03	100.47	100	99.34	99.34	100.36	99.54	100.55	99.59	100.20	97.06	101.4	99.76	95.30

(c) pale green inclusions in calcic plagioclase phenocrysts, and (d) mantling or replacing corundum xenocrysts in the volcanic matrix.

Orthopyroxene ($En_{65.2}Fs_{34.5}Wo_{0.30}$) is very aluminous (up to 5.91 wt. % Al_2O_3), with a high Mg# of 65, and rather calcium-poor. Accompanying biotite (Table 6) shows high TiO_2 content (4.74 wt. % TiO_2) and Mg# (72) that together yield a temperature of 800 ºC using the Henry *et al*. (2005) Ti-in-biotite geothermometer for biotite crystallization in the pseudomorph. Coexisting titanomagnetite and ilmenite also were used to obtain an independent estimate of the crystallization temperature for the pseudomorph, as discussed below.

Non-stoichiometric garnet xenocrysts with high pyrope content ($Al_{54}Pyr_{44}Sp_{1.36}Gr_{0.32}$) immersed in a sanidine-rich matrix, and titanite xenocrysts also found in the intrusion may indicate assimilation of deep crustal materials by the andesitic magma.

Evolution of the Puente Negro plumbing system

Although hornblende xenocrysts, "glomerocrysts", and microphenocrysts in the andesitic magma reproduce the assemblages in the gabbroic xenoliths (mafic and ultramafic), the order of crystallization cannot be established for the volcanic rock because of the strong mineral and textural modifications caused by interaction with the rocks that provided the gabbroic xenoliths. Thus, the crystallization sequence shown in Figure 6 is deduced only from the petrography of ultramafic cumulitic xenoliths, which represent an important plutonic component of the Puente Negro plumbing system. "Glomerocrysts" in the andesite and cumulitic gabbroic xenoliths, both rich in pargasitic amphibole, indicate fractional crystallization at high water pressures in an evolving magma chamber emplaced in the middle crust, followed by their disaggregation, possibly during magmatic recharge and rapid ascent of a subsequent magma batch with a different isotopic composition (see below). Sapphire, colorless corundum, high-Al orthopyroxene, and green spinel represent phases in the andesite that may be restitic xenocrysts after partial melting and assimilation of pelitic and quartzo-feldspathic gneisses at various depths in the lower crust or, alternatively, the first fractionated phases at high pressures in the mantle. The euhedral aspect of spinel and corundum xenocrysts (Figure 4g-4h) and their presence as inclusions in plagioclase of the andesite (Figure 4c) suggest their very early crystallization in the plumbing system rather than plucked crystals from a high-grade metamorphic rock. In fact, in the basaltic system CMAS (*cf.* Milholland and Presnall, 1998) spinel and corundum develop small windows for the early crystallization of these phases at high temperatures and pressures in the mantle.

The magma batch parental to the gabbroic xenoliths and hornblende xenocrysts in the andesite underwent sequential crystallization (Figure 6) in the middle or lower crust, apparently starting with minor clinopyroxene, hercynite and ilmenite, closely followed by abundant orthopyroxene and amphibole, and finally by abundant plagioclase and amphibole. Absence of olivine and early presence of clinopyroxene and some spinel in the liquidus indicate, in

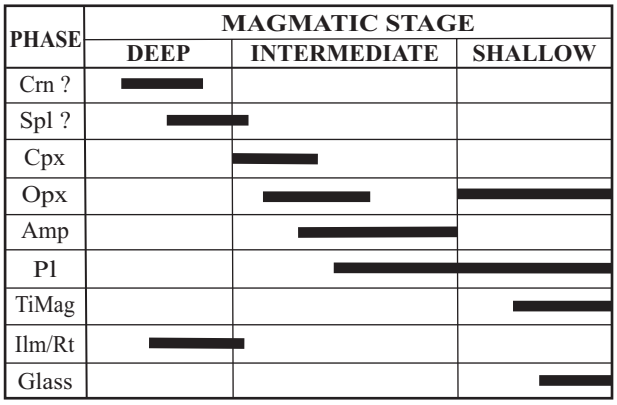

Figure 6. Inferred polybaric sequential crystallization in the Puente Negro "glomerocrysts", gabbroic xenoliths, and high-Al xenocrysts domains.

principle, fractional crystallization at high pressure (*e.g.*, Elthon and Scarpe, 1984), whereas the late appearance of plagioclase may be due to high water pressure during crystallization of the basic magma at depth. Virtually all amphiboles show simple to multiple decompression rims of opacite or anhydrous pyroxene-plagioclase-titanomagnetite assemblages, and their oscillatory color zoning may be due to isobaric T-f_{H_2O} changes caused by repeated injection of basaltic magma into a differentiating hydrous mafic magma chamber (*e.g.*, Bachmann and Dungan, 2002). Some magmatic pulses with extremely rapid ascent rates are indicated by very narrow to absent opacite rims for some amphiboles, as opposed to other crystals with broader opacite rims or complete recrystallization to the assemblages Pl-Cpx-Mag-Ilm ± Bt ± Rt ± Fa, and Pl-Opx-TiMag that indicate slower cooling rates (Buckley *et al*., 2006). In fact, given the pargasitic composition of all amphiboles, its presence in the silica-saturated andesite-dacite dikes suggests that this phase probably was derived from the postulated gabbroic body. Magmatic recharge, possibly by fresh basaltic batches, may have triggered rapid ascent to shallow levels of the differentiated magma, as deduced from the quenched plagioclase-glass patches and the partial to total dehydration of hornblende in gabbroic xenoliths (*cf*. Rutherford and Devine, 2003). QUILF (quartz-ulvospinel-ilmenite-fayalite) (Andersen *et al*., 1993) calculations on coexisting augite and orthopyroxene in the hornblende pyroxenite cumulitic xenolith (see Table 5) yield, at 4–6 kbar, temperatures of 944–949 ± 57 ºC for the crystal cores, and 900–906 ± 9 ºC for their rims, in this case probably indicating minor cation readjustment during cooling. Temperatures of 909 and 920 ºC are obtained for Hbl-Pl pairs (Holland and Blundy, 1994) for pressures of 4 and 6 kbar, respectively. Heating by crystallization and degassing, as proposed by Blundy *et al*. (2006) for many andesites in magmatic arcs, also remains a strong possibility to explain many features of Puente Negro, such as the abundance of microlites of plagioclase and orthopyroxene in the andesitic matrix, dehydration of hornblende, and the high temperatures of final emplacement above the quartz-tridymite phase transition. Further contamination by partial melting, assimilation and physical disruption of granitic gneisses near the surface resulted in the present complex mineralogy and bulk andesitic-dacitic composition of the Puente Negro dikes.

Figure 7 provides a simplified model for the possible plumbing system of Puente Negro, and Table 7 shows phase distribution according to the petrographic domains distinguished in the Puente Negro andesite.

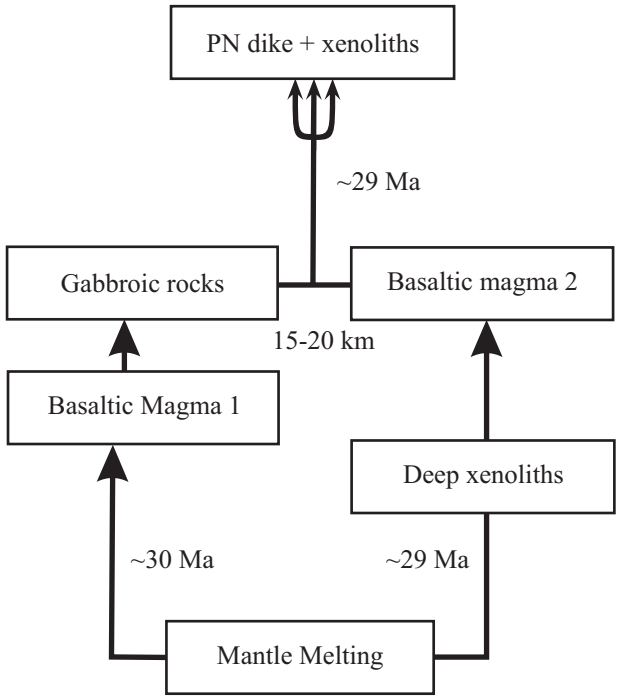

Figure 7. Simplified plumbing system model for the Puente Negro intrusion, including the uptake of xenoliths at different levels in the crust.

High-grade metamorphic xenoliths

Given the great diversity of mineral and melt assemblages found in the metamorphic xenoliths, the following data, obtained by microprobe analyses of a limited number of samples represent only a few, albeit essential petrologic aspects of the complex evolution of the Puente Negro magma-xenolith system.

The composition of important high-grade phases is given in Table 8 (silicates and oxides) and Table 9 (garnet and its decompression corona), but several other phases, such as mullite, corundum, staurolite, sillimanite and clinopyroxene, were not analyzed due to their very small size. Figure 8 gives our interpretation on the origin of the analyzed metamorphic phases in terms of two major events: deep-seated granulite facies superimposed by very shallow sanidinite facies.

Silica phases. SiO_2-rich phases in most xenoliths consist of quartz, tridymite, inverted tridymite (paramorphic laths in optical continuity with quartz), opal, and two fibrous phases, possibly chalcedony and metastable cristobalite. However, whereas optical properties of tridymite are diagnostic (biaxial positive, triangular facets, pie-shaped twinning, and very low birefringence and relief), identification of pristine cristobalite (very low relief, isotropic) is tentative. Most grains of tridymite are close to pure SiO_2, but show in cursory microprobe analyses (Table 8) small contents (<1 wt. %) of CaO, MgO, and FeO, with Al_2O_3 ranging from 0.48 to 1.02 wt. %, indicating incipient solid solution with mullite. The brittle behavior (polygonal cracking) of all quartz at these high temperatures attests to the extremely dry environment in which it recrystallized and may indicate contraction from high to low quartz.

Al-silicate$_{ss}$. Long prismatic to acicular silicate phases resembling sillimanite but occurring in bundles and intimately associated with other high temperature aluminous phases such as spinel and Al-rich hypersthene and glass

Table 7. Interpreted origin of most relevant petrographic objects (phases and domains) identified in the Puente Negro andesite and its metasedimentary and gabbroic inclusions.

Domains and phases	Metsed xenoliths	Garnet corona	Gabbroic xenoliths	Quenched gabbroic matrix	Volcanic matrix	Pheno-crystal	Xeno-crystal	Glomero-crystal	Hbl rims	Pseudo-morph
Pl	X	X	X	X	X	X	X	X	X	X
Cpx	X	X	X	X			X	X	X	X
Opx	X	X	X		X	X	X	X	X	X
Hbl			X				X	X		
Spl	X	X	X				X			X
Crn	X	X					X			X
TiMag	X			X	X				X	
Ilm	X		X						X	
Grt	X	X					X			
Sil	X									X
Mul	X									X
Qz	X						X			
Trd	X									
Crs	X									
St	X									X
Bt	X								X	
Sa	X								X	
Rt	X		X						X	X
Zrn	X						X			
Glass	X			X	X				X	X

are interpreted as mullite solid-solution phases (Figure 5h) based on EDS analyses (mol Al_2O_3/SiO_2 >1). Unfortunately, quantitative WDS analyses were hampered by the minute widths (<3 μm) of these crystals. On the other hand, relict sillimanite apparently coexisting with orthopyroxene and quartz in a microxenolith was identified optically in sample FO6605, and also inside a complex poikiloblast composed of bytownite-spinel-corundum-garnet-sillimanite-staurolite in FO8305.

Spinel. Spinel is present in all high-grade xenoliths and it is compositionally inhomogeneous. It is almost a pure hercynite-spinel solid solution ($Hc_{57–75}$) varying in color from opaque to pale green, olive green or brown, and is usually associated with titanomagnetite, glass, calcic plagioclase, aluminous orthopyroxene, quartz/tridymite, mullite, corundum, ilmenite, and rutile, depending on the original mineral assemblage replaced during decompression and pyrometamorphism. Analyses shown in Table 8 correspond to crystals in the glass-rich quartzose gneisses. Note the larger hercynite contents of spinels developed in the decompression mantles of garnets (Table 9). The stable assemblage Opx-Spl-Trd/Qz, in the absence of garnet, may be explained by the coupled reactions Grt + Crd = 2Opx + 3Spl + 6Qz/Trd, and Grt + 2Sil = 3Spl + 5Qz/Trd during heating and decompression. Commonly, spinel and corundum appear to grade into each other, but spinel also appears replaced by the assemblage Crn-Mag in some decompression coronas of garnet porphyroblasts (PN29) through the reaction 3Hc = 3Crn + Mag. Elongated crystals of spinel occur in one quartzose gneiss (FO8305) as cores to an $Al\text{-}silicate_{ss}$.

Garnet. Textural and chemical features of garnet porphyroblasts reveal different P-T histories, compositions, degree of fracturing, and zoning patterns. Analyzed grains (Tables 9 and 10) show high manganese and moderate calcium, low magnesium, and a remarkable chemical homogeneity of their interior cores. Results of a microprobe traverse performed on one of these cores and its fractured envelope are shown in Table 10 and Figure 9, where a flat profile stands out for all cations across the area. The internal zone around the core is strongly fractured and much richer in calcium, probably indicating contrasting P-T inherited conditions of recrystallization prior to incorporation in the magma. The outer zone of most garnets consists of kelyphitic coronas with the assemblage Pl-Opx-Spl/Mag ± glass ± Crn ± Rt where the presence of corundum and magnetite was probably controlled by the reaction 3Hc + O_2 = Mag + 3Crn, and rutile from possible biotite inclusions in the garnet. Minor clinopyroxene ($Jd_{1.9}CaTsch_{16.1}Hd_{15.4}Di_{66.6}$) was also found during routine microprobe studies of the corona. These features are important petrogenetically because they demonstrate that garnets are polyphase and remained at high temperature and relatively high pressure for a long time until entrainment and fast uplift in the magma.

Orthopyroxene. It is ubiquitous in all metamorphic xenoliths with granulite facies and sanidinite facies thermal imprints as: (a) strongly colored, stubby to acicular prisms immersed in glass of partially melted gneisses and quartzites (Table 8), (b) subhedral crystals in the coronitic alteration of garnet (Table 9), (c) mantling quartz/tridymite oval grains inside glass patches of the strongly melted shallow

Table 8. Electron microprobe chemical analyses of main phases composing high-grade metasedimentary xenoliths (PN1, PN17, PN19). For garnet, see Tables 9 and 10.

	Orthopyroxene					**Spl**				**Plagioclase**						**Ilmenite**		**Tridymite**	
Oxide wt. %																			
SiO_2	47.32	46.93	47.35	48.80	49.64	0.09	0.08	n.d.	n.d.	57.23	57.69	61.09	52.96	53.89	55.82	0.04	0.02	97.32	96.06
TiO_2	0.42	0.4	0.38	0.24	0.33	0.35	0.36	0.46	0.41	0.04	0.06	0.04	0.00	0.01	0.00	50.62	50.30	0.00	0.00
Al_2O_3	11.6	11.23	11.33	5.06	5.91	60.79	60.91	59.67	59.61	27.60	27.16	24.73	30.25	29.89	28.78	0.22	0.26	0.48	1.02
FeO_{Total}	21.9	23.14	23.08	20.98	20.58	27.97	28.06	28.21	28.73	0.21	0.36	0.24	0.38	0.28	0.21	43.76	44	0.31	0.65
MnO	0.15	0.11	0.12	3.40	1.84	0.11	0.12	0.10	0.10	n.d.	n.d.	n.d.	0.00	0.00	0.00	0.22	0.23	0.00	0.02
MgO	19.83	18.86	18.46	20.85	21.77	11.95	11.77	11.65	11.75	0.03	0.04	0.05	0.10	0.09	0.08	4.03	4.18	0.16	0.39
CaO	0.16	0.14	0.13	0.22	0.13	0.09	0.09	0.06	0.05	9.58	9.37	6.82	12.96	12.33	11.15	0.01	0.00	0.11	0.52
Na_2O	n.d.	n.d	n.d	n.d	n.d	n.d	n.d	n.d.	n.d.	6.81	6.40	8.34	4.25	4.62	5.22	n.d.	n.d.	0.07	0.06
K_2O	n.d.	n.d.	n.d.	n.d.	n.d.	n.d.	n.d.	n.d.	n.d.	0.07	0.07	0.11	0.03	0.04	0.06	n.d.	n.d.	n.d.	n.d.
Total	101.38	100.81	100.85	99.55	100.20	101.35	101.39	100.15	100.65	101.53	101.15	101.42	100.93	101.15	101.32	98.90	98.99	98.45	98.72
Cations	6 Oxygens					32 Oxygens				16 Oxygens									
Si	1.732	1.738	1.750	1.846	1.843	n.d.	n.d.	n.d.	n.d.	2.540	2.560	2.690	2.382	2.412	2.483				
Ti	0.011	0.011	0.010	0.007	0.009	0.056	0.058	0.075	0.067	n.d.	n.d.	n.d.	0.000	0.000	0.000				
Al	0.500	0.490	0.493	0.226	0.259	15.347	15.373	15.279	15.223	1.440	1.420	1.280	1.603	1.577	1.509				
Fe^{2+}	0.670	0.716	0.713	0.663	0.639	5.01	5.025	5.125	5.206	0.010	0.010	0.010	0.014	0.010	0.008				
Mn	0.005	0.003	0.004	0.109	0.058	0.02	0.022	0.018	0.018	n.d.	n.d.	n.d.	0.000	0.000	0.000				
Mg	1.081	1.040	1.016	1.176	1.205	3.816	3.758	3.774	3.796	n.d.	n.d.	n.d.	0.007	0.006	0.005				
Ca	0.006	0.005	0.005	0.009	0.005	0.021	0.021	0.014	0.012	0.460	0.550	0.710	0.624	0.591	0.531				
Na	n.d.	n.d.	n.d.	n.d.	n.d.	n.d.	n.d.	n.d.	n.d.	0.590	0.550	0.310	0.371	0.401	0.450				
K	n.d.	n.d.	n.d.	n.d.	n.d.	n.d.	n.d.	n.d.	n.d.	0.000	0.000	0.010	0.002	0.002	0.003				
Total	4.005	4.003	3.991	4.036	4.018	24.270	24.257	24.285	24.322	5.040	5.090	5.010	5.003	5.001	4.990				
An										44	45	31	63	59	54				
Mg #	62	59	59	64	65	43	43	42	42										
Wo	0.4	0.3	0.3	0.5	0.3														
En	61.5	59.1	58.6	60.0	63.2														
Fs	38.1	40.6	41.1	39.5	36.5														

Table 9. Electron microprobe chemical analyses of minerals composing the garnet corona in the garnetiferous gneiss (PN17).

	Components of garnet corona								
	Spl	Spl	Opx	Opx	Pl	Pl	Pl	Ilm	TiMag
Oxide wt. %									
SiO_2	0.54	0.07	52.71	53.44	45.20	44.79	46.66	0.04	0.70
TiO_2	0.80	0.77	0.12	0.19	0.50	0.34	0.06	46.28	17.52
Al_2O_3	45.84	50.36	0.77	1.72	34.02	35.54	35.24	0.09	3.46
Cr_2O_3	0.09	0.09	n.d.	n.d.	n.d.	n.d.	n.d.	0.03	0.47
FeO_{Total}	43.39	37.43	23.16	20.28	0.90	0.79	0.66	51.39	69.18
MnO	1.32	0.98	0.25	0.19	n.d.	n.d.	n.d.	0.32	0.90
MgO	8.57	10.28	23.72	24.86	0.10	0.04	0.09	2.20	3.90
CaO	0.04	0.03	0.73	0.55	17.35	17.97	17.39	0.01	0.40
Na_2O	n.d.	n.d.	n.d.	n.d.	1.00	1.21	1.31	n.d.	n.d.
K_2O	n.d.	n.d.	n.d.	n.d.	0.08	0.06	0.08	n.d.	n.d.
ZnO	0.22	0.35	n.d.	n.d.	n.d.	n.d.	n.d.	n.d.	n.d.
Total	100.8	100.4	101.46	101.2	99.15	100.7	101.5	100.4	96.53
Mg#	26	33	65	69	n.d.	n.d.	n.d.	n.d.	n.d.
Cations									
Si	n.d.	n.d.	1.944	1.944	2.120	2.060	2.120	n.d.	n.d.
Ti	0.145	0.134	0.003	0.005	n.d.	n.d.	n.d.	n.d.	n.d.
Al	13.02	13.75	0.033	0.074	1.880	1.930	1.890	n.d.	n.d.
Cr	0.003	0.003	0.000	0.000	n.d.	n.d.	n.d.	n.d.	n.d.
Fe^{2+}	8.745	7.253	0.714	0.620	0.040	0.030	0.030	n.d.	n.d.
Mn	0.269	0.192	0.008	0.010	n.d.	n.d.	n.d.	n.d.	n.d.
Mg	3.079	3.551	1.304	1.350	n.d.	n.d.	n.d.	n.d.	n.d.
Ca	0.010	0.007	0.029	0.020	0.870	0.890	0.850	n.d.	n.d.
Na	n.d.	n.d.	0.000	0.000	0.090	0.110	0.120	n.d.	n.d.
K	n.d.	n.d.	0.000	0.000	0.000	0.000	0.000	n.d.	n.d.
Total	25.27	24.89	4.035	4.023	5.000	5.020	5.010	n.d.	n.d.

continues

(buchite) xenoliths and (d) in pseudomorphic associations with high-Al phases and glass. Deformed or sharply color-zoned orthopyroxene crystals found occasionally in the andesite may be xenocrystic. Orthopyroxene coexisting with green spinel and immersed in glass inside an impure quartzite (PN1, Table 8) is extremely rich in alumina (average of three grains is 11.4 ± 0.19 Al_2O_3 wt. %) and poor in calcium, whereas the coronitic orthopyroxene around garnet only contains up to 1.72 wt. % Al_2O_3. In the shallow xenolith (Table 11), orthopyroxene shows up to 0.92 wt. % Al_2O_3, and considerable manganese and calcium. Intense green to brown or pale orange pleochroism distinguishes the most aluminous types, including grains that contain spinel and corundum inclusions (FO8305). These textures and compositions suggest variable P-T conditions of orthopyroxene crystallization recorded by the xenoliths. The Mg# in the coronitic pyroxene around garnet (Table 9) ranges from 65 to 69, whereas aluminous orthopyroxene in the high-grade metasedimentary xenoliths shows slightly lower values of 59 to 62 (Table 8).

Feldspar. Plagioclase in metamorphic xenoliths is common and of several types (Tables 8, 9, 11) one type crystallized as needles within glass, another type formed slender prisms nucleated on most quartz grain surfaces (PN19), and other grains form part of the symplectitic coronas around decompressed garnet (PN17), or occur closely associated with orthopyroxene. Plagioclase associated with garnet breakdown is of two types, one being nearly pure anorthite and the other labradorite. Anorthite contents in plagioclase varies according to their position in the internal or external parts of the corona (Table 9). Sodic sanidine ($Ab_{64}Or_{32}An_4$) was rarely found in the groundmass of a small xenolith in PN32, perhaps because most alkalis were partitioned to the glass phase on melting of the original biotite-plagioclase gneissic xenoliths.

Fe-Ti oxides. Fe-Ti oxides are present in all xenoliths and igneous rocks of Puente Negro. Representative analyses of ilmenite-magnetite-ulvospinel solid solutions from various domains appear in Tables 4, 6, 8 and 9. Ilmenite in the quartzo-feldspathic xenoliths is notable for its high content of MgO (geikielite) reaching up to 4.2 MgO wt. % with smaller contents of MnO (pyrophanite) (Table 8). Titanomagnetite also yields substantial contents of MgO, and up to 39 % ulvospinel component. One titanomagnetite

Table 9 (continued). Electron microprobe chemical analyses of minerals composing the garnet corona in the garnetiferous gneiss (PN17).

	Garnet internal zone											
	Rim					Core						Rim
Oxide wt. %												
SiO_2	37.65	37.68	37.56	37.37	37.37	37.38	37.58	37.58	37.52	37.34	37.32	37.39
TiO_2	n.d.	n.d.	n.d.	n.d.	n.d.	n.d.	n.d.	n.d.	n.d.	n.d.	n.d.	n.d.
Al_2O_3	21.19	21.11	21.09	20.95	21.11	21.14	21.05	21.11	21.16	21.13	20.95	21.11
Cr_2O_3	n.d.	n.d.	n.d.	n.d.	n.d.	n.d.	n.d.	n.d.	n.d.	n.d.	n.d.	n.d.
FeO_{Total}	25.69	25.62	25.65	25.51	25.67	25.48	25.38	24.98	25.59	25.74	25.92	25.98
MnO	12.98	12.83	13.18	13.04	12.98	13.24	12.96	13.17	12.97	13.14	13.17	13.04
MgO	1.38	1.39	1.42	1.42	1.37	1.36	1.39	1.37	1.38	1.38	1.36	1.36
CaO	1.54	1.60	1.63	1.73	1.69	1.70	1.64	1.65	1.69	1.65	1.54	1.56
Na_2O	n.d.	n.d.	n.d.	n.d.	n.d.	n.d.	n.d.	n.d.	n.d.	n.d.	n.d.	n.d.
K_2O	n.d.	n.d.	n.d.	n.d.	n.d.	n.d.	n.d.	n.d.	n.d.	n.d.	n.d.	n.d.
ZnO	n.d.	n.d.	n.d.	n.d.	n.d.	n.d.	n.d.	n.d.	n.d.	n.d.	n.d.	n.d.
Totals	100.4	100.22	100.53	100.01	100.19	100.30	99.99	99.86	100.31	100.37	100.25	100.45
Mg#	9	9	9	9	9	9	9	9	9	9	8	8
Cations						12 Oxygens						
Si	3.030	3.040	3.030	3.030	3.020	3.020	3.040	3.040	3.030	3.020	3.020	3.020
Ti	n.d.	n.d.	n.d.	n.d.	n.d.	n.d.	n.d.	n.d.	n.d.	n.d.	n.d.	n.d.
Al	2.010	2.010	2.000	2.000	2.010	2.010	2.010	2.010	2.010	2.010	2.000	2.010
Cr	n.d.	n.d.	n.d.	n.d.	n.d.	n.d.	n.d.	n.d.	n.d.	n.d.	n.d.	n.d.
Fe^{2+}	1.730	1.730	1.730	1.730	1.740	1.720	1.720	1.690	1.730	1.740	1.760	1.750
Mn	0.890	0.880	0.900	0.890	0.890	0.910	0.890	0.900	0.890	0.900	0.900	0.890
Mg	0.170	0.170	0.170	0.170	0.170	0.160	0.170	0.170	0.170	0.170	0.160	0.160
Ca	0.130	0.140	0.140	0.150	0.150	0.150	0.140	0.140	0.150	0.140	0.130	0.130
Na	n.d.	n.d.	n.d.	n.d.	n.d.	n.d.	n.d.	n.d.	n.d.	n.d.	n.d.	n.d.
K	n.d.	n.d.	n.d.	n.d.	n.d.	n.d.	n.d.	n.d.	n.d.	n.d.	n.d.	n.d.
Total	7.960	7.970	7.970	7.970	7.980	7.970	7.970	7.950	7.980	7.980	7.970	7.960

continues

analyzed for vanadium (EDS not shown) yielded 1.42 wt. % V_2O_3. Rutile is common in quartzose gneisses as individual crystals, and coring or rimming ilmenite, but often forms composite, coronitic and symplectitic aggregates with ilmenite, spinel, and rarely zircon. These aggregates sometimes suggest the breakdown of rutile-thialite and armalcolite or ferropseudobrookite solid solutions. Hexagonal plates of a reddish brown phase present in glass-rich portions of the quartzose xenoliths and associated with the high-Al xenocrystic pseudomorphs were tentatively identified as pyrophanite based on its distinctive optical properties.

Clinopyroxene. Clinopyroxene in the metamorphic xenoliths occurs as stubby, euhedral prisms isolated within strongly brown glass (FO6605) and abundantly in the calcsilicate xenolith, where it shows colors from brown in the center to green in the margin, suggesting a rather sodic composition. Only two analyses were made on this mineral corresponding to a secondary augite formed within the buchite xenolith FO6605 (Table 11).

Glasses. Glasses are abundant and diverse in all metamorphic xenoliths. Representative microprobe analyses (Table 12) are from restitic quartzose gneisses (PN1, PN19, PN23), garnetiferous gneisses (PN17, PN18), and a buchite shallow xenolith (FO6605, Table 11). Compositional differences are evident, with much lower silica and higher alumina, alkalis, and calcium contents within the garnetiferous xenoliths (deep-seated) than the silica-rich glasses of the shallow quartzose gneisses that contain normative corundum (up to 9.16 mol %), and large amounts of normative quartz (up to 70%). All glasses contain substantial amounts of iron.

Brown and colorless glasses in the shallow xenoliths differ in iron and silica contents, and water content may be 5% lower in the brown glass (see Table 11). However, both types commonly merge into each other, and the colorless glass also forms microscopic veins that cut across all other phases, including the brown glass. The silicic glasses formed in partially fused xenoliths and were locally mixed with the magma bearing the wall rock xenolith, as suggested by the gradual merging of the brown and clear glasses. Brown glass often remained *in situ* forming, with calcic plagioclase, symplectitic pseudomorphs probably after amphibole and sodic plagioclase.

Table 9 (continued). Electron microprobe chemical analyses of minerals composing the garnet corona in the garnetiferous gneiss (PN17).

	Garnet external zone					
	Rim			Core		Rim
Oxide wt. %						
SiO_2	37.87	36.78	37.98	38.51	37.62	37.39
TiO_2	n.d.	n.d.	n.d.	n.d.	n.d.	n.d.
Al_2O_3	21.19	21.88	21.45	21.32	20.83	21.02
Cr_2O_3	n.d.	n.d.	n.d.	n.d.	n.d.	n.d.
FeO_{Total}	22.42	24.05	22.70	22.67	23.24	24.42
MnO	10.87	10.42	10.11	9.83	9.30	8.47
MgO	0.94	0.88	0.93	0.92	0.92	1.06
CaO	7.34	7.35	7.32	7.67	7.70	6.99
Na_2O	n.d.	n.d.	n.d.	n.d.	n.d.	n.d.
K_2O	n.d.	n.d.	n.d.	n.d.	n.d.	n.d.
ZnO	n.d.	n.d.	n.d.	n.d.	n.d.	n.d.
Totals	100.63	101.36	100.49	100.91	99.62	99.34
Mg#	7	6	7	7	7	7
Cations			12 Oxygens			
Si	3.020	2.940	3.030	3.050	2.990	3.020
Ti	n.d.	n.d.	n.d.	n.d.	n.d.	n.d.
Al	1.990	2.060	2.010	1.990	2.050	2.000
Cr	n.d.	n.d.	n.d.	n.d.	n.d.	n.d.
Fe^{2+}	1.500	1.600	1.510	1.500	1.550	1.650
Mn	0.730	0.700	0.680	0.660	0.630	0.580
Mg	0.110	0.100	0.110	0.110	0.110	0.130
Ca	0.630	0.630	0.620	0.650	0.660	0.600
Na	n.d.	n.d.	n.d.	n.d.	n.d.	n.d.
K	n.d.	n.d.	n.d.	n.d.	n.d.	n.d.
Total	7.980	8.030	7.960	7.960	7.990	7.980

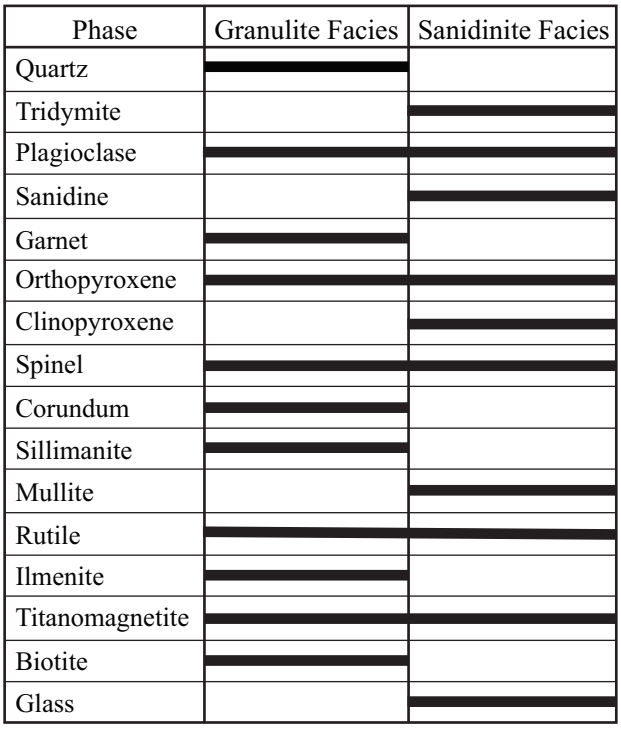

Figure 8. Phase stability bar diagram inferred for the two main metamorphic events registered in the Puente Negro xenoliths.

Geothermobarometry of the xenoliths

Quantification of the peak temperatures attained during deep-seated metamorphism can be derived from the FMAS phase diagram based on experimental and theoretical data for Al-orthopyroxene coexisting with sapphirine and quartz (Liermann and Ganguly, 2003; Hollis and Harley, 2003). According to the latter authors, at pressures between 12 and 16 kbars, and temperatures of 1250 and 1350 ºC, aluminum solubility in orthopyroxene shows a strong dependence on temperature, but very slightly on pressure. The Al content in Opx measured in those experiments varied from 0.374 to 0.547 a.p.f.u. (atoms per formula unit), which if compared to values of 0.49 to 0.50 a.p.f.u. measured for the most aluminous orthopyroxene of Puente Negro quartzose xenoliths, it would indicate very high temperatures and high pressures, albeit not precisely determinable at Puente Negro because of the actual absence of sapphirine due to inappropriate chemical composition (relatively high Fe/Mg bulk compositions) rather than different P-T conditions. The up to 44% a.p.f.u. content of the Mg-Fe-Tschermakite end member in the most aluminous orthopyroxene of quartzose xenoliths of Puente Negro coexisting with spinel is consistent with temperatures in excess of 1100 ºC (Kelsey *et al.*, 2003; Kosyakova *et al.*, 2005). Moreover, the maximum Al content of the enstatite found by Grochau and Johannes (1997) during a experimental study of phlogopite stability only yielded 7.6 Al_2O_3 wt. %, whereas Puente Negro orthopyroxenes contain up to 11.60 wt. % alumina, probably reflecting higher temperatures for the metamorphism that affected the xenoliths. Finally, zoned Al-orthopyroxene in the Napier Complex (Antarctica), with Al_2O_3 contents similar to those of Puente Negro, formed at temperatures above 1120 ºC and pressures around 10–12 kbar (Harley and Motoyoshi, 2000). Unfortunately, pressures for the crystallization of Puente Negro high-Al orthopyroxene cannot be accurately obtained solely from this system.

Several mineralogical and geothermometric criteria may be applied to Puente Negro xenoliths to estimate the very high temperatures of metamorphism, most of which converge to minimum values above 1000 ºC. Various magnetite-ilmenite thermometers calculated with the ILMAT Excel worksheet of Lepage (2003) yield variable, albeit consistent temperatures between 966 and 1072 ºC, with f_{O_2} between ($\log_{10}$) -7.60 and -10.71 for ilmenite/titanomagnetite pairs in the decompression coronas of garnet of the garnetiferous gneisses (PN17), and between 961 and 1035 ºC with f_{O_2} ($\log_{10}$) -9.07 to -11.52 for pairs in the decompressional xenocryst within the andesite PN32 (see Table 6). The QUILF program of Andersen *et al.* (1993) was also used for the garnet coronitic oxide assemblage

Table 10. Electron microprobe chemical analyses across the core zone of a garnet porphyroblast of PN17 and two garnet xenocrysts in the andesite.

	Left Rim					**Central Zone**						**Right Rim**		**1***	**2****
Oxide wt. %															
SiO_2	37.16	37.45	37.59	37.13	37.19	37.39	37.14	37.64	37.34	37.26	37.15	37.10	37.74	36.69	37.81
TiO_2	0.05	0.05	0.05	0.07	0.05	0.06	0.08	0.05	0.05	0.06	0.05	0.09	0.11	0.05	0.08
Al_2O_3	19.60	19.67	19.92	19.95	20.45	19.89	19.57	19.69	19.66	19.09	19.57	19.60	19.87	20.71	20.87
FeO_{Total}	31.50	31.14	30.76	30.64	29.84	30.31	30.16	30.21	30.65	32.02	30.42	30.09	30.53	29.94	27.46
MnO	6.94	7.46	7.62	8.06	7.85	8.48	8.46	8.31	8.20	7.74	8.37	8.17	7.46	7.70	6.44
MgO	2.17	2.09	1.99	2.02	2.10	1.94	2.01	1.91	2.00	1.91	2.04	1.94	2.10	2.59	1.95
CaO	2.60	2.83	2.67	2.86	2.68	2.91	3.01	2.81	2.74	2.82	2.81	3.00	2.94	2.54	3.35
Total	100.02	100.69	100.60	100.73	100.16	100.98	100.43	100.62	100.64	100.90	100.41	99.99	100.75	100.21	97.96
Cations								12 Oxygens							
Si	3.03	3.03	3.04	3.01	3.01	3.02	3.02	3.05	3.03	3.03	2.99	3.03	3.04	2.97	3.08
Ti	0.00	0.00	0.00	0.00	0.00	0.00	0.00	0.00	0.00	0.00	0.00	0.01	0.01	0.00	0.00
Al_{Total}	1.88	1.88	1.90	1.90	1.95	1.89	1.88	1.88	1.88	1.83	1.85	1.88	1.89	1.98	2.00
Fe^{2+}	2.15	2.15	2.08	2.08	2.02	2.05	2.05	2.04	2.08	2.18	2.18	2.05	2.06	2.03	1.87
Mn	0.48	0.51	0.52	0.55	0.54	0.58	0.58	0.57	0.56	0.53	0.57	0.56	0.51	0.53	0.44
Mg	0.26	0.25	0.24	0.24	0.25	0.23	0.24	0.23	0.24	0.23	0.24	0.24	0.25	0.31	0.24
Ca	0.23	0.25	0.23	0.25	0.23	0.25	0.26	0.24	0.24	0.25	0.24	0.26	0.25	0.22	0.29
Total	8.03	8.07	8.01	8.03	8.00	8.02	8.03	8.01	8.03	8.05	8.07	8.03	8.01	8.04	7.92
Alm	68.9	67.6	67.7	66.5	66.4	65.8	65.3	66.2	66.6	68.3	67.4	65.9	67.0	65.6	65.8
Prp	8.5	8.1	7.8	7.8	8.3	7.5	7.8	7.5	7.8	7.3	7.6	7.6	8.2	10.1	8.3
Spes	15.4	16.4	17.0	17.7	17.7	18.6	18.6	18.4	18.0	16.7	17.6	18.1	16.6	17.1	15.6
Gros	7.3	7.9	7.5	8.0	7.6	8.1	8.4	7.9	7.6	7.7	7.5	8.4	8.3	7.1	10.3

1* Average of six points from core to rim. 2**Average of four random points in the garnet xenocryst.

yielding similar values at 1020 ± 81 to 965 ± 72 ºC, with oxygen fugacity of (log_{10}) -10 and -10.5, respectively (oxides in Table 9). Garnet-orthopyroxene geothermometry (*e.g.*, Lee and Ganguly, 1988) applied to the coronas of decompressed garnets yield unrealistic low temperatures, probably because garnet is no longer in equilibrium with the coronitic orthopyroxene. The Ti-in-biotite thermometer of Henry *et al.* (2005), based on the presence of some biotite in the aluminous pseudomorphs (see Table 6), yields a temperature of 800 ± 12 ºC for formation of the Spl-Pl-Crn ± Opx ± Bt ± Rt pseudomorph, which is probably a minimum value because quartz and graphite are not present in the assemblage.

Unfortunately, precise geobarometry could not be performed with the assemblages of Puente Negro because garnet is no longer stable with the rest of the minerals, and cordierite was not positively identified. However, minimum depth conditions for the xenolith P-T path are suggested by textural evidence of reactions such as Al-Opx = Spl + Qz coexisting with melt, and the total absence of cordierite in the plutonic assemblages (garnet coronas), which requires pressures above 3.5 kbar according to thermodynamic phase-melt equilibria at very high temperature (*e.g.*, Vielzeuf and Holloway, 1988). Higher minimum pressures are derived from the crystallization of the cumulate ultramafic xenolith PN4 (Table 5), whose average pressure was calculated on the basis of total molar Al in hornblende (*cf.* Johnson and Rutherford, 1989) at about 5.75 ± 0.8 kbar for the gabbroic amphiboles, and 4.85 ± 0.8 kbar for the andesitic amphiboles. These pressures, however, may be overestimated by about 1.2 kbar, as the assemblages accompanying amphibole are quartz-free, implying a silica activity lower than unity. Other similar, but still minimum pressures affecting some of the xenoliths during entrainment in the hot, hornblende-

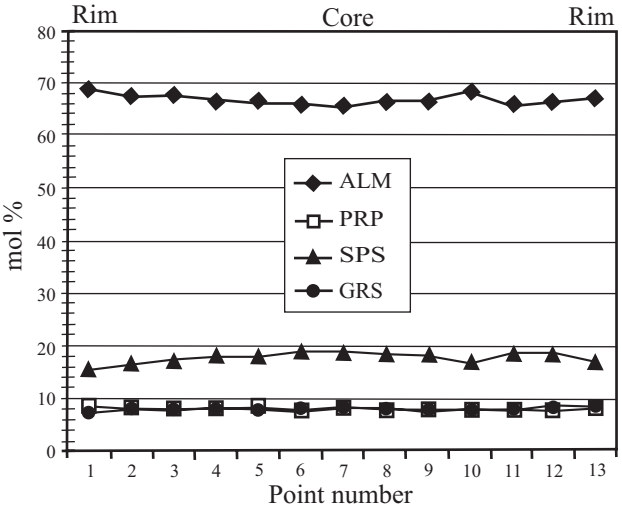

Figure 9. Microprobe transect across the unfractured core of a garnet xenocryst. Note lack of zoning for all elements.

Table 11. Electron microprobe chemical analyses of main silicates and glasses composing the buchite raft xenolith (c: clear glass, b: brown glass).

	Plagioclase					Spinel				Orthopyroxene					Clinopyroxene			Glasses			
																		c	c	c	b
Oxide wt. %																					
SiO_2	52.96	53.89	55.82	51.85	60.03	n.d.	n.d.	n.d.	n.d.	53.15	53.97	54.24	51.55	50.15	50.16	53.71		75.22	78.70	77.61	80.19
TiO_2	n.d.	n.d.	n.d.	0.20	0.01	0.57	0.47	0.48	0.46	0.12	0.14	0.14	0.23	0.97	0.40	0.29		0.33	0.21	0.48	0.18
Al_2O_3	30.25	29.89	28.78	28.39	23.17	59.65	60.08	59.78	60.16	0.47	0.92	0.43	0.58	0.84	9.30	1.29		12.47	10.06	11.06	10.85
FeO_{Total}	0.38	0.28	0.21	2.14	0.65	28.43	28.20	28.20	28.96	22.29	19.91	21.53	23.24	27.58	10.59	14.50		1.10	1.21	1.50	2.06
MnO	n.d.	n.d.	n.d.	n.d.	0.04	0.13	0.10	0.14	0.12	0.73	0.69	0.66	1.24	0.97	0.29	0.46		0.02	0.00	0.02	0.07
MgO	n.d.	n.d.	n.d.	0.06	0.14	12.02	12.13	12.05	11.66	23.39	23.71	24.48	21.60	17.09	6.44	6.79		0.10	0.12	0.13	0.18
CaO	12.96	12.33	11.15	13.81	7.22	0.05	0.06	0.06	0.07	0.46	0.91	0.28	1.54	1.94	20.66	21.48		1.19	0.28	0.62	0.85
Na_2O	4.25	4.62	5.22	3.49	6.51	n.d.	n.d.	n.d.	n.d.	n.d.	n.d.	0.03	n.d.	0.47	0.98	0.21		1.12	1.73	1.64	1.62
K_2O	0.03	0.04	0.06	0.34	1.40	n.d.	n.d.	n.d.	n.d.	n.d.	n.d.	0.00	n.d.	0.00	0.07	0.03		1.99	2.47	2.44	2.60
Total	100.83	101.05	101.24	100.28	99.17	100.85	101.04	100.71	101.43	100.61	100.25	101.79	99.98	100.01	98.89	98.76		93.61	94.78	95.50	98.59
Cations	16 Oxygens					32 Oxygens				6 Oxygens					6 Oxygens			*CIPW norm*			
Si	2.38	2.410	2.480	2.380	2.717	n.d	n.d	n.d	n.d	1.969	1.980	1.975	1.948	1.940	1.890	1.980	Qz	61.81	60.66	57.46	58.95
Ti	n.d.	n.d.	n.d.	n.d.	0.000	n.d	n.d	n.d	n.d	0.003	0.004	0.004	0.007	0.028	0.010	0.000	C	6.92	4.23	5.78	4.81
Al	1.60	1.580	1.510	1.540	1.236	n.d	n.d	n.d	n.d	0.021	0.040	0.018	0.026	0.038	0.410	0.050	Ab	10.15	15.48	15.91	14.55
Fe^{2+}	0.01	0.010	0.010	0.080	0.025	5.14	5.01	5.03	5.14	0.691	0.612	0.655	0.734	0.892	0.330	0.400	An	5.79	1.49	2.83	3.23
Mn	n.d.	n.d.	n.d.	n.d.	0.002	n.d.	n.d.	n.d.	n.d.	0.023	0.021	0.020	0.040	0.032	0.010	0.020	Or	12.59	15.42	14.42	15.07
Mg	n.d.	n.d.	n.d.	n.d.	0.009	3.87	3.84	3.83	3.69	1.292	1.298	1.329	1.217	0.985	0.360	0.560	Hy	1.90	2.31	3.04	2.44
Ca	0.62	0.590	0.530	0.680	0.350	n.d.	n.d.	n.d.	n.d.	0.018	0.036	0.010	0.062	0.080	0.830	0.970	Ilm	0.66	0.41	0.55	0.95
Na	0.37	0.400	0.450	0.310	0.571	n.d.	n.d.	n.d.	n.d.	n.d.	n.d.	n.d.	n.d.	0.035	0.070	0.030					
K	0.00	0.000	0.000	0.020	0.081	n.d.	n.d.	n.d.	n.d.	n.d.	n.d.	n.d.	n.d.	n.d.	0.000	0.000					
Total	4.980	4.990	4.980	5.010	4.991	n.d.	n.d.	n.d.	n.d.	4.017	3.991	4.011	4.034	4.030	3.910	4.010					
An	37.2	40.3	45.7	30.8	34.9																
Ab	62.6	59.5	53.9	67.3	57.0																
Or	0.20	0.20	0.30	2.00	8.10																
Mg #						43	43	43	42	65	68	67	62	53	51	58					
Wo										0.9	1.8	0.5	3.0	4.04	54.2	49.9					
En										63.8	66.0	66.0	59.3	49.53	23.5	28.9					
Fs										35.3	32.2	33.5	37.7	46.43	22.3	21.2					

Table 12. Electron microprobe chemical analyses of glasses in Puente Negro xenoliths

	1	2	3	4	5	6	7	8	9	10	11	12	13	14
Oxide wt. %														
SiO_2	61.77	62.95	63.10	61.48	65.73	78.72	80.41	75.22	78.70	77.61	79.33	79.72	80.19	80.41
TiO_2	0.11	1.85	0.07	1.85	0.03	0.00	0.18	0.33	0.21	0.48	0.18	0.29	0.18	0.18
Al_2O_3	19.74	17.33	19.14	17.35	14.35	12.92	10.47	12.47	10.06	11.06	9.95	12.61	10.85	10.47
FeO_{Total}	0.30	0.63	0.25	0.64	3.84	0.10	1.90	1.10	1.21	1.50	1.27	1.44	2.06	1.90
MnO	0.00	0.06	0.01	0.06	0.01	0.01	0.07	0.02	0.00	0.02	0.03	n.d.	0.07	0.07
MgO	0.00	0.11	0.00	0.11	2.81	0.00	0.11	0.10	0.12	0.13	0.13	0.22	0.18	0.11
CaO	2.06	1.75	2.10	1.75	3.36	3.73	0.84	1.19	0.28	0.62	0.26	0.44	0.85	0.84
Na_2O	6.81	6.01	6.80	6.01	4.32	4.30	0.99	1.12	1.73	1.64	1.29	1.46	1.62	0.99
K_2O	5.15	4.79	4.73	4.79	0.00	0.00	2.32	1.99	2.47	2.44	2.42	0.44	2.6	2.32
F	0.03	0.00	0.00	0.00	n.d.	n.d	0.00	0.07	0.00	0.00	0.05	n.d.	0.00	0.00
Total	95.97	95.48	96.20	94.04	94.46	99.81	97.29	93.61	94.78	95.50	94.91	96.62	98.59	97.29
CIPW norm														
Qz	-	6.60	1.39	5.13	27.55	60.08	64.05	61.81	60.66	57.46	64.17	69.49	58.95	64.05
C	-	-	-	-	1.20	-	4.94	6.92	4.23	5.78	5.00	9.16	4.81	4.94
Ab	56.29	53.22	59.82	54.07	38.67	36.47	8.63	10.15	15.48	15.91	11.51	12.78	14.55	8.63
An	8.4	6.46	8.03	6.63	17.66	15.99	4.27	5.79	1.49	2.83	1.34	2.48	3.23	4.27
Or	31.74	29.67	29.08	30.08	0.00	-	14.06	12.59	15.42	14.42	15.07	2.72	15.07	14.06
Ne	2.05	-	-	-	-	-	-	-	-	-	-	-	-	-
Hy	-	-	-	0.3	14.87	-	3.67	1.9	2.31	3.04	2.55	2.81	2.44	3.67
Di	0.73	-	-	-	-	0.38	-	-	-	-	-	-	-	-
Wo	0.52	-	0.83	-	-	0.89	-	-	-	-	-	-	-	-
Ilm	0.21	1.52	0.13	1.57	0.06	-	0.36	0.66	0.41	0.55	0.36	0.57	0.95	0.36
Rt	-	0.39	-	0.4	-	-	-	-	-	-	-	-	-	-
Ttn	-	1.84	-	1.83	-	-	-	-	-	-	-	-	-	-

rich magma, yield about 5 kbar using the empirical semi quantitative thermobarometer of Ernst and Liu (1998) at temperatures around 900 ºC calculated with QUILF on coexisting Cpx-Opx in the cumulitic hornblende pyroxenite xenolith. In addition, the paucity of plagioclase phenocrysts and common Opx-Hbl-Cpx "glomerocrysts", for an andesitic composition, would indicate (Blatter and Carmichael, 1998) minimum crystallization pressures around 4.3 kbar or about 15 km of depth.

Contiguous hornblende and plagioclase in the ultramafic xenolith, using the method of Holland and Blundy (1994), yielded crystallization temperatures between 886 and 930 ºC, whereas a temperature of 950 ºC was obtained using the method of Saxena *et al.* (1986) based on the distribution of Fe and Mg between orthopyroxene and clinopyroxene in igneous and metamorphic rocks.

On these bases, it may be concluded that maximum temperatures attained by the Puente Negro xenoliths inside the magma or in the solid crust varied between 961 ºC (pargasitic hornblende stable) to more than 1100 ºC (mullite-tridymite-highly siliceous melts), whereas peak pressures are only constrained to a minimum of about 5 kbar but probably reached 8 kbar or more. Quemographic representations of stable mineral assemblages of Puente Negro metamorphic high-Al xenoliths and the garnet coronas are illustrated in Figure 10, whilst a graphic summary of the peak thermal conditions as derived from their critical and inferred mineral assemblages is given in Figure 11.

Geochemistry of the Puente Negro intrusion

The whole rock geochemistry of the Puente Negro andesite (PN44, Table 3) is comparable to that of andesitic to basaltic andesite lavas of similar age exposed to the east, in the western sector of the state of Oaxaca (Martiny *et al*., 2000). In Harker diagrams of major and trace elements (not shown) as well as in chondrite-normalized rare earth element (REE) diagrams and primitive mantle normalized multi-element variation diagrams (Figures 12a and 13a), the least contaminated sample collected at Puente Negro (PN44) displays patterns similar to the Oaxaca lavas, although it is slightly more enriched in Pb and REE, particularly the heavy REE (HREE) and heavier middle REE (MREE). Enrichment in Pb can be explained by the participation of a crustal component in the genesis of the magmas. Amphibole, which is abundant in the Puente Negro andesite, controls enrichment in the heavier MREE relative to LREE and HREE (partition coefficients are particularly high from Dy to Er) (*e.g.*, Arth, 1976; Green and Pearson, 1985; Schnetzler

and Philpotts, 1970) and can explain MREE enrichment, whereas the probable presence of minute garnet xenocrysts in the andesite could explain HREE enrichment.

Preliminary data on Sr, Nd and Pb isotopic data presented in this work for Puente Negro intrusive body (Table 13) confirm substantial assimilation of ancient crust by the original magmas, since the more radiogenic sample (PN15b) displays an initial $(^{87}Sr/^{86}Sr)_i$ value of 0.706252, and initial $(\varepsilon Nd)_i$ of -2.4 (Figure 14). The depleted mantle model age (T_{DM}) is 0.98 Ga. Present-day $^{206}Pb/^{204}Pb$, $^{207}Pb/^{204}Pb$ and $^{208}Pb/^{204}Pb$ ratios of this sample are 18.846, 15.637, and 38.759, respectively. Another sample of the Puente Negro intrusive body (PN44) displays a smaller degree of assimilation and shows a $(^{87}Sr/^{86}Sr)_i$ ratio of 0.704635, an $(\varepsilon Nd)_i$ of -1.6, and a similar T_{DM} age of 1.01 Ga. PN44 lies on the radiogenic side of the field corresponding to the western Oaxaca lavas (Figure 14), which are slightly less contaminated by old crustal material. Present-day $^{206}Pb/^{204}Pb$, $^{207}Pb/^{204}Pb$ and $^{208}Pb/^{204}Pb$ ratios of PN44 are 18.768, 15.620, and 38.634, falling within the field of early Oligocene lavas from western Oaxaca, which display a linear trend with a positive slope in Pb isotope diagrams (Figures 15a and 15b). It is interesting to note that the linear array of these lavas points toward the gneissic xenoliths from Puente Negro (Figures 15a and 15b). The linear trend of the lavas suggests a mixing line between a mantle source and a crustal component rich in ^{206}Pb, ^{207}Pb, and ^{208}Pb, such as the upper crust or sediments, similar to the composition of the metapelitic gneiss (PN17).

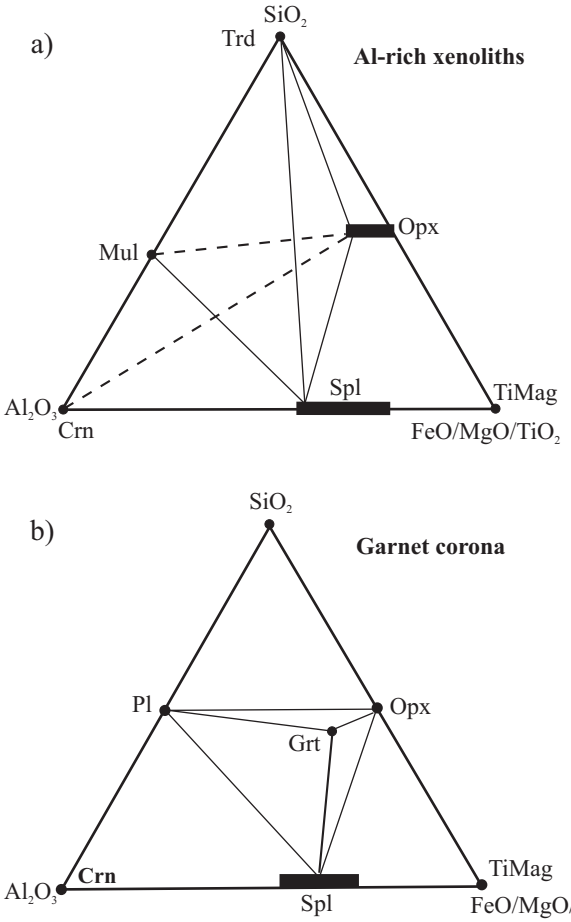

Figure 10. a) Quemographic phase relations in the system SiO_2-Al_2O_3-FeO/MgO/TiO_2 (PN1, PN17, PN19, PN 29, 29698). Rutile may be stable instead of TiMag. Note the aluminous nature of orthopyroxene. From textural observations Opx with corundum or mullite may not be in equilibrium, suggesting the decompression reactions Opx_{ss} + 2Crn = Spl + Al-Sil_{ss}, and Al-Sil_{ss} + Opx = Spl + 2Trd. b) Quemographic phase relations in the system CaO-Al_2O_3-FeO/MgO/TiO_2 (partially melted xenoliths FO6605 and 11679). Note the absence of aluminous phases (including Al-Opx) in these xenoliths entrained at a very shallow level. Zoisite, although stable with glass and tridymite/quartz, may be incompatible with orthopyroxene considering the oxidizing-dehydration reaction Opx + 2Zo + Qz + ½O_2 = 3An + Di + H_2O, suggested by crossing tie lines in the triangle and the high temperature nature of the event.

Geochemistry and isotopic composition of the Puente Negro xenoliths

In chondrite-normalized diagrams, the REE patterns of the xenoliths analyzed are roughly sub-parallel, particularly the two gneisses (PN17 and PN1b). The deep-seated garnetiferous gneiss is strongly REE enriched, with elevated HREE concentrations of 27 times the chondritic values (Figure 12b) that can be accounted for by the presence of garnet. PN17 is also characterized by LREE enrichment with chondrite-normalized $(La/Yb)_N = 7.3$, and a very slight negative Eu anomaly (Eu/Eu* = 0.80). The quartzose gneiss (PN1b) has much lower REE concentrations, with HREE

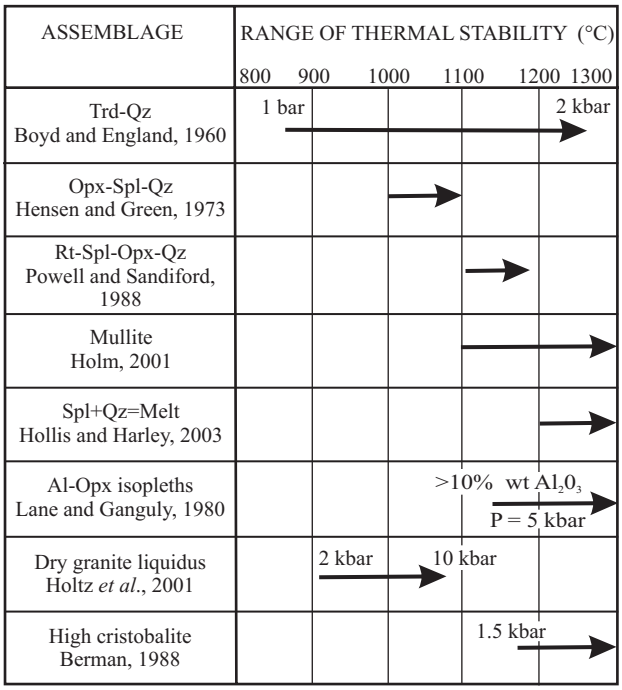

Figure 11. Thermal stability range for phases and assemblages that characterize Puente Negro.

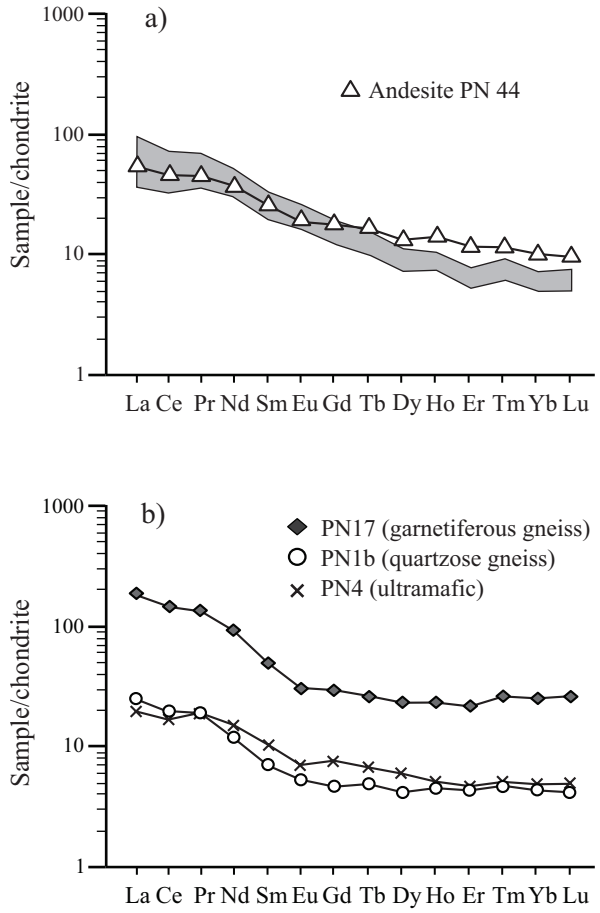

Figure 12. Chondrite-normalized rare earth element (REE) composition of (a) the Oligocene Puente Negro andesite (PN44) and, for comparison, andesites and basaltic andesites of similar age from nearby western Oaxaca (shaded area). Slight enrichment of the heavy REE (Dy-Lu) in the Puente Negro dikes with respect to western Oaxaca lavas may be due to the presence of common garnet xenocrysts. (b) Puente Negro xenoliths. Data for western Oaxaca lavas from Martiny *et al.,* (2000). Chondrite values from Nakamura (1978) and Haskin et al. (1968).

concentrations of 4–5 times the chondritic values, and shows a comparable LREE enrichment [$(La/Yb)_N = 6$]. The amphibole pyroxenite (PN4) displays a slightly fractionated REE pattern [$(La/Yb)_N = 4$], has a very slight negative Eu anomaly (Eu/Eu* = 0.78), and HREE concentrations of 5 times the chondritic values. The presence of amphibole in this xenolith can explain the slight enrichment in the heavier MREE.

In primitive mantle normalized multi-element variation diagrams, trace element contents of the xenoliths display strong enrichment in Cs, Pb, Th, and U. The relative depletion in fluid immobile incompatible elements, such as Nb, Ta and Ti (Figure 13b) suggests a subduction component in the protolith. Enrichment in Zr, Hf, and U, and Th in the gneiss xenoliths is likely controlled by zircon, which has high distribution coefficients for these elements.

The Sr, Nd and Pb isotopic compositions of the Puente Negro xenoliths provide a preliminary insight on the nature of the basement under the Acatlán Complex (Table 13). For reference, Sr and Nd isotope ratios were also determined for the basement rocks outcropping in the uppermost crust intruded by the Puente Negro andesite (Esperanza Granitoids of the Acatlán Complex, Figure 2b). The gneissic xenoliths (PN1, PN1b, PN17), which originated in the lower crust, display little variation in initial $^{87}Sr/^{86}Sr$ ratios (calculated for 30 Ma), with ratios between 0.7144 and 0.7148, and $(\varepsilon Nd)_i$ values varying from -10.9 to -8.2. Sr and Nd isotope ratios of the country rock (Esperanza Granitoids) of the Puente Negro andesite is much more radiogenic (Figure 14, Table 13), indicating that there is probably no genetic relationship to the xenoliths. Surprisingly, the ultramafic cumulate xenolith (PN4) is more radiogenic than the hosting andesite [$(^{87}Sr/^{86}Sr)_i = 0.711$, $(\varepsilon Nd)_i = -3.7$] (Table 13), suggesting participation of at least two magma batches, one substantially more contaminated at depth and parental to the gabbroic xenoliths and hornblende xenocrysts, and a new basaltic magma that entrained all the xenolithic material; these magmas further assimilated upper crustal rocks yielding the present andesitic-dacitic composition of the Puente Negro intrusion. Pb isotope ratios of the amphibole pyroxenite are slightly more radiogenic (19.011, 15.683, 39.001) than those of the gneissic xenoliths ($^{206}Pb/^{204}Pb$=18.808–18.878, $^{207}Pb/^{204}Pb$=15.650–15.677, and $^{208}Pb/^{204}Pb$=38.790–38.937) (Figure 15, Table 13).

The gneissic xenoliths analyzed have pre-Grenvillian model ages (T_{DM} = 1.26, 1.40 and 1.52 Ga), which hint at the presence of old components in the local lower crust. It has been suggested previously that the Acatlán Complex overlies an unknown Precambrian continental crust, tentatively considered Grenvillian in age (Ortega-Gutiérrez *et al*., 1990). Model ages of the Grenvillian Oaxacan Complex (1.49–1.60), situated to the east, are relatively close to those of the studied gneissic xenoliths and seem to support this hypothesis.

DISCUSSION

Polymetamorphic evolution of the gneissic xenoliths

Petrologically distinguishing between original metamorphic assemblages and source of xenoliths from the superimposed low pressure, purely thermal event was difficult to establish. Thermal resetting and absence of appropriate mineral geobarometers (*i.e.*, absence of quartz, olivine, or cordierite in the decompression coronas of garnet) did not permit pressure determinations, but this central issue eventually may be addressed through the study of abundant fluid-solid and melt inclusions present in most xenoliths of Puente Negro (*e.g.*, Sachs and Hansteen, 2000).

Pyrometamorphism

Phase stability in the sanidinite facies and pyrometa-

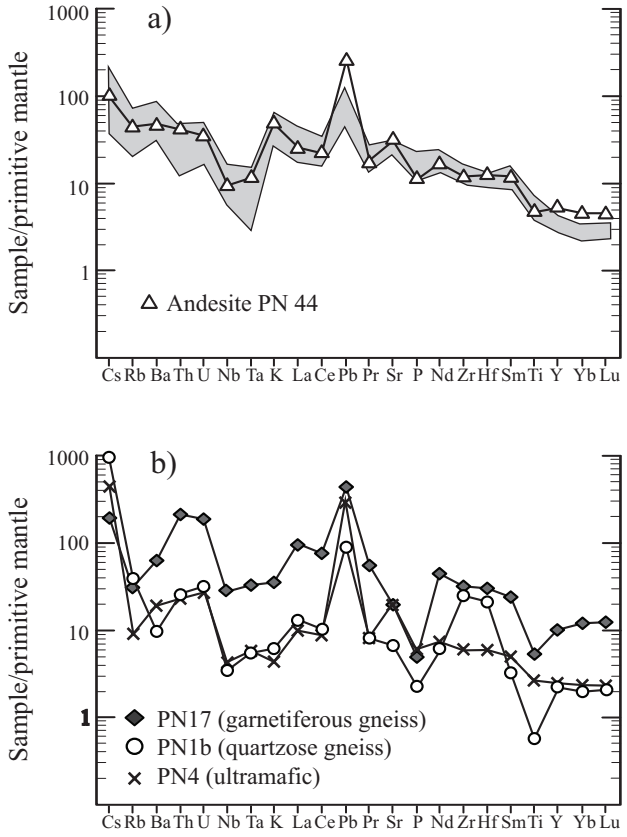

Figure 13. Primitive mantle normalized multi-element variation diagrams for (a) Puente Negro andesite and nearby western Oaxaca lavas (shaded area) of similar age, and (b) Puente Negro xenoliths. Data for western Oaxaca lavas from Martiny *et al.,* (2000). Primitive mantle values from Sun and McDonough (1989).

morphism (*e.g.*, Grapes, 2006 and references therein) is well established at Puente Negro by the abundance of glass and tridymite, both fresh (high tridymite) and inverted to quartz, as well as by coexisting sanidine, orthopyroxene, clinopyroxene, spinel, mullite, and calcic plagioclase. The former presence of high-tridymite rims about quartz in most quartzose xenoliths would indicate minimum temperatures of 867 ºC at 1 bar pressure, and above 1100 ºC at pressures around 1 kbar (Boyd and England, 1960). Moreover, textural and mineralogical data indicate even more extreme contact metamorphism involving several dry partial melting reactions such as Spl + Qz/Trd = Mul + melt, Pl = Mul + melt, and Ab + Qz = melt, or Or + Qz = melt, all of which would occur at temperatures above 1000 ºC at low pressures. Pseudomorphic assemblages in xenoliths of Opx-glass, Spl-Opx-glass ± Al-silicate$_{ss}$, Spl-Opx-Pl-Crn ± glass after garnet or biotite, and Spl-Pl-Cpx-Ilm after amphibole, constitute evidence of incongruent melting of those mafic phases at very high temperature and variable pressures. Sillimanite in fact should be converted to mullitic Al-silicate$_{ss}$ above 1000 ºC at low pressure (*cf.* Pugin and Kuskov, 1968; Schreyer, 1976; Cameron, 1976; Grapes, 2006). Based on the interpretation of textures and secondary mineral assemblages in symplectites, it is assumed that biotite was present in some of the metasedimentary xenoliths, and that it melted incongruently to symplectitic pseudomorphs of Opx-Spl-glass ± Al-silicate$_{ss}$. Temperatures in excess of 1100 ºC at low pressures also may explain the virtual absence of cordierite in the Puente Negro xenoliths, as it probably was replaced in the reaction Crd = 2Spl + 5Trd (*cf.* Harris, 1981). At near surface conditions, the anhydrous assemblage albite + quartz melts at ~1015 ºC (Wen and Nekvasil, 1994), a reaction suggested at Puente Negro by colorless glass mantling albite grains in former contact with quartz. Finally, orthorhombic mullite, would require temperatures above 1150 ºC (Johnson *et al.*, 2001; Grapes, 2006), whilst the presence of Spl-Opx-Qz/Trd-Rt-Ilm in many of the Puente Negro xenoliths also implies temperatures in excess of 1100 ºC and low $a(O_2)$ (Powell and Sandiford, 1988).

The breakdown of igneous pargasite before and during the final ascent of the gabbroic xenoliths from the middle crust suggests magmatic recharge and heating above 1000 ºC, whereas the occasional presence of tridymite in gneissic xenoliths stoped from the adjacent country rocks would imply minimum emplacement temperatures near the quartz-tridymite transition at 867 ºC. At the maximum temperatures (>1000 ºC) and very low pressure envisaged for the Puente Negro intrusion, high cristobalite would form metastably from high quartz in a narrow window between 1.5 and 2 kbar (Berman, 1988). High tridymite at these pressures would form in its own stability field at temperatures near 1200 ºC, remaining stable to temperatures of about 900 ºC during the final emplacement of the andesite. The stability of tridymite is consistent with temperatures calculated from ilmenite-magnetite pairs present in the shallow buchitic xenolith (FO6605), the values of which vary from 861 to 909 ºC applying the ILMAT program of Lepage (2003), and geothermometry by Powell and Powell (1977), Spencer and Lindsley (1981), and Andersen and Lindsley (1988). Finally, titanite coexisting with orthopyroxene and spinel suggests (*cf.* Xirouchakis *et al.*, 2001) high f_{O_2} and temperatures below 650 ºC at some point in the final cooling history of the intrusion.

Deep-seated metamorphism?

The evidence suggesting that some of the xenoliths and high-Al xenocrysts represent very high-grade metamorphic rocks that suffered considerable decompression before contact metamorphism consists of: (a) xenoliths with abundant relict garnet showing unfractured, inclusion-free calcium-poor unzoned cores in sharp contact with calcium-rich fractured rims mantled by kelyphitic coronas with the assemblage Pl-Spl-Opx ± Crn ± glass, (b) xenocrysts of Al-rich orthopyroxene rimmed by an Al-poor type associated with the decompression coronas of some garnets, (c) xenocrysts of sapphire, corundum, and spinel in the andesitic intrusion, and (d) the rare occurrence of Opx-Sil (PN42), implying pressures close to or above 8

Table 13. Sr, Nd and Pb isotope data for selected samples of the Puente Negro intrusion and xenoliths, and units of the Acatlán Complex.

(a) Sample	Rock type	Rb	Sr	Sm	Nd	$(^{87}Sr/^{86}Sr)_m$	$1s_{abs}$	$^{87}Rb/^{86}Sr$	$(^{87}Sr/^{86}Sr)_i$	$(^{143}Nd/^{144}Nd)_m$	$1s_{abs}$	$^{147}Sm/^{144}Nd$	$(^{143}Nd/^{144}Nd)_i$	$(\varepsilon Nd)_0$	$(\varepsilon Nd)_i$	T_{DM}
Puente Negro																
PN15b	Puente Negro intrusion (dacite)	22.1	645	4.36	20.7	0.706295	± 36	0.0991	0.706253	0.512503	± 18	0.1272	0.512478	-2.6	-2.4	0.98
PN44	Puente Negro intrusion (andesite)	28.9	662	5.27	23.5	0.704689	± 37	0.1264	0.704635	0.512544	± 16	0.1356	0.512517	-1.8	-1.6	1.01
PN17	Garnetiferous gneiss xenolith	19.2	468	10.77	58.2	0.714481	± 37	0.1191	0.714430	0.512199	± 19	0.1118	0.512177	-8.6	-8.2	1.26
PN1	Quartzose gneiss xenolith	20.6	127	1.31	6.8	0.714855	± 40	0.4703	0.714655	0.512064	± 26	0.1170	0.512041	-11.2	-10.9	1.52
PN1b	Quartzose gneiss xenolith	23.7	143	1.42	7.6	0.714999	± 39	0.4803	0.714794	0.512114	± 16	0.1130	0.512092	-10.2	-9.9	1.40
PN4	Amphibole pyroxenite xenolith	5.4	421	2.31	9.5	0.710988	± 36	0.0375	0.710972	0.512439	± 16	0.1470	0.512410	-3.9	-3.7	1.37
Acatlán Complex																
Chaz-1	Schist (Chazumba Formation)	81.6	254	6.03	32.1	0.714651	± 51	0.9316	0.714254	0.512120	± 13	0.1134	0.512098	-10.1	-9.8	1.39
Cos-1	Schist (Cosoltepec Formation)	226.5	85	10.61	55.4	0.751238	± 44	7.7070	0.747954	0.511973	± 16	0.1157	0.511950	-13.0	-12.7	1.63
CON-300	Augen gneiss (Esperanza Granitoids)	124.9	118	10.29	54.6	0.732326	± 38	3.0688	0.731018	0.512236	± 22	0.1139	0.512214	-7.8	-7.5	1.24
MD202	Augen gneiss (Esperanza Granitoids)	91.0	176	9.05	54.1	0.726175	± 35	1.5036	0.725534	0.512039	± 20	0.1011	0.512019	-11.7	-11.3	1.35
AC-05W #	Augen gneiss (Esperanza Granitoids)	91.3	176	9.07	44.3	0.726560		1.5036	0.725919	0.512101		0.1238	0.512077	-10.5	-10.2	1.57
Toto-1	Trondhjemite (Totoltepec stock)	6.5	195	4.04	13.1	0.704991	± 33	0.0958	0.704950	0.512685	± 14	0.1868	0.512648	0.9	1.0	1.85

(b) Sample	Material analyzed	Material	$^{206}Pb/^{204}Pb$	$1s_{rel}$	$^{207}Pb/^{204}Pb$	$1s_{rel}$	$^{208}Pb/^{204}Pb$	$1s_{rel}$
Puente Negro								
PN15b	Puente Negro intrusion (dacite)	WR	18.846	0.020	15.637	0.021	38.759	0.024
PN44	Puente Negro intrusion (andesite)	WR	18.768	0.021	15.620	0.025	38.634	0.031
PN17	Garnetiferous gneiss xenolith	WR	18.808	0.030	15.650	0.029	38.790	0.031
PN1	Quartzose gneiss xenolith	WR	18.878	0.040	15.677	0.041	38.937	0.055
PN1b	Quartzose gneiss xenolith	WR	18.824	0.026	15.672	0.029	38.909	0.030
PN4	Amphibole pyroxenite xenolith	WR	19.011	0.071	15.683	0.070	39.001	0.074
Acatlán Complex								
Chaz-1	Schist (Chazumba Formation)	WR	18.678	0.022	15.654	0.026	38.686	0.030
Cos-1	Schist (Cosoltepec Formation)	WR	19.900	0.080	15.796	0.098	40.469	0.124
CON-300	Augen gneiss (Esperanza Granitoids)	WR	19.047		15.672		39.103	
CON-300	Augen gneiss (Esperanza Granitoids)	Kfs	18.621	0.035	15.679	0.048	38.334	0.063
Xaya-1	Ultramylonite (Xayacatlán Formation)	WR	20.584	0.020	15.684	0.022	39.761	0.022
MM-2	Magdalena migmatite	Kfs	18.596	0.043	15.618	0.045	38.389	0.047
MM-5	Magdalena migmatite	Kfs	18.607	0.016	15.631	0.019	38.429	0.019
Toto-1	Trondhjemite (Totoltepec stock)	WR	18.475	0.021	15.612	0.022	38.284	0.023
Toto-1	Trondhjemite (Totoltepec stock)	Pl	18.329	0.017	15.597	0.018	38.142	0.019

WR: whole rock. Element concentrations (in ppm) obtained by isotope dilution, with the exception of PN44 (ICP-MS). Initial Sr and Nd isotope ratios calculated for 30 Ma, using a $^{143}Nd/^{144}Nd$ (CHUR) of 0.512638. $1s_{abs}$ errors refer to the last two digits. Laboratory values of the NBS 987 standard, the Nd La Jolla standard and the NBS 981 Pb standard are: $^{87}Sr/^{86}Sr = 0.710235 \pm 18$ ($1s_{abs}$, $n = 250$); $^{143}Nd/^{144}Nd = 0.511877 \pm 21$ ($1s_{abs}$, $n = 138$); $^{206}Pb/^{204}Pb = 16.8926 \pm 0.04\%$ ($1s_{rel}$), $^{207}Pb/^{204}Pb = 15.4272 \pm 0.06\%$ ($1s_{rel}$), $^{208}Pb/^{204}Pb = 36.5089 \pm 0.08\%$ ($1s_{rel}$). Total blanks during these runs were 8.04 ng for Sr, 8.87 ng for Nd, and 509 pg for Pb. # taken from Yañez *et al*. (1991).

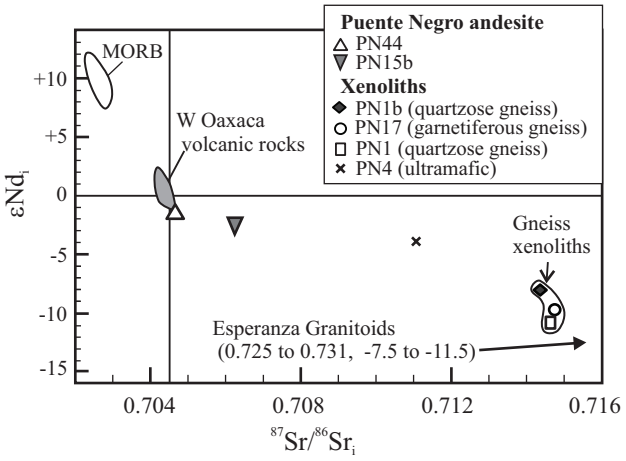

Figure 14. Initial Sr and Nd isotope values for the Puente Negro intrusion and xenoliths, Esperanza Granitoids, and early Oligocene lavas from western Oaxaca. Data for western Oaxaca lavas from Martiny *et al.,* (2000).

kbar (*e.g.*, Carrington and Harley, 1995; Harley, 2004). The stable presence of corundum with orthopyroxene in some of the pseudomorphs and garnet coronas may indicate very restricted bulk chemical compositions and P-T conditions proper of the lower crust (Kelly and Harley, 2004). In granulites of Sri Lanka, coronas of Opx-Crn around garnet formed on decompression from 9 to 7.5 kbar (Kriegsman and Schumacher, 1999). The fact that relatively high-pressure phases such as garnet and aluminous hornblende suffered decompression melting, as discussed above, also suggests relative deep crustal levels for the entrainment of some of the xenoliths. Hayob *et al.* (1989) described rims of orthopyroxene and green spinel with interstitial glass or plagioclase around garnets in deep-seated granulites from northern Mexico, and suggested an origin by incongruent melting of garnet, as xenoliths ascended in the basaltic magma from a deep source. Similar conditions may have prevailed during the kelyphitic breakdown of garnets at Puente Negro.

An alternative explanation for the presence of high-Al xenoliths in Puente Negro is to consider the presence at crustal depth of a high-temperature thermal aureole around a gabbroic intrusion similar in many aspects to the Voisey's Bay Intrusion of Labrador, Canada (Mariga *et al*., 2006a, 2006b). There, small xenoliths (2–10 cm) were converted through reaction of country gneisses with the gabbroic magma into aggregates of spinel-plagioclase-corundum in proportions very similar to those found in the high-Al pseudomorphs at Puente Negro. Here, further injection of subcrustal magmas may have traversed this hypothetical aureole carrying the pseudomorphic xenoliths near to surface conditions. However, gabbroic xenoliths other than the hydrous porphyries and ultramafic cumulates are lacking, and the high temperatures required to produce the assemblages described above could not be provided by a hydrous magma from which the hornblende-rich rocks crystallized.

Ascent history and source of xenoliths

Insights into the magma ascent rates for the final pulse may be gained from the nature of opacite and gabbroic coronas developed virtually on all amphiboles, both in the andesite and in the gabbroic xenoliths. These rims usually form by dehydration during ascent and dewatering of hydrous magmas (Blatter and Carmichael, 2001). Because opacitic rims may range from almost absent to the complete replacement of amphibole, injection of different batches of magma into a chamber or variable position in the flow channel of the Puente Negro intrusion probably controlled the ascent rates to the surface. The anhydrous gabbroic opacitic replacement of pargasite would require interaction with a hot magma and ascent times much longer

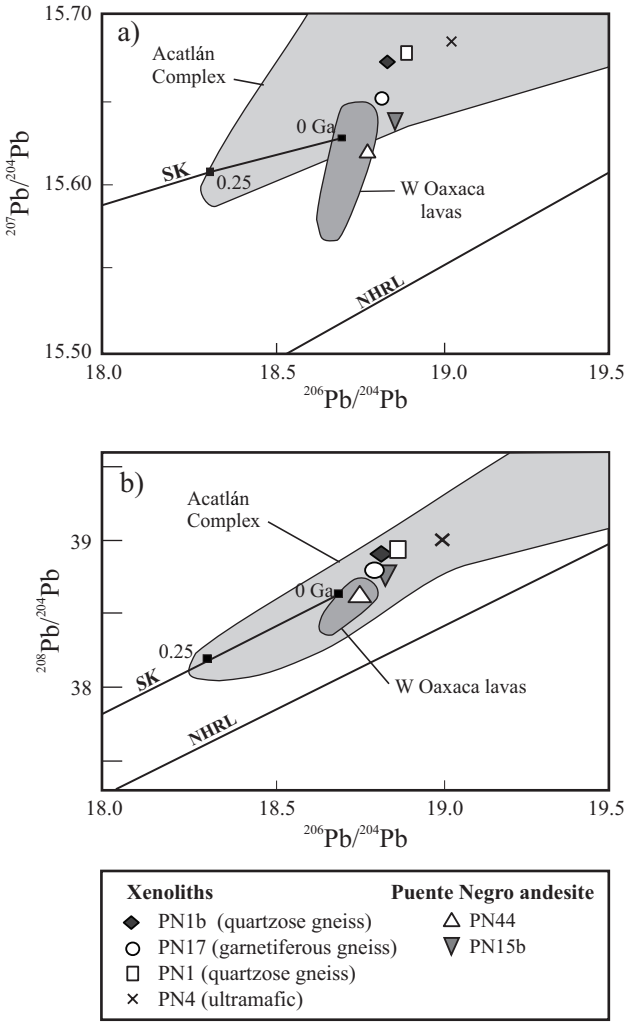

Figure 15. Pb isotope ratios for the Puente Negro intrusion and xenoliths, and early Oligocene andesitic and basaltic andesite lavas from western Oaxaca. The field for representative samples from Acatlán Complex is indicated. Shown for reference are the NHRL (Northern Hemisphere Reference Line, defined by Hart, 1984), along which most northern hemisphere MORB and OIBs lie, and SK, the Pb isotopic evolution curve, as defined by Stacey and Kramers (1975).

than a few days, whereas pristine amphibole in some pulses of the Puente Negro magma would require ascent rates >2 cm/s (Rutherford and Devine, 2003). Assuming a mean depth of about 15 km for the gabbroic differentiating body, this distance would be traversed in less than a week, as envisaged for the Santa Elena eruption on the basis of the absence of opacite rims in amphibole (Rutherford and Hill, 1993).

Moreover, the common preservation of glass and abundance of microlites in the andesite, as well as glass with quenched plagioclase in the gabbroic and ultramafic xenoliths, suggest (*e.g.*, Cashman and Blundy, 2000) explosive ascent rates (*ca*. 1 m/s) for some pulses of the Puente Negro intrusion.

Figure 16 shows selected very high temperature phase equilibria in the system FMAS and a tentative P-T trajectory for the Puente Negro granulitic xenoliths, whereas Figure 17 illustrates a preferred albeit simplified mantle-crust scenario where the magma-xenolith plumbing system might have evolved. An original basaltic batch envisaged for the first intrusive event at Puente Negro (hydrous gabbroic magma) requires a primary source in the upper mantle underlying a hot Cenozoic crust more than 40 km thick (*ca*. 11 kbar) (*cf.* Valdés *et al.*, 1986); and its transient stagnation in the middle crust (15–20 km) at temperatures near 1000 ºC and pressures of 5–6 kbar. There, the basaltic magma cooled and differentiated by fractional crystallization in a chamber at high water pressures, with the successive but overlapping crystallization of clinopyroxene, orthopyroxene, amphibole, and plagioclase, forming a mafic-ultramafic cumulate complex represented by "glomerocrysts" and hornblende-pyroxene rich xenoliths. The more siliceous residual melt eventually mixed with high temperature basaltic batches that recharged the evolving magma chamber and triggered the rapid extrusion of the residual magma and both gabbroic and metamorphic xenoliths. Interactions between multiple basaltic sills emplaced at temperatures above 1200 ºC and a hot lower crust could in theory melt and assimilate much of that crust, leaving residues of refractory phases, such as anorthite, corundum, spinel, Al-orthopyroxene, sillimanite, and garnet, which are present in the actual xenocrysts and xenolithic phases of the Puente Negro intrusion. Refractory xenoliths and xenocrysts would have been taken from the local lower crust by the new magma, decompressed and cooled *en route* to its final emplacement near the surface, together with fragments of the partially crystallized hornblende-rich gabbroic batch.

Although another possible source for the high-grade xenoliths could be the exposed units of the local Acatlán Complex (augen gneisses), which during pyrometamorphism may in principle also yield the anhydrous, high-Al assemblages that characterize the gneissic xenoliths, the isotopic compositions of those rocks are indeed different (Table 13). Also, the abundance of garnet in Puente Negro xenoliths and xenocrysts excludes the low-grade phyllites and quartzites of the underlying Cosoltepec Formation as the

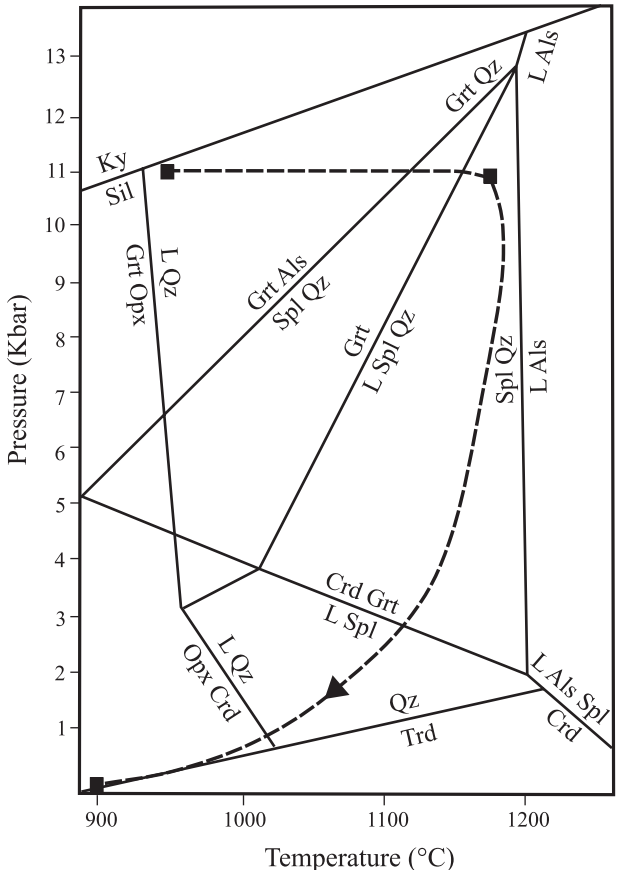

Figure 16. A model proposed for the origin and evolution of the Puente Negro xenoliths and transporting magma. Position and temperatures of magmatic bodies are inferred from geothermobarometric data as determined for the deep, intermediate and shallow emplacement levels represented by the studied petrologic systems.

source for the high-grade xenoliths. Likewise, the different composition of garnets from the Acatlán Complex high-pressure rocks (Reyes-Salas, 2003) also seems to exclude the gneissic rocks exposed in the surface as the source for the Puente Negro garnetiferous xenoliths. In fact, the local Acatlán Complex lacks staurolite, and its possible presence in the corundum-spinel-plagioclase pseudomorphs, or in combination with spinel, garnet, sillimanite, and corundum, thus strongly suggests entrainment of metapelitic xenoliths from crustal levels under the Acatlán Complex. Moreover, eclogitic garnets of that complex usually contain abundant inclusions of epidote, rutile, and quartz, contrary to the clean, unfractured nature of all garnet xenocrysts in the volcanic rock, and porphyroblasts found in the Puente Negro xenoliths. On the other hand, polyphase, very high-grade deep-seated metamorphism in the xenoliths is suggested by assemblages with spinel, plagioclase, orthopyroxene, garnet, and titanomagnetite defining foliated fabrics, where spinel or magnetite are mantled by Al-orthopyroxene, and garnet porphyroblasts display compositions unlike those of garnets in the local, high pressure quartzo-feldspathic gneisses of the Acatlán Complex (Reyes-Salas, 2003), which

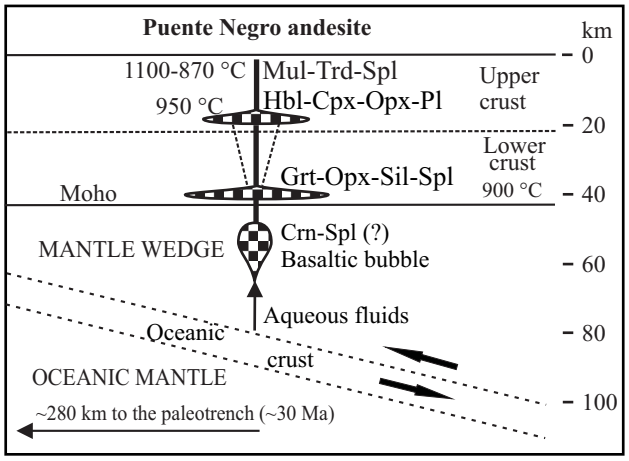

Figure 17. Schematic geological model for the depth-temperature history path of the Puente Negro magma-xenolith-xenocryst system, from inception in the mantle wedge (basalt) to emplacement near the surface (andesite).

are extremely rich in calcium (10–20 CaO wt. %). Rare coronitic textures of spinel-orthopyroxene around garnet that exclude plagioclase suggest strong decompression of almandine-pyrope garnet at UHTM (ultrahigh temperature metamorphism) conditions by the reaction Grt = 2Opx + Spl + Qz_{melt} (73 % molar volume increase).

This complex petrologic content of Puente Negro gneissic xenoliths is considered to be the result of high or ultrahigh temperature pre-Mesozoic granulitic metamorphism followed by Oligocene sanidinite facies pyrometamorphism. The presence of relict orthopyroxene and sillimanite in two of the studied xenoliths stands as direct evidence of ultrahigh temperature granulite facies metamorphic rocks underlying the Acatlán Complex. Finally, the common presence of spinel and corundum inclusions in plagioclase phenocrysts, and sapphire, spinel, and high-Al orthopyroxene xenocrysts in the andesitic volcanic matrix, would also support the subcrustal or lower crustal provenance and therefore original basaltic character of the Puente Negro andesite.

CONCLUDING REMARKS

The abundance and diversity of xenoliths in the Puente Negro shallow intrusion and paragenetic textural relationships of the magmatic-metamorphic system posed several questions, some of which remain poorly resolved: (a) Did the host magma (now andesitic) originally have a basaltic composition?. The answer in this case may be positive because the coexistence of basaltic magma stagnated in the middle crust and represented by xenoliths of mafic-ultramafic cumulates (hydrous, relative low temperature, low silica) and the following "andesitic" magma (high silica, relative high temperature) in principle indicate the presence of a typical basaltic magma chamber periodically replenished by hot basaltic magma (*e.g.*, Murphy *et al*., 2000). The andesitic dikes hosting the xenoliths would represent the latest, originally basaltic batch that interacted with the deep crust (high-grade metapelites), sampled the mafic cumulitic products of previous basaltic magma differentiated in the middle crust (gabbroic xenoliths), and strongly interacted with the upper exposed crust (buchitic xenoliths). The final result of these processes was the present andesite-dacite subvolcanic complex and its load of xenoliths taken at three different levels in the crust. Textural, chemical, geochronological, and isotopic data, as discussed above, support this conclusion.

(b) Do some of the xenoliths represent Paleogene residues of partial melting at depth beneath the Acatlán Complex? The answer to this question also may be positive because the minimum emplacement pressures calculated for the underplated gabbroic magma equivalent to 15–20 km require that some xenoliths were entrained at this or greater depth, where rocks of the Acatlán Complex most probably are no longer present. Moreover, the extremely aluminous composition of many xenoliths and the actual presence of high-grade calcsilicate xenoliths indicate protoliths that are rare or absent in the Acatlán Complex. Finally, complex decompressional coronas and composite zoning patterns of garnet xenocrysts and in garnetiferous xenoliths also indicate a deep and distinct crustal source other than the Acatlán Complex.

(c) Are the high-alumina phases and pseudomorphs in the andesitic magma former phenocrysts that crystallized at mantle pressures, or just xenocrysts remaining as a product of metapelitic xenolith disaggregation? This question remains open because evidence of magmatic crystallization of corundum or spinel is texturally inconclusive, while many of the metamorphic xenoliths are corundum and spinel-bearing, thus providing another plausible source for these crystals.

(d) What were the magma ascent rates? Magma-crust interactions occurred at different levels in Puente Negro, one being very shallow (a few hundreds meters at most), but other, much deeper levels are evident. Complex decompression reaction textures and preserved mineral assemblages stable at middle or lower crustal levels (hypersthene-sillimanite, staurolite-spinel-sillimanite, hypersthene-corundum-spinel), and quenched, glass-rich residual magma in gabbroic xenoliths, require fast movement of some magmas towards the surface. The presence of rare pristine amphibole (without dehydration rims) in gabbroic xenoliths and host magma is considered strong evidence for explosive ascent rates of magmas from its middle crust chamber.

(e) Which were the main processes of magmatic differentiation? Fractional crystallization is supported by abundance of cumulate mafic-ultramafic xenoliths and "glomerocrysts" of gabbroic composition in the extrusive andesite, whereas assimilation is physically visible in the melting and metasomatic reactions that occurred between xenoliths and magma at different levels in the crust. Moreover, abundant quartz xenocrysts, extensive melting

of xenoliths, the presence of other exotic high-Al phases that could be considered xenocrysts (corundum, spinel, Al-orthopyroxene), and highly radiogenic Nd, Sr, and Pb isotopes of the magmas further support crustal assimilation as an important additional process in the evolution of the Puente Negro magmas.

ACKNOWLEDGMENTS

This research was partly funded by PAPIIT grant IN104706 from the DGAPA at UNAM, and benefited by the kindness of many people at UNAM: Rufino Lozano, and Patricia Girón made some of the XRF analyses, and Diego Aparicio prepared and polished thin sections on which the study was based; we specially thank Hugo Delgado and Carlos Linares for facilitating the use of the electron microprobe at the Laboratorio Universitario de Petrología at UNAM. We thank Gilles Levresse, of the Centro de Geociencias, UNAM, for ICP-MS analyses of the xenoliths. We are also grateful to the following persons at the Instituto de Geología and the Instituto de Geofísica, UNAM, who helped in different ways with the analytical work: At the Laboratorio Universitario de Geoquímica Isotópica Gabriela Solis assisted in the clean lab, and Juan Julio Morales measured the isotopes, María del Sol Hernández measured the K content of the plagioclase used for dating the andesite, and Elena Lounejeva carried out some of the ICP-MS analyses. This work was substantially improved by the extremely careful and constructive review of J. Jorge Aranda-Gómez.

REFERENCES

Aguirre-Díaz, G., Dubois, M., Laureyns, J., Schaaf, P., 2002, Nature and P-T conditions of the crust beneath the central Mexican Volcanic Belt based on a Precambrian crustal xenolith: International Geology Review, 44, 222-242.

Andersen, D.J., Lindsley, D.H., 1988, Internally consistent solution models for Fe–Mg–Mn–Ti oxides: Fe–Ti oxides: American Mineralogist, 73, 714-726.

Andersen, D.J., Lindsley, D.H., Davidson, P.M., 1993, QUILF: a Pascal program to assess equilibria among Fe-Mg-Mn-Ti oxides, pyroxenes, olivine, and quartz: Computers and Geosciences, 19, 1333-1350.

Arth, J.G., 1976, Behavior of trace elements during magmatic processes – A summary of theoretical models and their applications: Journal of Research, U.S. Geological Survey, 4(1), 41-47.

Bachmann, O., Dungan, M.A., 2002, Temperature-induced Al-zoning in hornblendes of the Fish Canyon magma, Colorado: American Mineralogist, 87, 1062-1076.

Beard, J.S., Ragland, P.C., Crawford, M.L., 2005, Reactive bulk assimilation: A model for crust-mantle mixing in silicic magmas: Geology, 33, 681-684.

Berman, R.G., 1988, Internally-consistent thermodynamic data for minerals in the system Na_2O-K_2O-CaO-MgO-FeO-Fe_2O_3-Al_2O_3-SiO_2-TiO_2-H_2O-CO_2: Journal of Petrology, 29, 445-522.

Blatter, D.L., Carmichael, I.S.E., 1998, Hornblende peridotite xenoliths from central Mexico reveal the highly oxidized nature of subarc upper mantle: Geology, 26, 1035-1038.

Blatter, D.L., Carmichael, I.S.E., 2001, Hydrous phase equilibria of a Mexican high-silica andesite: A candidate for a mantle origin?: Geochimica et Cosmochimica Acta, 65, 4043-4065.

Blundy, J., Cashman, K., Humphreys, M., 2006, Magma heating by decompression-driven crystallization beneath andesite volcanoes: Nature, 443, 76-80.

Boyd, F.R., England, J.L., 1960, The quartz-coesite transition: Journal of Geophysical Research, 65, 749-756.

Buckley, V.J.E., Sparks, R.S.J., Wood, B.J., 2006, Hornblende dehydration reactions during magma ascent at Soufrière Hills volcano, Montserrat: Contributions to Mineralogy and Petrology, 151, 121-140.

Cameron, K.L., Robinson, J.V., Niemeyer, S., Nimz, G.J., Kuentz, D.C., Harmon, R.S., Bohlen, S.R., Collerson, K.D., 1992, Contrasting styles of pre-Cenozoic and mid-Tertiary crustal evolution in northern México: evidence from deep crustal xenoliths from La Olivina: Journal of Geophysical Research, 97, 17353-17376.

Cameron, W.E., 1976, Coexisting sillimanite and mullite: Geological Magazine, 113, 497-592.

Cameron, W.E., 1977, Nonstoichiometry in sillimanite: Mullite compositions with sillimanite-type superstructures: Physics and Chemistry of Minerals, v. 1, p. 265-272.

Campa, M.F., Coney, P.J., 1983, Tectono-stratigraphic terranes and mineral resource distributions in Mexico: Canadian Journal of Earth Sciences, 20, 1040-1051.

Carrington, D.P., Harley, S.L., 1995, Partial melting and phase relations in high-grade metapelites: an experimental petrogenetic grid in the KFMASH system: Contributions to Mineralogy and Petrology, 120, 270-291.

Cashman, K., Blundy, J., 2000, Degassing and crystallization of ascending andesite and dacite: Philosophical Transactions Royal Society London, 358, 1487-1513.

Elías-Herrera, M., Ortega-Gutiérrez, F., 2002, Caltepec fault zone: an Early Permian dextral transpressional boundary between the Proterozoic Oaxacan and the Paleozoic Acatlán complexes, southern Mexico, and regional tectonic implications: Tectonics, 21, doi:10.1029/2000TC001278.

Elthon, D., Scarpe, C.M., 1984, High-pressure phase equilibria of a high-magnesia basalt and the genesis of primary oceanic basalts, American Mineralogist, 69, 1-15.

Ernst, W.G., Liu, J., 1998, Experimental phase-equilibrium study of Al- and Ti-contents of calcic amphibole in MORB –A semiquantitative thermobarometer: American Mineralogist, 83, 952-969.

Garnier, V., Ohnenstetter, D., Giuliani, G., Fallick, A.E., Phan Trong, T., Hoa Ng Quang, V., Pham Van, L., Schwarz, D., 2005, Basalt petrology, zircon ages and sapphire genesis from Dak Nong, southern Vietnam: Mineralogical Magazine, 69, 21-38.

Ghent, E.D., Edwards, B.R., Russell, J.K., Mortensen, J., 2008, Granulite facies xenoliths from Prindle volcano, Alaska: Implications for the northern Cordilleran crustal lithosphere: Lithos, 101, 344-358.

Gill, J., 1981, Orogenic andesites and plate tectonics: New York, Springer-Verlag, 390 pp.

Gómez-Tuena, A., Orozco-Esquivel, T., Ferrari, L., 2005, Petrogénesis ígnea de la Faja Volcánica Transmexicana: Boletín de la Sociedad Geológica Mexicana, 57, 227-283.

Grapes, R., 2006, Pyrometamorphism: Berlin, Springer-Verlag, 275 pp.

Green, T.H., Pearson, N.J., 1985, Experimental determination of REE partition coefficients between amphibole and basaltic to andesitic liquids at high pressure: Geochimica et Cosmochimica Acta, 49, 1465-1468.

Grochau, B., Johannes, W., 1997, Stability of phlogopite in granitic melts, an experimental investigation: Contributions to Mineralogy and Petrology, 126, 315-330.

Guo, J., O'Reilly, S.Y., Griffin, W.L., 1996, Corundum from basaltic terrains: a mineral inclusion approach to the enigma: Contributions to Mineralogy and Petrology, 122, 368-386.

Halliday, A.N., Dickin, A.P., Hunter, R.N., Davies, G.R., Dempster, T.J., Hamilton, J.P., Upton, B.G.J., 1993, Formation and composition of the lower continental crust: Evidence from Scottish xenolith suites: Journal of Geophysical Research 98, B1, 581-607.

Harley, S.L., 2004, Extending our understanding of ultrahigh temperature

crustal metamorphism: Journal of Mineralogical and Petrological Sciences, 99, 140-158.

Harley, S.L., Motoyoshi, Y., 2000, Al zoning in orthopyroxene in a sapphirine quartzite: evidence for >1120 ºC UHT metamorphism in the Napier Complex, Antarctica, and implications for the entropy of sapphirine: Contributions to Mineralogy and Petrology, 138, 293-307.

Harris, N., 1981, The application of spinel-bearing metapelites to P/T determinations: An example from south India: Contributions to Mineralogy and Petrology, 76, 229-233.

Hart, S.R., 1984, A large-scale isotope anomaly in the Southern Hemisphere mantle: Nature, 309, 753-757.

Haskin, L.A., Haskin, M.A, Frey, F.A., Wildeman, T.R., 1968, Relative and absolute terrestrial abundances of the rare earths, *in* Ahrens, L.H. (ed.), Origin and Distribution of the Elements: Oxford, Pergamon, 889-912.

Hayob, J.L., Essene, E.J., Ruiz J., Ortega-Gutiérrez, F., Aranda-Gómez, J.J., 1989, Young high-temperature granulites from the base of the crust in central Mexico: Nature, 342, 265-268.

Henry, D.J., Guidotti, C.V., Thomson, J.A., 2005, The Ti-saturation surface for low-to-medium pressure metapelitic biotites: Implications for geothermometry and Ti-substitution mechanisms: American Mineralogist, 90, 316-328.

Hensen, B.J., Green, D.H., 1973, Experimental study of the stability of cordierite and garnet in pelitic compositions at high pressures and temperatures. III synthesis of experimental data and geological applications: Contributions to Mineralogy and Petrology, 38, 151-166.

Holland, T.J.B, Blundy, J.D., 1994, Non-ideal interactions in calcic amphiboles and their bearing on amphibole-plagioclase thermometry: Contributions to Mineralogy and Petrology, 116, 433-447.

Hollis, J.A., Harley, S.L., 2003, Alumina solubility in orthopyroxene coexisting with sapphirine and quartz: Contributions to Mineralogy and Petrology, 144, 473-483.

Holm, J.L., 2001, Kaolinites-mullite transformation in different Al_2O_3-SiO_2 systems: Thermo-analytical studies: Physical Chemistry and Chemical Physics, 3, 1362-1365.

Holtz, F., Becker, A., Freise, M., Johannes, W., 2001, The water-undersaturated and dry Qz-Ab-Or system revisited. Experimental results at very low water activities and geological implications: Contributions to Mineralogy and Petrology, 141, 347-357.

Johnson, B.R., Kriven, W.M., Schneider, J., 2001, Crystal structure development during devitrification of quenched mullite: Journal of European Ceramic Society, 21, 2541-2562.

Johnson, M.C., Rutherford, M.J., 1989, Experimental calibration of the aluminum-in-hornblende geobarometer with application to Long Valley Caldera (California) volcanic rocks: Geology, 17, 837-841.

Kelly, N.M., Harley, S.L., 2004, Orthopyroxene–corundum in Mg–Al-rich granulites from the Oygarden Islands, East Antarctica: Journal of Petrology, 45, 1481-1512.

Kelsey, D.E., White, RW., Powell, R., 2003, Orthopyroxene-sillimanite-quartz assemblages: distribution, petrology, quantitative P-T-X constraints and P-T paths: Journal of Metamorphic Geology, 21, 439-453.

Kosyakova, N.A., Aranovich, L.Y., Podlesskii, K.K., 2005, Equilibria of aluminous spinel with orthopyroxene in the system FeO-MgO-Al_2O_3-SiO_2: new experimental data and thermodynamic assessment: Doklady Earth Sciences, 400, 57-61.

Kriegsman, L.M., Schumacher, J.C., 1999, Petrology of sapphirine-bearing and associated granulites from central Sri Lanka: Journal of Petrology, 40, 1211-1239.

Lane, D.L., Ganguly, J., 1980, Al_2O_3 solubility in orthopyroxene in the system MgO-Al_2O_3-SiO_2; a reevaluation, and mantle geotherm: Journal of Geophysical Research, 85, B12, 6963-6972.

Le Bas, M.J., Le Maitre, R.W., Streckeisen, A., Zanettin, B., 1986, A chemical classification of volcanic rocks based on the total alkali-silica diagram: Journal of Petrology, 27, 745-750.

Lee, C.-T., Rudnick, R.L., Brimhall, G.H., Jr., 2001, Deep lithospheric dynamics beneath the Sierra Nevada during the Mesozoic and Cenozoic as inferred from xenolith petrology: Geochemistry Geophysics Geosystems, 2(12), doi: 10.1029/2001GC000152.

Lee, H.Y., Ganguly, J., 1988, Equilibrium compositions of coexisting garnet and orthopyroxene: Experimental determinations in the system FeO-MgO-Al_2O_3-SiO_2, and applications: Journal of Petrology, 29, 93-113.

Lepage, L.D., 2003, ILMAT: an Excel worksheet for ilmenite-magnetite geothermometry and geobarometry: Computers & Geosciences, 29, 673-678.

Liermann, H.P., Ganguly, J., 2003, Fe^{2+}-Mg fractionation between orthopyroxene and spinel: experimental calibration in the system FeO-MgO-Al_2O_3-Cr_2O_3-SiO_2, and applications: Contributions to Mineralogy and Petrology, 145, 217-227.

Lozano, R., Bernal, J.P., 2005, Characterization of a new set of eight geochemical reference materials for XRF major and trace element analysis: Revista Mexciana de Ciencas Geológicas, 22, 329-344.

Luhr, J.F., Aranda-Gómez, J.J., 1997, Mexican peridotite xenoliths and tectonic terranes: correlations among vent location, texture, temperature, pressure, and oxygen fugacity: Journal of Petrology, 38, 1075-1112.

Luhr, J.F., Aranda-Gómez, J.J., Pier, J.G., 1989, Spinel-lherzolite-bearing Quaternary volcanic centers in San Luis Potosí, Mexico: I. Geology, mineralogy and petrology: Journal of Geophysical Research, 94, B6, 7916-7940.

Mariga, J., Ripley E.M., Li, C., 2006a, Petrologic evolution of gneissic xenoliths in the Voisey´s Bay intrusion, Labrador, Canada: Mineralogy, reactions, partial melting, and mechanisms of mass transfer: Geochemistry Geophysics Geosystems, 7(5), doi: 10.1029/2005GC001184.

Mariga, J., Ripley, E.M., Li, C., McKeegan, K.D., Schmidt, A., Groove, M., 2006b, Oxygen isotopic disequilibrium in plagioclase-corundum-hercynite xenoliths from the Voisey's Bay Intrusion, Labrador, Canada: Earth and Planetary Science Letters, 248, 263-275.

Martiny, B., Martínez-Serrano, R.G., Morán-Zenteno, D.J., Macías-Romo, C., Ayuso, R.A., 2000, Stratigraphy, geochemistry and tectonic significance of the Oligocene magmatic rocks of western Oaxaca, southern Mexico: Tectonophysics, 318, 71-98.

Milholland, C.S., Presnall, D.C., 1998, Liquidus phase relations in the CaO-MgO-Al_2O_3-SiO_2 system at 3·0 GPa: the aluminous pyroxene thermal divide and high-pressure fractionation of picritic and komatiitic magmas: Journal of Petrology, 38, 3-27.

Morán-Zenteno, D. J., Martiny, B., Tolson, G., Solís-Pichardo, G., Alba-Aldave, L., Hernández-Bernal, M.S., Macías-Romo, C., Martínez-Serrano, R.G., Schaaf, P., Silva Romo, G., 2000, Geocronología y características geoquímicas de las rocas magmáticas terciarias de la Sierra Madre del Sur: Boletín de la Sociedad Geológica Mexicana, 53, 27-58.

Murphy, M.D., Sparks, R.S.J., Barclay, J., Carrol, M.R., Brewer, T.S., 2000, Remobilization of andesite magma by intrusion of mafic magma at the Soufriere Hills volcano, Montserrat, West Indies: Journal of Petrology, 41, 21-42.

Nakamura, N., 1974, Determination of REE, Ba, Fe, Mg, Na and K in carbonaceous and ordinary chondrites: Geochimica et Cosmochimica Acta, 38, 757-775.

Ortega-Gutiérrez, F., 1978, Estratigrafía del Complejo Acatlán en la Mixteca Baja, Estados de Puebla y Oaxaca: Revista, 2(2), 112-131.

Ortega-Gutiérrez, F., Mitre Salazar, L.M, Roldán Quintana, J., Sánchez Rubio, G., de la Fuente, M., 1990, North American Ocean-Continent Transects Program, Transect H-3 from Acapulco Trench to the Gulf of México across southern México: Boulder, CO, Geological Society of America, Decade of North American Geology (DNAG), Transect 13, map with sections and text, 9 pp.

Ortega-Gutiérrez, F., Elías-Herrera, M., Dávalos-Elizondo, M.G., 2008, On the nature and role of the lower crust in the volcanic front of the Trans-Mexican Volcanic Belt and its fore-arc region, southern and central Mexico: Revista Mexicana de Ciencias Geológicas,

25, 346-364.

Powell, M, Powell, R., 1977, Plagioclase-alkali feldspar geothermometry revisited: Mineralogical Magazine, 41, 253-256.

Powell, R., Sandiford, M., 1988, Sapphirine and spinel phase relationships in the system FeO-MgO-Al_2O_3-SiO_2-TiO_2-O_2 in the presence of quartz and hypersthenes: Contributions to Mineralogy and Petrology, 98, 64-71.

Pugin, V.A., Kuskov, O.L., 1968, P-T equilibria in the system Al_2O_3-SiO_2 according to thermodynamic data: Geochemistry International, 5, 804-808.

Ray, R., Shukla, A.D., Sheth, H.C., Ray, J.S., Duraiswami, R.A.,Vanderkluysen, L., Rautela, C.S., Mallik, J., 2008, Highly heterogeneous Precambrian basement under the central Deccan Traps, India: Direct evidence from xenoliths in dykes: Gondwana Research, 13, 375-385.

Reyes-Salas, A.M., 2003, Mineralogía y petrología de los Granitoides Esperanza del Complejo Acatlán, sur de México: Morelos, México, Universidad Autónoma del Estado de Morelos, Facultad de Ciencias Químicas e Ingeniería, Ph.D. thesis, 165 pp.

Rudnick, R.L., Cameron, K.L., 1991, Age diversity of the deep crust in northern Mexico: Geology, 19, 1197-1200.

Rudnick, R.L., Fountain, D.M., 1995, Nature and composition of the continental crust: a lower crustal perspective: Reviews in Geophysics, 33, 267-309.

Ruiz, J., Patchett, P.J., Ortega-Gutiérrez, F., 1988, Proterozoic and Phanerozoic basement terranes of Mexico from Nd isotopic studies: Geological Society of America Bulletin, 100, 274-281.

Rutherford, M.J., Hill, M., 1993, Magma ascent rates from hornblende breakdown: an experimental study applied to the 1980-1986 Mount St. Helens eruptions: Journal of Geophysical Research, 98, B11, 19667-19685.

Rutherford, M.J., Devine, J.D., 2003, Magmatic conditions and magma ascent as indicated by hornblende phase equilibria and reactions in the 1995–2002 Soufrière Hills magma: Journal of Petrology, 44, 1433-1454.

Sachs, P.M., Hansteen, T.H., 2000, Pleistocene underplating and metasomatism of the lower continental crust: a xenolith study: Journal of Petrology, 41(3), 331-356.

Saxena, S.K., Sykes, J., Eriksson, G., 1986, Phase equilibria in the pyroxene quadrilateral: Journal of Petrology, 27, 843-852.

Schaaf, P., Heinrich, W., Besh, T., 1994, Composition and Sm-Nd isotopic data of the lower crust beneath San Luis Potosi, central Mexico: Evidence from a granulite facies xenolith suite: Chemical Geology, 118, 63-84.

Schaaf, P., Stimac, J., Siebe, C., Macías, J.L., 2005, Geochemical evidence for mantle origin and crustal processes in volcanic rocks from Popocatépetl and surrounding monogenetic volcanoes, central Mexico: Journal of Petrology, 46, 1243-1282.

Schnetzler, C.C., Philpotts, J.A., 1970, Partition coefficients of rare-earth elements between igneous matrix material and rock-forming mineral phenocrysts –II: Geochimica et Cosmochimica Acta, 34, 331-340.

Schreyer, W., 1976, Experimental metamorphic petrology at low pressures and high temperatures, *in* Bailey D.K. MacDonald, R. (eds.), The Evolution of the Crystalline Rocks: London, Academic Press, 261-331.

Sedlock, R.L., Ortega-Gutiérrez, F., Speed, R.C., 1993, Tectonostratigraphic terranes and tectonic evolution of Mexico: Geological Society of America Special Paper 278,153.

Solé, J., Enrique, P., 2001, X-ray fluorescence analysis for the determination of potassium in small quantities of silicate minerals for K-Ar dating: Analytica Chimica Acta, 440, 199-205.

Spencer, K.J., Lindsley, D.H., 1981, A solution model for coexisting iron-titanium oxides: American Mineralogist, 66, 1189-1201.

Stacey, J.S., Kramers, J.D., 1975, Approximation of terrestrial lead isotope evolution by a two-stage model: Earth and Planetary Science Letters, 26, 207-221.

Steiger, R.H., Jäger, E., 1977, Subcommission on geochronology: Convention on the use of decay constants in geo- and cosmochronology: Earth and Planetary Science Letters, 36, 359-362.

Sun, S.-s., McDonough, W.F., 1989, Chemical and isotopic systematics of oceanic basalts: implications for mantle composition and processes, *in* Saunders, A.D., Norry, M.J. (eds.), Magmatism in the ocean basins, Geological Society Special Publication 42, 313-345.

Sutherland, F.L., Hoskin, P.W.O., Fanning, C.M., Coenraads, R.R., 1998, Models of corundum origin from alkali basaltic terrains: a reappraisal: Contributions to Mineralogy and Petrology, 133, 356-372.

Valdés, C.M., Mooney, W.D., Singh, S. K., Meyer, R.P., Lomnitz, C., Luetgert, J.H., Helsley, C.E., Lewis, B.T.R., Mena, M., 1986, Crustal structure of Oaxaca, from seismic refraction measurements: Bulletin of the Seismological Society of America, 76, 547-563.

Vielzeuf, D., Holloway, J.R., 1988, Experimental determination of the fluid-absent melting relations in the pelitic system. Consequences for crustal differentiation: Contributions to Mineralogy and Petrology, 98, 257-276.

Wen, S., Nekvasil, H., 1994, Ideal associated solutions: Application to the system albite-quartz-H_2O: American Mineralogist, 79, 316-331.

Whitney, D.L., Evans, B.W., 2010, Abbreviations for names of rock-forming minerals: American Mineralogist, 95, 185-187.

Xirouchakis, D., Lindsley, D.H., Andersen, D.J., 2001, Assemblages with titanite ($CaTiOSiO_4$), Ca-Mg-Fe olivine and pyroxenes, Fe-Mg-Ti oxides, and quartz: Part 1. Theory: American Mineralogist, 86, 247-253.

Yañez, P., Ruiz J., Patchett, P.J, Ortega-Gutiérrez, F., Gehrels G.E., 1991, Isotopic studies of the Acatlan Complex, southern Mexico: Implications for Paleozoic North American tectonics: Geological Society of America Bulletin, 103, 817-828.

Manuscript received: June 9, 2010
Corrected manuscript received: July 22, 2011
Manuscript accepted: July 27, 2011